HIGH-ACCURACY P-ρ-T MEASUREMENTS

OF PURE GAS AND NATURAL GAS LIKE MIXTURES

USING A COMPACT MAGNETIC SUSPENSION DENSIMETER

A Dissertation

by

SAQUIB EJAZ

Submitted to the Office of Graduate Studies of
Texas A&M University
in partial fulfillment of the requirements for the degree of

DOCTOR OF PHILOSOPHY

May 2007

Major Subject: Chemical Engineering

HIGH-ACCURACY P-ρ-T MEASUREMENTS

OF PURE GAS AND NATURAL GAS LIKE MIXTURES

USING A COMPACT MAGNETIC SUSPENSION DENSIMETER

A Dissertation

by

SAQUIB EJAZ

Submitted to the Office of Graduate Studies of
Texas A&M University
in partial fulfillment of the requirements for the degree of

DOCTOR OF PHILOSOPHY

Approved by:

Co-Chairs of Committee,	Kenneth R. Hall
	James C. Holste
Committee Members,	John Baldwin
	Maria A. Barrufet
Head of Department,	N. K. Anand

May 2007

Major Subject: Chemical Engineering

ABSTRACT

High-Accuracy P-ρ-T Measurements of Pure Gas and Natural Gas Like Mixtures
Using a Compact Magnetic Suspension Densimeter. (May 2007)
Saquib Ejaz, B.S.; M.S., Bangladesh University of Engineering and Technology, Dhaka,
Bangladesh;
M.E., Texas A&M University
Co-Chairs of Advisory Committee: Dr. Kenneth R. Hall
Dr. James C. Holste

Highly accurate data for density measurements are required for engineering calculations as well for developing equations of state (EOS) for use in the custody transfer of natural gas through pipelines. The widely used present industry standard, the AGA8-DC92 EOS, was developed against a database of reference quality natural gas mixtures with compositions containing less than 0.2 mole percent of the heavier C_{6+} fraction. With the advances in technology in the late nineties, it is possible to produce gas from deep and ultra-deepwater of the Gulf of Mexico where the pressures and temperatures encountered are much higher. Produced gas mixtures have compositions containing higher percentages of the C_{6+} fraction. As AGA8-DC92 is a statistical fit equation developed for one set of conditions, time has come to evaluate its performance to assess whether it is still viable for gas custody transfer with a new set of conditions encountered.

A highly accurate, high pressure and temperature, compact single sinker magnetic suspension densimeter has been used first to determine densities of pure component's densities for which very reliable data are available. After validating its performance, the densities of four light natural gas mixtures, containing no C_{6+} fraction and two heavy gas mixtures containing more than 0.2 mole percent of the heavier C_{6+} fraction, were measured. The light mixtures were measured in the temperature range of 250 to 450 K and in the pressure range of 10 to 150 Mpa (1450 to 21,750 psi); the heavy mixtures were measured in the range of 270 to 340 K and in the pressure range of 3.45 to

34.45 MPa (500 to 5,000 psi). Out of those, the data of only two light natural gas mixtures have been presented in the dissertation. Data on two heavy mixtures have not been published due to reasons of confidentiality.

Measured densities of light mixtures, not containing the C_{6+} fraction show less than expected relative deviations from the AGA8-DC92 EOS predictions except at low temperature. The deviation with the recently developed GERG02 EOS was more pronounced. A force transmission error analysis and uncertainty analysis was carried out. The total uncertainty was calculated to be 0.105 %.

The data measured as a part of this research should be used as reference quality data either to modify the parameters of AGA8-DC92 EOS or develop a more reliable equation of state with wider ranges of pressure and temperature.

DEDICATION

In loving memory of our daughter

Lamiya Zahin

(March 13, 2000 – August 2, 2004)

ACKNOWLEDGMENTS

I am indebted to Dr. Kenneth R. Hall and Dr. James C. Holste for giving me the opportunity to work in this project and for their advice, both professional and personal. I want to cherish their patience and understanding during the difficult times with the project. I would like to thank Dr. Maria Barrufet and Dr. John Baldwin for their time, advice and for serving on my research advisory committee.

I gratefully acknowledge the contributions of the National Institute of Standards and Technology (NIST), Mr. Ronald E. Beaty of Premier Measurement Services and Mr. James E. Gallagher of Savant Measurement Corporation for providing financial support for the project. I am grateful to Dr. Hall for financially supporting me for the last 5 years, well beyond the expected time of completion.

During the research, I had to communicate with many people for technical support. I am thankful to Dr. Mark O. McLinden and Dr. Eric W. Lemmon of NIST; Dr. Mclinden for doing calibration for us and Dr. Lemmon for providing us with NIST-12 and REFPROP software. Dr. Cornelia Lösch and Dr. Reza Seif, of Rubotherm Präzisionsmesstechnik GmbH, Bochum, Germany, offered their sound advice in solving countless technical problems with the magnetic suspension densimeter.

I sincerely appreciate the help I received from various people in the department, directly or indirectly related to my research. Mr. Randy Marek of the machine shop helped us with our mechanical works. Ms. Valerie Green, Ms. Towanna Hubacek, Ms. Missy Newton and Ms. Ninette Portales helped me with academic and personal matters. Mr. Jeff Polasek and Mr. Joel James helped me with computer hardware problems.

I am very appreciative of Mr. Jayson Caswell of the Physics electronic shop for spending countless hours with us advising on electrical connections and on Labview and for building constant power supply and temperature control box for the research.

I am very indebted to all my colleagues in the group for the valuable time spent with them. I am exceptionally grateful to Dr. Prashant V. Patil for guiding me through the initial stages of research and proving me with the support following the fire incident

I am most grateful to my wife, Lufthansa Kanta for being an exceptionally good mother to Lamiya and Nashita, our second child. She sacrificed three years of study at TEXAS A&M just to take care of Lamiya. Despite the loss of Lamiya, despite suffering almost fatal injuries that sent her to intensive care unit for three weeks, she has been a steady source of support for me and has been carrying on with her PhD at Texas A&M University. Finally, I am very grateful to the Almighty for having survived our second daughter Nashita Zahin; she is my biggest source of inspiration for continuing my work at Texas A&M.

NOMENCLATURE

a	Calibration constant in the deviation equations of ITS-90 for a PRT or coil radius (in)
A	Cross sectional area of piston cylinder assembly of dead weight gauge (in^2)
b	Calibration constant in the deviation equations of ITS-90 for a PRT
b_1, b_2	Elastic distortion coefficients
B	Second virial coefficient (cm^3/mole) or Constant in the reference function of ITS-90 for a PRT calibration
C	Third virial coefficient (cm^6/mole^2) or coefficient of superficial expansion in DWG or magnetic effect on density measurements
C_p	Isobaric heat capacity
D	Fourth virial coefficient or constant in the reference function of ITS-90 for a PRT calibration
E	Young's modulus (GPa)
g	acceleration of gravity (m/s^2)
G	Magnetic field gradient
H	magnetic field
I	Current through platinum resistance thermometer (mA)
L	length representing linear thermal expansion and contraction
m	Mass of sinker (g)
M	Molar mass (kg/kmole) or magnetic moment
M_X	Mass of DWG calibration weights in vacuum (kg)
n	Number of pairs of thermocouples forming a thermopile
N	Number of components in a natural gas mixture or constant in a polynomial equation
P, p	Pressure (MPa) [psia]
q	Charge, coulomb

R	Resistance of platinum resistance thermometer (ohm) or universal gas constant (8.314 J/mole K)
S	Seebeck coefficient (µV/ ^{o}C) or Slope of pressure transducer calibration linear fit
T	Temperature (K)
u	Uncertainty or speed of sound
U	Potential energy
V	Volume of sinker (cm^3) or voltage drop, volt
W	Ratio of the resistance of a platinum resistance thermometer at a temperature to its resistance at the triple point of water or balance reading or weight
x	Composition as mole fraction

Abbreviations

AC	Alternating Current
AGA	American Gas Association
AGA8-DC92	Detailed Characterization method of the American Gas Association
BP	British Petroleum
CB	Cricondenbar
CP	Critical Point
CT	Cricondentherm
DC	Direct Current
DMM	Digital Multimeter
DPDT	Double Pole Double Throw
DPI	Differential Pressure Indicator
DWG	Dead Weight Gauge Piston
DWRRA	Deep Water Royalty Relief Act
EOS	Equation of State

FPS	Floating Production System
FT	Fischer-Tropsch
FTE	Force transmission Error
GERG	European Group for Gas Research
GERG02	GERG EOS for gas mixtures
GOM	Gulf of Mexico
GTL	Gas to Liquids
HCCI	Homogeneous charge compression ignition
HIP	High Pressure Equipment Company
HP	Hand Pump
IC	Isochore
IEA	International Energy Agency
IGCC	Integrated Gasification Combined Cycle
IPTS-68	International Practical Temperature Scale of 1968
IT	Isotherm
ITS-90	International Temperature Scale of 1990
LNG	Liquefied natural gas
LVDT	Linear variable differential transformer
M78C1	Natural gas mixture with 78 mole percent methane
M88C1	Natural gas mixture with 88 mole percent methane
MMS	Minerals Management Service
MP	Measurement Point
MSA	Magnetic Suspension Assembly
NIST	National Institute of Standards and Technology
NEL	National Engineering Laboratory
OCS	Outer Continental Shelf
PID	Proportional Integral Derivative
PPM	Parts per Million
PRT	Platinum Resistance Thermometer

PT6K	6,000 psia range Pressure Transducer
PT30K	30,000 psia range Pressure Transducer
SC	Suspension Control
SNG3	Synthetic natural gas mixture
SNG5	Synthetic natural gas mixture
SSR	Solid State Relay
T	Tee fitting
Ta	Tantalum
Ti	Titanium
TLP	Tension Leg Platform
V	Valve
ZP	Zero Point

Greek letters

α	Temperature distortion coefficient (K^{-1}) or thermal coefficient of expansion (K^{-1}) or balance calibration factor
κ	Pressure distortion coefficient (MPa^{-1})
Δ	Difference or deviation
μ	Average or the permeability of free space
X	Internal temperature period of pressure transducer quartz crystal (μs)
ρ	Density (kg/m^3)
σ	Standard deviation or deviation at the 68% confidence level or normal stress
τ	Pressure period of vibration of transducer quartz crystal (μs)
υ	Poisson's ratio
φ	Coupling factor
ε	Apparatus specific constant or strain (inch/inch)
χ	Magnetic Susceptibility, m^3/kg

| π_∞ | Zero pressure cell constant |
| γ | Pressure distortion coefficient (MPa^{-1}) |

Subscripts

0	Index for constants B and D in reference functions of ITS-90 for PRT calibration
6+	Hexane and components heavier than hexane such as heptane, octane, etc
i	Component number or index for constants in the reference function of ITS-90 for PRT calibration
e-mag	Electromagnet
o	Reference condition of 23 ^{o}C for cross sectional area of piston cylinder assembly of dead weight gauge or reference condition of 20 ^{o}C and 1 bar pressure for sinker volume
p-mag	Permanent magnet
s	Initial set-point
S	Sinker
v	Vacuum condition

TABLE OF CONTENTS

Page

LIST OF FIGURES

Page

LIST OF TABLES

1. INTRODUCTION

1.1 Energy: Present and Future

Energy is important to maintain our ways of life, to raise and sustain our living standards and to attain economic progress. The quest for economic growth and a better quality of life fuels global energy demand not only in developed countries but also in developing countries. New supplies of reliable and affordable energy are necessary to meet this rising demand. At the same time, concerns about energy supply and its adverse impact on the environment has renewed interest in energy supply options, energy prices, energy efficiency and environmentally benign technologies (Exxon Mobil, 2006). Environmental issues now command center stage in the fuel sector; attempts to maintain or modify current modes of fuel generation or usage must acknowledge and respond to public and regulatory concerns over how fuel technologies may affect human health and ecosystems (Peters and Serio, 1993).

The global economy should double in size by 2030 with most of the growth taking place in the developing nations. World energy needs may grow by 50%; again most of the expansion happening place in the developing countries (Exxon Mobil, 2006). The world population should reach 8 billion by that time with 95% of the growth occurring in the developing world (World Bank, 2004). Currently, about 1.6 billion people have no access to electricity, and about 2.4 billion people use basic fuels such as dung and wood for heating and cooking (International Energy Agency, 2004). These factors must have a significant and dramatic impact upon energy demand and trade patterns worldwide.

Over time, a diverse range of energy sources including non fossil fuels and efficient technologies will be needed to meet the energy demand. But at least through

_____

This dissertation follows the style of *AIChE Journal*.

2030, fossil fuels will continue to play the major role in satisfying the energy demand. Oil and gas combined will represent about 60% of the overall energy consumption in 2030, as is the case today. Oil usage will grow by 1.4% annually despite significant improvements in vehicle fuel economy. Natural gas usage will grow by 1.8% annually because of strong growth in global electricity demand. Coal, the fastest growing fuel in 2005, will maintain about 20% of the share of the total energy demand through 2030. Aided by expanding power generation and easy availability, coal will grow annually at about 1.8%. The remaining 20% will be supplied by non fossil fuels such as nuclear, hydropower, bio-fuels (such as ethanol and bio-diesel), wind and solar energy. Energy concern and rising greenhouse gas emissions have brought these old and new technologies to the forefront of public discussion (Exxon Mobil, 2006; British Petroleum, 2006).

Fossil fuel is a general term for buried organic geological deposits formed from decayed plants and animals. Hundreds of millions of years of exposure to heat and pressure in the earth's crust have converted them to oil, natural gas, coal or heavy oils (US EPA, 2000). Coal is a carbon-based composite material consisting of a large variety of organic and inorganic compounds including alumina, silica, ferric oxides, magnesium oxides etc. It is a porous material with polymeric character consisting of aromatic and hydro-aromatic units connected by oxygen, methylene and sulphur cross-links (Mirzaeian and Hall, 2006). Anthracite coal has more carbon and has more energy content. Lignite is soft and low in carbon but high in oxygen and hydrogen content. Natural gas is a mixture of hydrocarbon gases found with petroleum deposits and composed mainly of methane (CH_4) and smaller amounts of paraffinic hydrocarbons such as ethane, propane, butanes, pentanes, and other gases such as hydrogen sulphide, nitrogen, carbon dioxide, benzene, helium (http://www.glossary.oilfield.slb.com). Petroleum is a mixture of liquids varying from colorless to jet black, thinner than water to thicker than molasses, light gases to asphalts heavier than water. It consists of hydrocarbon such as paraffins, cycloparaffins and aromatics with the number of carbon atoms in each molecule going up to hundred or more. It also includes compounds like

sulfur, nitrogen, oxygen, and metal atoms with the proportion of these atoms increasing with increasing size of the hydrocarbon molecule.

The availability of fossil fuel-based energy is estimated by proven and unproven reserves. Proven reserves are those quantities of hydrocarbons identified with a reasonable certainty to be commercially viable and recoverable from known reservoirs. These reservoirs have been drilled, the reserves have been evaluated and are producing fuel or are about to go into production. On the other hand, unproven reserves have been evaluated with some uncertainty to be potentially recoverable, but no commitment yet exists to develop the fields (Richardson et al., 2004).

The total global consumption of oil at the end of 2005 was 82.5 millions barrel/day whereas the world-wide proven reserves were estimated at about 1.2 trillion barrels. In the USA, the total proven reserves were about 29.3 billions barrel. The total global consumption of gas in 2005 was 2749.6 billion cubic meter and the total world proven reserves were 179.83 trillion cubic meters. The total proven reserves in the USA were 5.45 trillion cubic meters. The total global consumption of coal in 2005 was 2929.8 million tonnes oil equivalent. The total world proven reserves were 909 billion tonnes. The total proven reserves in the USA were 246.6 billion tonnes. At the end of 2005, the domestic reserves-to-production ratio, the length of time remaining reserves would last if production were continued at the current level, was 11.8, 10.4 and 240 years for oil, gas and coal, respectively (BP, 2006).

1.2 Fossil Fuels and Environmental Concern

Presently fossil fuels account for approximately 80% of the commercial energy used. The situation has not changed much over the last 50 years and should persist 50 more. Fossil fuels are an excellent source of energy. The variety of fossil fuels combined with the technology developed to produce and convert them for useful purposes has led to tremendous growth. The reservoirs were filled rather ubiquitously as a consequence of biomass production 100 to 300 million years ago when the planet was much warmer. As

a result, fossil fuels are found everywhere and some are easily transportable. Technical advances have led to discoveries and production from remote and inhospitable places as well as to more complete recovery (Judkins et al., 1993).

The perception that the coal is a major contributor to global warming is a major hurdle to overcome. Coal has the highest carbon to hydrogen ratio among the fossil fuels, thereby producing a higher proportion of CO_2 per unit of energy than fuels such as oil or gas. Other greenhouse gases include CH_4, which is released during deep hard coal production, and nitrous oxide that is produced in small quantities when coal is used. Nitrous oxide is responsible for stratospheric ozone depletion. Ozone is also a green house gas formed from complex reactions with several pollutants in the air. Nitric oxide and nitrogen dioxide are also released from coal emissions; they are not greenhouse gases but nitric oxide quickly converts to nitrogen dioxide in the atmosphere, which reacts with water vapor to form nitric acid (Smith and Thambimuthu, 1993; Mallet et al., 1997).

The relative contribution of greenhouse gases may be estimated from the increase of the gases in the atmosphere over a period. Factors such as differing times that gases remain in the atmosphere, their greenhouse effects while in the atmosphere and the period over which climatic changes are of concern should all be taken into account while determining the relative global warming potential of each gas (Shine et al., 1990). Most greenhouse gas concentration decays exponentially with time, which is not the case for CO_2. It declines fast over the first 10-year period, gradually over the next 100 years and very slowly over the thousand-year time scale. This is because CO_2 is exhausted from the atmosphere on different time scales into different carbon storage sinks, in vegetation soils, and the deep oceans (Smith and Thambimuthu, 1993). The approximate lifetime of CO_2 is calculated to be about 120 years with a range of 50-200 years (Watson et al., 1990).

The natural gas has a comparatively benign effect on the environment as far as greenhouse gases are concerned. The heat of combustion per molecule of CO_2 generated is about 70% more than that of coal and natural gas can be used more efficiently to

produce the same energy. However, this advantage may be offset to some extent by the leakage of natural gas from the production and transport systems. The principal component CH_4 has about 30 times more greenhouse effect than CO_2. Fortunately, the effective lifetime of CH_4 in the atmosphere is much shorter than CO_2 (Judkins et al., 1993).

1.3 Abatement of Greenhouse Gas Emissions

Abatement technologies are available that aim to reduce greenhouse gas emissions per unit of useful energy in the large-scale use of fossil fuels, especially coal. One way to tackle the emission issue is to improve the efficiency of coal use in steam power plants with supercritical steam cycles. Sophisticated steel alloys used to fabricate steam tubing enable its use in high temperature and pressure service. The improvement in plant efficiency reduces fuel intake, which also reduces nitrogen and sulphur input to the boiler by a similar input.

The application of combined cycles may remove the efficiency limitations in conventional steam cycles. In such a cycle, called integrated gasification combined cycle (IGCC) coal, water and oxygen are fed into a high-pressure gasifier where coal is converted into syngas, i.e. carbon monoxide and hydrogen. The syngas, after cleaned of particles, mercury and sulfur, is combusted and the resulting hot, pressurized flue gas expands through a gas turbine thus producing power in an open gas turbine (Brayton) cycle. The exhaust passes to a heat recovery steam generator that produces superheated steam, which drives a steam turbine in a closed cycle. An advantage of the IGCC process is that natural gas, oil or even biomass can replace coal (Beyer and Bolland, 1998).

For all fossil fuels, the amount of CO_2 released is inversely proportional to the process efficiency. All the improved methods should be able to maintain CO_2 concentration at an acceptable level based upon international standards. Among other major pollutants that need attention are: NO_X, SO_X and particulates. The formation of NO is inhibited by lower temperature, lower residence time and lower concentration of

oxygen in the fuel-air mixture; unfortunately, these same conditions prevent complete combustion of carbon monoxide to CO_2. Optimization of residence time and mixing conditions reduce NO emissions and at the same time avoid increasing the concentrations of incompletly combusted components (Beyer and Bolland, 1998).

A major source of air pollution is the exhaust gas emissions from the internal combustion engine. Researchers have investigated homogeneous charge compression ignition (HCCI) as a lean burn combustion concept that reduces the emissions of NO and particulate matter with high efficiency, something that has not been possible for diesel engines. In such a HCCI engine, fuel is premixed homogeneously with air, as is the case in a spark ignition engine, but with a high proportion of air to fuel. When the piston reaches the point where compression ratio is highest, it auto-ignites from compression heating, as in a diesel engine. The knocking generated does not damage the engine with a high air to fuel ratio because the presence of excess air keeps the maximum temperature of the burned gases relatively low. The most important characteristic of HCCI is that ignition occurs at several places simultaneously. Ongoing work seeks to design microprocessors that, by knowing the precise conditions (fuel species, temperature and density) at the start of compression, can predict accurately the beginning of combustion. At that point small amounts of dimethyl ether can be injected. With advances in microprocessors and a physical understanding of the ignition process, HCCI can achieve gasoline engine-like low NO emissions along with diesel engine-like efficiency (Ando et al., 2003; Westbrook, 1999).

1.4 Control of Greenhouse Gas Emissions

The control of greenhouse gas emissions by recovery and disposal is a last resort because of the high energy costs involved. Adsorption, membrane separation and cryogenic methods have excellent potentials for CO_2 removal, and they might become excellent alternatives in the future. Adsorption selectively removes CO_2 from a gas stream using adsorbent like zeolites, followed by regeneration, which can be achieved either by increasing the temperature or by reducing pressure. A novel method of

regeneration includes electrical swing adsorption where electrical current is passed through the adsorbent. Low capacity and low CO_2 selectivity have prevented this method from becoming commercially viable. In the cryogenic method, flue gas is cooled below the CO_2 boiling point and is separated from other gaseous products. However, the process is energy intensive and would result in large efficiency reduction. Membrane separation, which is a relatively new concept, has not seen large-scale application because of problems like selectivity, permeability and durability at higher temperatures (European Carbon Dioxide Network, 2004).

Depleted natural gas fields are attractive targets for carbon sequestration by direct CO_2 injection because of their proven records of gas recovery and integrity against gas leakage. According to International Energy Agency (IEA), as much as 140 giga tons of carbon can be sequestered in depleted natural gas reservoirs worldwide. The process includes scrubbing CO_2 from flue gases at fossil-fueled power plants, pressurizing CO_2 to supercritical conditions and transporting it in a pipeline to the depleted natural gas reservoir, injecting the CO_2 into the reservoir and increasing the production of CH_4 from the reservoir. After a period of enhanced methane production, the production wells would be sealed and the reservoir filled with CO_2 to maintain the initial reservoir pressure (Oldenburg and Benson, 2001). Supercritical, liquid-like carbon dioxide is a well-established compound for use in such applications for a number of reasons. It has the unique ability to diffuse through the solids like a gas, and high density results in solvent properties similar to liquids. Low viscosity and surface tension enables it to penetrate even small pores. In addition, these properties are strongly pressure-dependent in the vicinity of the critical point, making supercritical fluids highly tunable solvents.

Ocean disposal is generally regarded as the one with the greatest potential of all the disposal options. The CO_2 is first compressed, transported and injected into the deep ocean. At the high pressures prevailing at such depths, the CO_2 would form a liquid pool or hydrates and would stay on the ocean floor. In the presence of water and at high pressures and low temperatures, CO_2 would form solid hydrate with a clathrate structure

having density greater than seawater. However, very little is known about their stability and effects on environment (Judkins et al., 1993).

1.5 Natural Gas Conversions to Liquid Fuels and Chemicals

The BP Statistical Review of World Energy (BP, 2006) has predicted a world reserve-to-production ratio of 65.1 and 40.6 years remaining for natural gas and oil, respectively. With this depletion in liquid petroleum, natural gas containing primarily methane should become the major source of chemicals and liquid fuels. Even a few years ago, the cost of gasoline and diesel fuel was very low. With the price of gas, especially in Western Europe and the cost of gas conversions, there was no prospect of developing a process with gasoline as an-end product at a price that is competitive with the price of gasoline derived directly from crude oil. However, with the high price of liquid fuel at present, the focus has shifted towards natural gas conversions.

A few general observations are possible regarding the present state of natural gas conversions to liquid fuels and chemicals. First, the volume of the transport market, for gasoline and diesel is enormous. The demand for chemical product is much smaller but the demand for these products is growing at a steady and attractive rate compared to the more-or-less static transport fuel market. Second, the prohibitive cost of transporting natural gas over large distances should be taken into account. Gas has a low energy density per unit volume compared to petroleum liquids. Liquefied natural gas (LNG) has a high production cost, but it can play an important role in transporting natural gas to areas where it commands a high value as a premium fuel but is too expensive to deliver at a price that is attractive to chemical industry. On the other hand, the cost of transporting liquids for 6,000 miles, such as fuel or methanol, does not add more than 10 % to the cost of product delivered at the point of use. Third, the steadily increasing proven reserves of natural gas compared to stagnate proven reserves of petroleum has given new impetus to the efficient conversion of natural gas to transportable liquid fuels and chemicals (Renesme et al., 1992; Parkyns et al., 1993).

Two different methods convert CH_4 to chemicals and liquid fuels, namely, direct and indirect methods. The direct method is the oxidative coupling of CH_4 (OCM) into C_2 products (ethane and ethylene). The announcement in 1982 that CH_4 could be directly converted into ethylene initiated a great deal of interest and investigations for better catalysts and process schemes (Keller and Bhasin, 1982). The indirect route involves the production of syngas. Syngas can be produced by steam reforming or partial oxidative reaction of methane, which finally is converted to higher hydrocarbons by a Fischer-Tropsch (FT) process. The need for air separation process in the syngas production step has made the FT process less attractive. The direct method is economically more promising, but its application is limited by the low yield of C_2 as they are easily oxidized because of their high reactivity (Tan and Li, 2006).

Various membrane reactors can achieve economically attractive C_2 yields in OCM method. One example is $La_{0.6}Sr_{0.4}Co_{0.2}Fe_{0.8}O_{3-\alpha}$ (LSCF), which is a hollow-fiber ceramic membrane with an asymmetric structure with a thin dense and separating layer integrated with a porous substrate of the same material. The local CH_4-to-O_2 ratio can be kept high in the reaction zone by the addition of O_2 discretely through the membrane along the length of the reactor. As a result, once the amount of O_2 introduced in the reactor is large enough for methane conversion to C_2 and less O_2 is available for CH_4 conversion to CO_2, higher selectivity than a conventional reactor results. Higher selectivity also results from increasing the CH_4 (mixed with Argon) flow rate; this suggests that more O_2 reacts with CH_4 into C_2 than into carbon oxides as the flow rate increases. Yield and selectivity are also controlled by parameters such as operating temperature and residence time of CH_4 in the reactor. After 4 weeks of OCM experiments, the LSCF membrane could maintain its structural integrity, mechanical strength and OCM performance (Tan and Li, 2006).

Given the prospect that the OCM method may become viable, it should also be noted that it may not be globally applicable because of local economics. In North America, the abundance of natural gas has made the case for oxidative coupling unfavorable because natural gas liquids, particularly ethane, are already the preferred

feedstocks for steam cracking to ethylene. Europe and Japan have no large domestic gas production and imported naphtha is the main feedstock for ethylene. A viable coupling process would make gas competitive with naphtha, thus making the oxidative coupling a promising method for future. In the Middle East, the absence of large domestic demand and high export transport cost has made the demand for ethylene negligible. Consequently, the future of oxidative coupling in that part of the world is still in doubt because future demand would be met by large quantities of ethane, LPG and natural gas liquids readily available (Renesme et al., 1992; Parkyns et al., 1993).

Because of the aforementioned problems, the OCM method has so far been unable to receive worldwide acceptance. This is evident by the fact that all most all the new gas to liquid plants is based on the proven FT technology. Patil (2005) has discussed the gas to liquid conversions in details.

1.6 Deepwater Gulf of Mexico: America's Expanding Frontier

The deepwater Gulf of Mexico (GOM) is a crucial oil and gas region and an essential part of America's oil and gas supply. Production of oil and gas in the deepwater GOM began in 1979; and since 1995, a sustained and robust expansion of exploration activities has continued and has shown no signs of letting up. Generally, deepwater is defined as water depths greater than or equal to 1,000 ft and ultra-deep water is defined as water depths greater than or equal to 5,000 ft. In the beginning of 2004, 90 hydrocarbon production projects were on line. Production from deepwater reservoirs grew to approximately 959 thousand barrels of oil per day and 3.6 billion cubic feet of natural gas per day. Since 1995, there had been a rise of 535 percent and 620 percent in production, respectively. In the period between 1995 to 2003, about 750 exploration wells were drilled and at least 100 deepwater discoveries were announced. Between 2001 and 2003, there were 11 industry-announced discoveries in the water depth greater than 7,000 ft and these ultra-deepwater discoveries have opened up a new geological frontier (Richardson et al., 2004).

The massive expansion in deepwater and ultra-deepwater production in GOM can be attributed to various factors. One reason is that the production from already saturated shallow water reservoirs and the northern slope of Alaska cannot keep pace with the massive demand in energy; environmental restrictions in case of Alaska has inhibited further growth in onshore energy production. The acquisition of huge volumes of high-quality three-dimensional seismic data has reduced the inherent risk of traditional hydrocarbon exploration and allows imaging of previously hidden objects under salt canopies. Pre-stack depth migration (PrSDM) of seismic data has strengthened the interpretation capabilities in deep water. Time-lapse seismic surveys have been developed that can monitor production efficiency and characterize reservoir properties. Better understanding of ocean currents, and especially deep-ocean currents, has improved fatigue-forecasting models and established responsible design criteria leading to more reliable deepwater structures. The Outer Continental Shelf (OCS) Deep Water Royalty Relief Act (DWRRA), which provides economic incentives for operators to develop fields in water depth greater than 656 ft, also has had a positive and significant impact on deepwater GOM activities (Richardson et al., 2004).

Different types of production systems have been used to develop deepwater discoveries. Fixed platforms are built on concrete or steel legs. Because of their immobility, they are designed for long-term use and have an economic water depth of about 1,400 ft. Compliant towers built on narrow, flexible towers are designed to sustain significant lateral deflections and can be considered for water depths of approximately 1,000-3,000 ft. Tension-leg platforms (TLP) consist of floating rigs tethered to seabed such that most vertical movements of the structures are eliminated frequently are used in 1,000-5,000 ft water depths. Spars, semi-submersible production units and floating, production and offloading (FPSO) may be used in water depths of 10,000 ft or more. A spur is a circular cross-section vessel sitting vertically in the water supported by a buoyancy chamber at the top, with a flooded mid section hanging from the top and a stabilizing keel section. Because of the keel and presence of mooring lines, the spur is more stable than a TLP.

Semi-submersible platforms are multi-component seafloor and surface facilities for production in such water depths where it is not possible to install fixed or other platforms. These units can be moved from place to place, can be ballasted up or down by controlling the amount of flooding in buoyancy tanks and can be anchored by cable or by dynamic positioning. FPSO are large ships with processing and seafloor facilities, similar to semi-submersible platforms. Sub-sea developments have allowed fields to be connected to hub facilities miles away through tie-backs. The fields can be operated remotely using the latest technology in fiber optic and automation technology (http://www.bp.com/sectiongenericarticle, November 2006). The improvement in the technology of these sub-sea production facilities has made the ultra-deepwater production a reality in GOM.

The production facilities are connected to the onshore networks through a series of pipelines such as the Mardi Gras oil and gas transportation system. The BP operated Mardi Gras system, the largest capacity deepwater pipeline system ever built, when completed, can transport more than 1 million bpd of oil and 1.5 bcfd of gas. The five pipelines in the system, with diameters between 16 in and 30 in and a total length of 485 miles, will be laid in water depths of 4,500 ft to 7,300 ft (Sauer and Wiseman, May 2006).

British Petroleum estimates that more than 40 billion barrels of oil and gas lie in the deepwater gulf, but only 15 billion barrels of oil and gas reserves have been discovered so far (http://www.bp.com/sectiongenericarticle, November 2006). The availability of this huge reserve will make deepwater and ultra-deepwater GOM a viable energy source for years to come.

 This deepwater gas will meet rising demand of natural gas whose consumption will double worldwide by 2030. As is the case now, gas will be preferred over coal for environmental advantages, lower capital cost and operational flexibility. Gas-to-liquid plants will emerge as new markets for natural gas in the near future. All these factors will make natural gas the principal energy source until the transition is made to the hydrogen economy (International Energy Agency, 2004).

1.7 Objective of the Current Research

Measurements of pressure-density-temperature data and development of vapor-liquid equilibrium data is the principal objective of our research. Density is an important property of matter and its accurate measurements have significant repercussions in industrial and scientific research. Very accurate measurements of Pressure-Density-Temperature (P-ρ-T) are not only important for custody transfer of natural gas in terms of energy content, but also necessary for development of equations of state (EOS). The measurements can be used to determine thermal and calorific properties of fluids and mixtures required for industrial process design and process implementation. A loss of accuracy affects correct determination of these values from densities; so, only exceptionally good density values can ensure good thermal and calorific properties (Wagner and Kleinrahm, 2004).

Present energy and density measurement systems for the natural gas industry contain: volume metering, volume conversion from field conditions to reference conditions and calorific value determination. The meters required for flow measurement may cause experimental uncertainties of 0.4 percent in heating values. (Jaeschke M., 2002). Installation effects, such as undeveloped flow caused by piping configuration just upstream of the meter may produce additional uncertainties regardless of the type of system.

Because of difficulties encountered in the use of flow meters and conventional gas densitometers for natural gas mixtures, many operators prefer to determine the density of gas indirectly using gas chromatography. Knowledge of temperature, pressure and compositions enables determination of the density from an equation of state. The equation most widely used with the gas chromatographic technique is the Detailed Characterization Method or AGA8-DC92 equation developed by American Gas Association (AGA, 1992). The coefficients of this equation result from regression of an extensive and reliable experimental data bank for natural gas mixtures and for binary and higher order mixtures of hydrocarbons with nitrogen, carbon dioxide and other gases.

Although the AGA8 equation can be applied for temperatures from -130 to 200 °C at pressures up to 40,000 psia (275 MPa), it ensures 0.1 percent uncertainty in density (at one standard deviation) in Region 1 only, i.e. from -8 to 62 °C and up to 1750 psia (12 MPa) (AGA, 1992). The equation is valid only for lean natural gas mixtures over this wide range of conditions; its application to rich natural gases (containing over 0.4 mole percent of hexane plus) is untested. Also, the equation is valid for gas phase only and use of the calculation methods is not recommended in the vicinity of the critical point. Not surprisingly, for gases from condensate fields in North Sea at metering conditions between 8 MPa and 17 MPa pressure and 40 to 80 °C, differences of some 2.0 to 2.5 percent are observed between density values determined from the AGA8 and those monitored by gas densitometers (Watson, 1998).

In the mid-nineties, the Gas Research Institute (GRI) in collaboration with the National Engineering Laboratory (NEL) undertook a joint industry project to extend the range of applicability of the AGA8 equation of state for natural gas mixtures to include the gas compositions encountered in the North Sea operations (Watson, 1998). The re-evaluation of AGA8 has taken on added significance lately with deep drilling into the offshore reservoirs in the Gulf of Mexico, as discussed earlier. Previous drillings occurred in 2000 feet of water at a gas pressure of 8000 psia (55 MPa) and a temperature of 340-365 K. Explorations now occur in 5000 feet of water (or more) at 13000-18000 psia (90-124 MPa) and 365-408 K temperature. The typical compositions of these gas samples differ from the lean gas samples in the data banks used to develop AGA8. For example, in AGA8 region 1 the hexane plus fraction should be less than 0.2 mole percent, whereas for the Gulf samples this number is generally in the range of 0.3 to 0.4 mol% or larger. The presence of these additional heavies has a significant effect upon density calculations and phase behavior. It is important to avoid conditions in the pipelines, processing plants and storage facilities that lead to condensation of heavier components. Such condensation not only leads to operational problems that increase the cost of compression but also to loss of energy content in the processed gas.

In the light of these problems, we have undertaken a project that has short and long-term goals:

- Experimentally measure the densities of ultra-high purity, single-component gases at pressures up to 35 MPa and in the temperature range of 270 to 340 K using a magnetic suspension densimeter. These values should be compared to the NIST-12 program, which is based on reliable EOS's for pure components. A small deviation between the experimental and theoretical values should serve as an indicator of our data quality.

- Then experimentally measured densities of simulated natural gas samples similar to the expected compositions of the Gulf of Mexico gas at the production platforms at the above-mentioned pressures and temperatures should be compared to AGA8 to check its validity.

- Experimentally measure the phase envelopes of the same samples using an isochoric apparatus and compare the phase envelopes with Peng-Robinson and Soave-Redlich-Kwong equations.

- Measure densities of a wide range of synthetic natural gas mixtures at very high temperatures and pressures to simulate reservoir conditions and build a data base. Phase envelopes should also be developed for these samples.

- Investigate the error analysis in details.

- Develop a new EOS for pure components and gas mixtures with a wide range of temperature and pressure applicable to both lean and rich gas mixtures; this EOS could replace AGA8 and become the industry standard. This equation can also be used in orifice equation measurements for accurate gas custody transfer.

1.8 Organization of Dissertation

The present section makes an overview of the future growth of energy demand, of measures to improve efficiency and also addresses environmental concern. It also has explained the importance of Gulf of Mexico as major source of energy for the country's growing demand and the inspiration for doing research to develop a new equation of

state in light of enhanced production from the gulf. Section II discusses different types of density measuring devices including two-sinker device which is the most accurate for density measurement, especially at low pressures. Section III discusses the applications of single and two-sinker densimeters as well methods to calculate force transmission errors. Section IV explains the development of the non-contact force measuring devices. Section V describes experimental set up, the fundamentals of analytical balance and single-sinker densimeter, a modified form of determining force transmission analysis, temperature and pressure measurements basics, propane cooling system and LabVIEW programs for balance and for temperature control. Section VI presents the density data and analysis on pure components and two light natural gas mixtures, each containing about 90 mole percent methane. Conclusions and recommendations derived from the measurements are presented in section VII.

2. DENSITY MEASURING DEVICES

2.1 Introduction

In order to apply general thermodynamic relationships in practice, the properties of the substances must be known for use in the thermodynamic equations. These properties are described by equations of state (EOS). Reliable data are required for the thermal and calorific variables for determining the EOS.

Density is such a variable that must be measured, and the measured values should be approximated by suitable empirical EOS. Accurate density measurements should be traceable to the International System of Units (Kuramoto et al., 2004). The most important decision at the beginning of the research project is the selection of density measurement method. The criteria for the selection of the suitable method include: large ranges in pressure, temperature and density, high accuracy for the method over the total range (of the order of $\pm\ 10^{-4}$ relative or on the order of $\pm\ 0.001$ kg/m^3 absolute), simplicity in design, high operating safety and low time requirement for each measured value (Kleinrahm and Wagner, 1984).

2.2 Density Measurement Techniques

Various types of fluid-density measurement techniques or devices appear in this section. They include: (1) fixed volume devices such as continuously weighed pycnometers and isochoric apparatus (2) expansion devices such as Burnett apparatus (3) vibrating objects such as vibrating tube and vibrating wire densimeters (4) methods which use speed of sound to measure density (5) buoyancy densimeters.

2.2.1 Continuously Weighed Pycnometers

In the continuously weighed pycnometer method, the mass of the sample is determined by direct weighing of the cell or supply vessel. In such a method, the supply

connection to the cell remains attached during the weighing process, thus eliminating the need to remove the cell from the isothermal enclosure and to sever pressure connections. A typical pycnometer (Lau et al., 1997) consists of: a weight measurement system, an isothermal bath with temperature control and data acquisition system, a variable volume bellows cell for changing pressure and density without transferring mass, and a high vacuum system. The mass is determined with an electronic force balance and the weighing pan has no vertical displacement during the weighing operation. This enables a capillary feed line to remain attached to the pycnometer cell without affecting the mass measurement. Using calibration fluids, for which reliable density data exist, it is possible to determine the cell volume and its pressure and temperature dependence. Densities result from the measured mass values and the known volume of the pycnometer.

2.2.2 Expansion Devices

In an expansion device, the sample is expanded from one volume into a second, evacuated volume and the ratio of the final volume to the original volume equals the ratio of density before and after the expansion. In a multiple expansion device, like the Burnett apparatus, a given amount of gas (at the beginning) goes through a series of isothermal expansions into a chamber, which is evacuated every time the expansion takes place; this method can be used to determine gas densities and virial coefficients. For each expansion, the ratio of the densities before and after the expansion is

$$\rho_i = \rho_m \, \pi_\infty{}^{m-i} \, \Pi \left[\frac{1 + \gamma_{ab} P_j}{1 + \gamma_a P_{j-1}} \right] \tag{2.1}$$

Where $\pi_\infty = \lim \dfrac{V_a + V_b}{V_a}$ as $P \to 0$ $\tag{2.2}$

Here γ_a and γ_{ab} are the pressure distortions of the volumes V_a and $(V_a + V_b)$ respectively, π_∞ is the zero pressure cell constant, ρ_m is the density at the lowest pressure and subscripts i and m indicate the value after the i-th and m-th (last) expansions, respectively.

There are two principal sources of error while measuring density in the multiple expansion method. One problem is the propagation of error as an equation of state is used to calculate the density at the lowest pressure. This is evident from equation 2.1. The second problem is fluid adsorption, which is difficult to detect and describe quantitatively because of its nature and its pressure dependence. The Burnett method works well for gases at temperatures well above their critical temperatures where the physical adsorption of gas onto the surface of apparatus is not significant. However, at reduced temperature near unity or less, adsorption introduces negative deviations in the pressure measurements. When this happens, the assumption of conservation of mass during successive expansion, upon which equation 2.1 is based, is no longer valid.

The adsorption affect can be minimized by the design of Tillner-Roth and Baehr (1992) that uses two cells with a surface area ratio almost equal to the volume ratio. On the other hand, Eubank et al., (1988) have formulated new adsorption correction schemes, based upon the BET adsorption isotherm. Warowny and Eubank (1995) have derived generalized equations for the Burnett method in the presence of adsorbing gas. They also presented a method for accurate determination of density and virial coefficients.

2.2.3 Vibrating Devices

Vibrating–wire and vibrating-tube densimeters are the most important applications of vibrating-bodies to the measurement of density of fluids. In a vibrating-wire, a wire carrying a diamagnetic weight suspended in the measurement fluid, is mounted vertically and perpendicular to a uniform magnetic field provided by a permanent magnet. An alternating current from a power source is fed through the wire and its interaction with the permanent magnetic field gives rise to a harmonic driving force, which is perpendicular to both the wire and the magnetic field and sets the wire into a transverse motion. If the masses, densities and dimensions of all the solid components are known and the resonant frequency under vacuum can be determined experimentally, then measurements of the resonant frequency of the wire's velocity

determines the fluid density, provided the viscosity of the fluid is known. Majer and Padua (2003) and Padua et al., (1998) have discussed the theories of vibrating-wire densimeter in details.

The vibrating-wire technique is suited for precise measurement of density for pure fluids and mixtures. The simplicity of the system allows development of an exact physical model, and density, in principal, can be directly calculated from the theory. This makes it a good candidate for a primary device. However, it suffers from few problems such as: surface tension on the wire, adsorption on the weight, the need to know the exact dimensions of the wire, etc.

A typical vibrating tube assembly consists of two hollow metallic or glass thin-walled tubes bent in 'U' or 'V' shaped. Permanent magnet and coil assemblies, forming a drive circuit, are mounted on the center of the tubes. Wire coils are mounted on the side legs of one of the tubes, and magnets are mounted on the side legs of the opposing tube. Each coil and magnet on the side leg forms a pick up circuit. An alternating current supplied to the coil of the drive circuit generates alternating attractive and repulsive magnetic field between the coils and magnets. This produces oscillations and induces sinusoidal electrical signal in the coils in the pick up circuits, one placed on the inlet side and the other at the outlet side of the device.

Because the coils are mounted on one tube and the magnets on the opposing tube, the sine wave generated by the two pick up circuits represents the motion of one tube relative to the other. When there is no flow, the sine waves are in phase. When a fluid is moving through the tubes, Coriolis forces are introduced that create bending moments between two points (on the opposing arm of the same U-tube) where the fluid velocity is opposite but equal. This leads to a phase shift between two pick-up circuits, which is proportional to mass flow rate.

The density comes from the following working equation:

$$\rho = K\tau^2 + L \tag{2.3}$$

Where, tube parameters K and L are both pressure and temperature dependent and τ is the period of vibration. However, it is not exactly possible to define the pressure and

temperature dependence on K and L. For this reason, measurements are done at the same temperature and pressure with the sample and a reference fluid of well-known properties. Then the corresponding density difference is obtained as:

$$\rho - \rho_r = K\,(\tau^2 - \tau_r^2) \tag{2.4}$$

where subscript r relate to the reference fluid.

The vibrating tube is suited to perform very precise measurements of density differences. However, several simplifying assumptions prevent density measurements when highest levels of accuracy are sought. The linearity between τ^2 and ρ is not exact and must be taken into account. All these issues mean that calibration of vibrating-tube densimeter should be very frequent to preserve the highest accuracy.

2.2.4   Density from Speed of Sound Measurement

Densities and other physical properties like isothermal and isentropic compressibility factors can be obtained from speed of sound measurements. In a typical measurement process described by Daridon et al. (1998), a cylindrical-shaped cell is used to measure ultrasonic speed waves. This system is based upon a pulse technique in which the piezo-electric elements are isolated from the fluid studied and hence from the effects of pressure. The speed is deduced from the measurements of the transit time through the sample and the length of passage. Length of passage is a function of temperature and pressure with the coefficients of the equation, which are the properties of the material, are determined by calibration with water.

Density can be determined from the following equation:

$$\rho\,(p,\,T) = \rho_o\,(p_o,\,T) + \int_{p_o}^{p} u^{-2}dp \ + \ T\int_{p_o}^{p}(\alpha^2/C_p)dp \tag{2.5}$$

where u is the sound speed, α denotes the isobaric coefficient of thermal expansion, C_p the isobaric heat capacity and p_o is the atmospheric pressure.

In this equation, the density with respect to pressure at different temperatures is defined by the sum of three terms. The first term, which provides the main contribution,

can be obtained by measuring density at atmospheric pressure using a vibrating-tube densimeter. The first integral, where u^{-2} can be expressed as a polynomial of pressure with coefficients expressed as a polynomial of temperature, can be evaluated along the isotherms considered. The second integral, which is numerically few percent of the first integral, can be calculated iteratively using thermodynamic relationships for $(\partial \alpha / \partial p)_T$ and $(\partial C_p / \partial p)_T$. Daridon et al. (1998) and Davis and Gordon (1967) have discussed the numerical procedures at length.

2.2.5 Buoyancy Densimeters

There are different kinds of buoyancy densimeters such as hydrostatic balance densimeters; magnetic float and magnetic suspension densimeters; hydrostatic balance densimeters in combination with the magnetic float or magnetic suspension method; and hydrostatic balance densimeters in combination with magnetic suspension couplings (Wagner et al., 2003).

In a hydrostatic balance, a sphere or a cylinder of glass or metal, called a sinker, is suspended by a thin wire hanging from a weighing hook of a commercial balance. The fluid, whose density is to be measured, is kept in a thermostated cell placed below the balance, and the sinker is totally immersed in the sample liquid. According to Archimedes' principal, the apparent loss in the true weight of the sinker is equal to the weight of the displaced fluid. Therefore, the density of the liquid can be calculated from the following equation:

$$\rho = \frac{m_v - m_a}{V_s(T, P)} \qquad (2.6)$$

Where m_v is the 'true' mass of the sinker in vacuum, m_a is 'apparent' mass of the sinker submerged in the liquid and V_s is the volume of the sinker, which is a function of temperature and pressure. Several corrections must be considered, such as the affect of surface tension between the sample liquid and the immersed part of the wire, the effect of the buoyant force of air on the masses of the analytical balance, etc.

In a magnetic float densimeter, densities of liquids within small density ranges are measured. The sinker or float consists of a hollow glass body with a magnet or soft iron core inside and the density of the sinker is less than the density of the fluid. The position of the sinker inside the cell, which is full of fluid, is controlled by current passing through a solenoid. The solenoid, placed below the cell, generates a magnetic force such that the float is held in a fixed position with zero net force acting on the float. The relation between current acting on the solenoid and the magnetic force on the float (or the density of the fluid) must be calibrated with liquids of known density. This kind of device is limited by the range of fluid density; if the fluid density is very large then large amounts of solenoid current are needed for float stability. This might produce self-heating and affect the accuracy of the calibration curve.

A magnetic suspension densimeter, developed by Haynes et al. (1976) can cover fluids with wider ranges of temperature and pressure and uses a float with density greater than the density of the fluid. A three-coil air-core system creates a region of definite magnetic flux density and adds an upward magnetic force to the buoyancy force to balance the downward gravitational force. Each of the coils is symmetric about the cylindrical axis of the magnetic buoy. The main coil, which is independent of the other two coils (called gradient coils), provides the main part of the force to lift the float. The float is supported such that its horizontal position is fixed and is approximately midway between the gradient coils. These two coils are connected in series such that their magnetic field intensity contributions cancel at the float position.

The position of the float is controlled by signal from the linear variable differential transformer (LVDT). When the float deviates from the 'null position', it is brought back to that position by the net attractive/repulsive effect of the two secondary or gradient coils, depending on the polarity of the current flow.

For this three-coil arrangement with a constant main coil current I_M, the density of the fluid ρ is related to the gradient coil current I_G by the equation:

$$\rho = A + BI_G \tag{2.7}$$

where *A* and *B* are constants and are determined by calibration with reference fluids. As the magnetic moment of the float is temperature dependent, the constants *A* and *B* should be determined at each temperature of interest.

Beams and Clarke (1962) combined the hydrostatic balance method with the magnetic float method. With this method, a sample cell, which contains the experimental fluid and the float, is suspended from a balance by a thin wire. A core-solenoid is placed above the cell and this provides the force for free magnetic suspension of the float. When the float comes into magnetic suspension, the change in the weight of the cell is measured with the balance. The mass and the volume of the float must be determined using calibration fluids. A significant problem for construction of such device is the construction of the thermostating device for the sample cell.

Masui et al. (1984) combined the hydrostatic balance method with the magnetic suspension method. A float inside a cell containing the fluid can be suspended by current passing through a support coil and it is the coil, not the cell that is suspended from the electronic balance. The position of the float is sensed by a capacitive sensor and is held constant by a feedback loop controlling the coil current. To determine the density of the fluid, the apparent weight of the float is measured as the change in the balance reading when the float is brought into stable levitation by the magnetic field produced by the coil.

A similar densimeter was developed by Fujii et al. (1988) where the float consisted of superconducting material with a high transition temperature of about 94 K. A ring shaped permanent magnet placed outside the cell brings the float to a stable magnetic levitation by the 'Miessner Effect', a phenomena caused by the exclusion of the magnetic field from the interior of the superconductor below a transition or critical temperature. The position sensor and the feedback control system are not necessary in such a system.

2.2.6   Two-Sinker Densimeter

Kleinrahm and Wagner (1986) developed the two-Sinker densimeter for accurate measurements of saturated liquid and vapor densities. Densities in the homogeneous gas and liquid region can also be measured over a wide range of temperature, pressure and density. This method uses Archimedes principal in a differential way. Two sinkers, a solid gold disc and a gold- coated quartz glass sphere, have identical mass and identical surface area but they have significantly different volumes. For density measurements, the sinkers can be put on a sinker support system alternately and can be lifted using a sinker-changing device. The sinker support is connected to a commercial analytical balance.

The major feature of the weighing system is the magnetic suspension coupling. (Wagner and Kleinrahm, 2004). The suspension force is transmitted without contact from a pressurized measuring cell to the balance, which is exposed to ambient conditions. The coupling consists of an electromagnet suspended from a weighing hook connected to the underside of the balance and a permanent magnet connected by a thin shaft to the sinker support. The permanent magnet is placed in a pressure-proof coupling housing that separates the permanent magnet from the electromagnet. The coupling is made of beryllium copper which is nearly non-magnetic. When the coupling is switched on, the permanent magnet is attracted to the electromagnet by the action of a position sensor and a control system. The distance between the two magnets is controlled in such a way that the net current through the electromagnet is zero on average and the suspension force is completely transmitted by the action between the magnets. This avoids self-heating of the electromagnet and its surroundings and prevents convection flows. Once, the coupling is switched on, it takes only few seconds to reach a magnetically stable suspended state.

The avoidance of self heating due to large current is also important from the point of view of the balance stability. The heat can change the radius of the electromagnet coil and hence the magnetic gradient and force according to

$$\frac{\delta G}{\delta T} = \frac{\delta G}{\delta a}\frac{\delta a}{\delta T} = \alpha\frac{\delta G}{\delta a} \tag{2.8}$$

Where G is the magnetic field gradient and proportional to current in the coil, T is temperature of the coil and a is the radius of the coil. The term $\frac{\delta a}{\delta T}$ the linear thermal expansion coefficient α of the material. It can be shown that for a 1 K change in the temperature of the coil, the relative change in the magnetic gradient is 18×10^{-6} when z, the distance between the electromagnet and the permanent magnet, is equal to $0.8a$. This may cause fluctuations in force measurement as well as instability in balance reading. However, it can also be shown that when $z = \pm \sqrt{(3/2)}a$, the term $\frac{\delta G}{\delta a}$ is zero, i.e. force measured is insensitive to temperature (Bignell, 2006).

The density of the sample fluid, ρ can be calculated from:

$$\rho = \frac{(m_{2,v} - m_{2,a})}{V_{2,S}(T,P)} = \frac{(m_{1,v} - m_{1,a})}{V_{1,S}(T,P)} = \frac{(\Delta m_v - \Delta m_a)}{(V_{2,S}(T,P) - V_{1,S}(T,P))} \tag{2.9}$$

Where $m_{1,a}$ and $m_{2,a}$ are the apparent masses of the respective sinkers at a given temperature and pressure, $m_{1,v}$ and $m_{2,v}$ are their respective masses in vacuum and $V_{1,S}$ and $V_{2,S}$ are their respective volumes at the same temperature and pressure.

Because of the differential application of the Archimedes principal, all effects that can reduce the accuracy of the measurements are eliminated; they include buoyant forces on the sinker suspension, surface tension between suspension wire and fluid, electronic drift of the balance with time, etc. (Nowak et al., 1997 a; and Pieperbeck et al., 1991). For the same reason as well as the fact that the permanent magnet is nearly in the same position for all measurements, force transmission errors caused by magnetic interactions with the housing and fluid are almost eliminated (Wagner and Kleinrahm, 2004). Force transmission error is defined as the influence of the nearby magnetic materials, external magnetic fields, and the fluid being measured.

Adsorption on the sinker surfaces and surface tensions are also eliminated because of the same surface area and same surface material (Nowak et al., 1997 a). As

Δm_v as well as Δm at low density are very small numbers and the differential volume of the sinkers is large, the method can measure even low gas densities very accurately (Wagner and Kleinrahm, 2004). We subtract one small number from another in the numerator, so the error propagation is not significant (Kreyszig, 2004). Finally, high-accuracy in density is obtained because of the large difference in the volume of the sinkers. All these factors make the two-sinker method suitable for precise density measurements both in low and high density region.

3. LITERATURE REVIEW

3.1 Two-Sinker Densimeter Applications

The two-sinker densimeters have been used to develop the (p, ρ, T) relation of several technically and scientifically important pure fluids, including methane, carbon dioxide, argon, ethene, ethane, nitrogen, sulphur hexafluoride, dichlorodifluoromethane (R 12), and chlorodifluoromethane (R22). Nitrogen was extensively investigated by Nowak et al. (1997 a; 1997 b). Nitrogen was chosen, because its accurate thermodynamic properties are important for process and plant design, cryogenic storage, and custody transfer. In the field of science and industry, nitrogen is an excellent reference fluid for testing and calibration of densimeters and flow meters. Nitrogen is chemically inert, inexpensive, non-poisonous, non-flammable, and has a nearly constant isotopic composition. Because it is almost spherically symmetric, it is one of the most widely used molecules for the development of theoretically based models to predict thermodynamics properties of elongated pure substances. Lack of reliable data especially in the homogeneous liquid region and along vapor-liquid coexistence curve prompted this comprehensive (p, ρ, T) measurement of nitrogen by Nowak et al. (1997 a; 1997 b). For this purpose, they used a modified two-sinker densimeter, which can also be used for measurements near the critical region.

Their measurements were at pressures up to 12 MPa over the temperature range 66 to 340 K on 36 isotherms, and they compared their data to experimental (p, ρ, T) values from other selected studies. Comparison between a preliminary equation of state (EOS) based only on their data to the works of others such as Cockett et al. (1968), Straty and Diller (1980), Friedman (1950), EOS of Jacobsen et al. (1986), Achtermann et al. (1986), Crain and Sonntag (1966), Canfield et al. (1965), Jaeschke et al. (1991), Pieperbeck et al. (1991) resulted in a percentage deviation in the range of -0.2 to 0.3 between 70-98 K, -0.2 to 0.2 between 105-120 K, -0.1 to 0.1 between 145-220 K and -0.03 to 0.03 between 260-320 K. The preliminary EOS was the reference for the comparison. The total relative uncertainty in density was in the range of $1.0 \cdot 10^{-4} \cdot \rho$ to

$1.5 \cdot 10^{-4} \cdot \rho$; near the critical region, it was in the range of $0.8 \cdot 10^{-4} \cdot \rho$ to $3.0 \cdot 10^{-4} \cdot \rho$. The uncertainty was calculated using a Gaussian error-propagation formula and the reliability of these uncertainties was about 95%.

For determining saturated vapor densities, a small reference cell built into the densimeter, ensures that a hydrodynamic gradient does not effect the measurements in the main cell. The reference cell is filled with the sample substance in the vapor liquid equilibrium at p_σ (T). The reference cell is connected through a differential pressure indicator to the main cell, where density is measured at pressure p. Densities are measured in the homogeneous gas region on a corresponding isotherm at pressure p just below the vapor pressure p_σ, and then the saturated vapor is estimated by linear extrapolation to the vapor pressure so that ($p - p_\sigma$) is zero. Near the critical region, however, linear extrapolation is no longer suitable. In that case, extrapolation to $p - p_\sigma = 0$ uses the power law equation:

$$\left| p - N_1 \right| = N_2 \left| \rho - N_3 \right|^d \tag{3.1}$$

Where, the constants N_1, N_2, N_3 and d are non-linearly adjusted to the experimental values for each isotherm in the critical region (Nowak et al., 1997 b). In this way, the problem of condensation when measuring directly at saturation is circumvented.

To determine saturated-liquid densities near the critical region, several liquid densities were measured at various small pressure differences ($p - p_\sigma$) on an isotherm. These pressure differences were achieved using different liquid levels above the sinkers in the main cell. The saturated-liquid density was determined by extrapolating the isothermal liquid densities to $p - p_\sigma = 0$, again by non-linearly fitting equation 3.1 to (p, ρ, T) values (Nowak et al., 1997 b). They observed that the saturated-liquid densities measured by this method had an uncertainty of about 0.012%, ten times smaller than that of the previous measurements. Similar observations could also be made for saturated-vapor densities. These results highlight the accuracy and efficiency of two-sinker densimeters for measurements of saturated densities (Wagner and Kleinrahm, 2004).

3.2 Single-Sinker Densimeter Applications

A two-sinker device is rather complex consisting of the sinker-changing device and two sinkers. This design makes the two-sinker method suitable for very accurate density measurements over a wide range of gas densities. However, such accuracy, especially at low densities, may not be important in many applications (Wagner and Kleinrahm, 2004). Therefore, to simplify density measurement, especially in the medium and high density regions, Wagner et al. (1995) developed a single-sinker densimeter. A detailed description of this device appears in the experimental section of this dissertation.

Using the single-sinker densimeter, the (p, ρ, T) relationships of many technically or scientifically important pure fluids such as argon (Klimeck et al., 1998), nitrogen (Klimeck et al, 1998), methane (Klimeck et al., 2001), carbon dioxide (Klimeck et al., 2001), ethene (Claus et al., 2003), ethane (Claus et al., 2003), and sulfur hexafluoride (Claus et al., 2003) have been measured. The total uncertainty (k=2) of these measurements is 0.015% to 0.02% in density. Other measurements by Klimeck et al. (1998) have shown very good agreement with the reference measurements of Nowak et al. (1997 a) measured with the two-sinker densimeter at pressures up to 12 MPa. In general, measurements of other investigators (Straty and Diller, 1980; Jaeschke et al., 1991; Jacobsen et al., 1986) agree with the accurate values of Klimeck et al. (1998) within their given uncertainty of about 0.05% to 0.10%.

Watson et al. (1998) at the National Engineering Lab (NEL) in Glasgow, Scotland, have built a single-sinker densimeter designed for density measurements on liquids covering a temperature range from 233 K to 423 K at pressures up to 30 MPa. The total uncertainty in density is 0.015%. Kinoshita and Fujii (1999) have built a compact version and Kuramoto and Fujii (2001) have improved it. This densimeter has been built with the purpose of making very accurate density measurements on several reference liquids such as n-nonane, n-tridecane, water and 2, 4-dichlorotoluene. These fluids are liquid-density standards for the calibration of vibrating-tube instruments, which is an indirect measuring method. This densimeter covers a temperature range of

253 K to 473 K at pressures up to 20 MPa. The density measurements of the reference liquids at ambient conditions achieve relative uncertainties in the range of $5.6*10^{-6}$ to $11*10^{-6}$.

A compact single-sinker densimeter has been built at the University of Valladolid (Villamañán and Chamorro, 2001) for measuring pure gases and gas mixtures. It covers a temperature range from 233 K to 523 K at pressures up to 20 MPa and densities up to 20 kg m^{-3}. An uncertainty value of $\pm$ (0.01%+0.004 kg m^{-3}) is given for the measurements. Blanke et al. (1995; 1996), investigating vapor-liquid equilibria of pure fluids and mixtures, developed a system for simultaneous measurement of liquid and vapor densities. The system consists of a single-sinker densimeter to measure density in the liquid phase. A similar densimeter for the gas density measurement also is connected to the first densimeter, a component for the temperature stabilization and control, and instruments for adjusting and measuring the saturation pressure. They have investigated the densities of tetrafluoroethane (R134a), 1-Chloro-1-2-2-2-tetrafluoroethane (R124), R125 and difluromethane (R32) in the temperature range from 120 K to 395 K at pressures up to 5 MPa. The reported total uncertainty in pure component density measurement is 0.02% for the saturated-liquid region and 0.1% for the saturated-vapor region. Iwagai et al. (1999) have used a similar system to measure densities of R32 and pentafluroethane in the homogeneous phase and on the vapor-liquid phase boundary. The apparatus covers a temperature range from 223 K to 423 K at pressures up to 15 MPa and densities up to 2000 kg m^{-3}. From the measurements of CO_2, the uncertainty is estimated to be 0.03% (Wagner and Kleinrahm, 2004).

A single-sinker densimeter with a specially designed measuring cell has been built in Universität für Bodenkultur in Vienna, Austria. The vapor-liquid equilibrium of binary mixtures of natural-gas components can be measured with this apparatus. First, the density of saturated liquid is directly measured. The density of the saturated-vapor is then calculated from a material balance, knowing the liquid level, the saturated-liquid density, the composition of the liquid and vapor phase, the total amount of substance in the cell, and the total volume of the cell. Test measurements on pure substances such as

water (compressed liquid densities), CO_2 (saturated-liquid densities), and nitrogen (supercritical gas densities) have been performed in the temperature range of 213 K to 373 K at pressures up to 6.7 MPa (Saleh and Wendland, 2005).

3.3 Force Transmission Error

As already discussed, the interaction of an electromagnet and a permanent magnet permits stable magnetic levitation of the permanent magnet, thus causing the sinker to float in single and two sinker magnetic suspension assemblies. After proper design, the efficiency of force transmission is almost one, but it is influenced by the presence of magnetic materials including sample fluids and any other external magnetic fields. These interactions produce a force transmission error (FTE) that must be taken into account to realize the full potential of these systems. The FTE can be either the error in the balance reading using the magnetic coupling or the error in the density because of magnetic effects. The first one can be explained in-terms of the effect of the di-magnetic housing. The second error is caused by the fluid itself as well as by the distribution of the fluid around the permanent magnet as the position of the magnet changes with density. This effect is called the "fluid specific effect" (McLinden et al., 2006).

The FTE has been explained from an empirical point of view by Wagner and Kleinrahm (2004) and McLinden et al. (2006) for both single and two-sinker methods. Kuramoto et al. (2004) has approached the problem based upon a physical problem; however, it is complex and requires detailed knowledge of the apparatus and fluid magnetic properties.

3.3.1 Force Transmission Error Analysis for Two-Sinker Densimeter

McLinden et al. (2006) have done a detailed analysis of the FTE in a two sinker densimeter. They used a tantalum and a titanium sinker and two external calibration weights. The external weights are fabricated of stainless steel, have equal volume but different mass and were initially intended to provide automated balance calibration.

Each of the weights is weighed one at a time and the following equations were suggested:

$$\beta = \varphi\left(m_{p-mag} - \rho_{fluid}V_{p-mag}\right) + \left(m_{e-mag} - \rho_{air}V_{e-mag}\right) + W_{zero} \tag{3.2}$$

$$\alpha = \frac{W_{cal} - W_{tare}}{(m_{cal} - m_{tare}) - \rho_{air}(V_{cal} - V_{tare})} \tag{3.3}$$

$$\beta = \frac{W_{cal}}{\alpha} - (m_{cal} - \rho_{air}V_{cal}) \tag{3.4}$$

$$\varphi = \frac{W_1/\alpha - \beta}{m_1 - \rho_{fluid}V_1} \tag{3.5}$$

$$\rho_{fluid} = \left[(m_1 - m_2) - \frac{(W_1 - W_2)m_1}{W_1 - \alpha\beta}\right] \bigg/ \left[(V_1 - V_2) - \frac{(W_1 - W_2)V_1}{W_1 - \alpha\beta}\right] \tag{3.6}$$

Where, α is the balance calibration factor, which drifts slowly with time as ambient temperature and pressure changes. The parameter β includes the buoyancy forces on the electromagnet, the permanent magnet and the zero shift of the balance (W_{zero}); it is a constant for density determination at a given point. φ is the coupling factor, which includes the apparatus magnetic effect as well as the fluid magnetic susceptibility and the relative position of the permanent magnet. m_{cal} and m_{tare} are the mass of the external calibration weights and m_1 and m_2 are mass of sinker 1 and 2, respectively; all these are in vacuum. W_1 and W_2 are the "ideal" balance readings when sinker 1 and 2 are weighed respectively, taking into account α, φ, β and the buoyancy. W_1 and W_2 should be slightly different from actual balance readings. Similarly, W_{cal} and W_{tare} are the readings of the external weights taking into account α, β and the effect of buoyancy.

Knowing the external weights and sinkers volumes (V_1, V_2) and their masses in vacuum from calibration, the corrected density of the fluid can be calculated as follows, provided that we can determine air density accurately in ambient conditions: first assume ρ_{fluid} (from any EOS), α and φ; then determine β from (3.2). Using these values, calculate W_{cal}, W_{tare}, W_1 and W_2 by using force balance. Then calculate α from (3.3), β

from (3.4), φ from (3.5) and ρ_{fluid} from (3.6). Using this new set of value for α, β and φ, start all over again by calculating $W_{cal,}$ W_{tare}, W_1 and W_2. Repeat the steps until the values of α, β, φ and ρ_{fluid} are converged. This final ρ_{fluid} is the corrected density value, which takes in to consideration all the factors (except very slightly different measurement position for the permanent magnet for the two sinkers weighing at same density) that otherwise, would decrease the accuracy of the two-sinker density measurement technique.

Finally, to make a one-to-one correspondence between the corrected density ρ_{fluid} and the uncorrected density $\rho(\varphi=1,\alpha=1)$, the following equation is used:

$$\rho(\varphi=1,\alpha=1)-\rho_{fluid} = \frac{1}{(V_1-V_2)}\left[W_1-W_2-\frac{(W_1-W_2)}{\alpha\varphi}\right] \qquad (3.7)$$

Where, the uncorrected density is directly obtained from the densimeter without the correction for the balance calibration factor and the correction for the FTE.

3.3.2 Force Transmission Error Analysis for Single-Sinker Densimeter

For the single-sinker densimeter, two weighings instead of four are performed. One at the zero point (zp) when the permanent magnet is suspended, and one at the measurement point (mp) when the permanent magnet and the sinker are suspended by an electromagnet shaft. One compensation weight is placed on the balance pan each time. Weight of the electromagnet shaft is considered both the time. McLinden et al. (2006) have suggested the following equations:

$$\varepsilon_\rho = \frac{\chi_{s0}}{\chi_s}\left(\frac{\rho_0}{\rho_{s,2}-\rho_{s,1}}\right)\left[\frac{\rho_1-\rho_{EOS}(T_1,p_1)}{\rho_{EOS}(T_1,p_1)}-\frac{\rho_2-\rho_{EOS}(T_2,p_2)}{\rho_{EOS}(T_2,p_2)}\right] \qquad (3.8)$$

$$W_1 = \alpha \left[\begin{array}{c} \varphi \{ m_s + m_{p-mag} - \rho_{fluid}(V_s + V_{p-mag}) \} + m_{e-mag} + m_{c1} \\ - \rho_{air}(V_{e-mag} + V_{c1}) + W_{zero} \end{array} \right] \tag{3.9}$$

$$W_2 = \alpha \left[\begin{array}{c} \varphi \{ m_{p-mag} - \rho_{fluid} V_{p-mag} \} + m_{e-mag} \\ + m_{c2} - \rho_{air}(V_{e-mag} + V_{c2}) + W_{zero} \end{array} \right] \tag{3.10}$$

$$\varphi_0 = \frac{-(m_{c1} - m_{c2}) + (W_1 - W_2)/\alpha}{m_s} \tag{3.11}$$

$$\rho_{fluid} = \frac{\varphi_0 m_s + (m_{c1} - m_{c2}) - (W_1 - W_2)/\alpha}{V_s \varphi_0} - \varepsilon_\rho \frac{\chi_s}{\chi_{s0}} \left(\frac{\rho_s}{\rho_0} - \frac{\rho_{fluid}}{\rho_0} \right) \rho_{fluid} \tag{3.12}$$

$$\varphi = \varphi_0 + \varepsilon_\rho \frac{\chi_s}{\chi_{s0}} \frac{\rho_{fluid}}{\rho_0} \tag{3.13}$$

Where, m stands for calibrated mass in vacuum, V for calibrated volume, subscripts s for sinker, $c1$ and $c2$ for external compensation weights (titanium and tantalum, respectively) and p-mag and e-mag for permanent and electro magnet respectively. W_1 and W_2 are the corrected balance reading at measurement and zero point respectively. ε_ρ is the apparatus specific constant independent of the fluid, temperature and pressure. Moreover, ρ_0 and χ_{s0} are reducing constants with positive signs, χ_s is the specific magnetic susceptibility of the fluid in $m^3.kg^{-1}$ and a known quantity. φ_0 is coupling factor extrapolated to zero density and α and φ have the same implications as before.

In order to determine the corrected density, ε_ρ is first calculated by using (3.8). Two sinkers are used to determine the density of the same fluid at almost same temperature, pressure and density at different times. p, ρ, T values for measurements with sinkers 1 and 2 are p_1, ρ_1, T_1 and p_2, ρ_2, T_2 respectively. ρ_1 and ρ_2 are the experimental uncorrected densities. Any Eos could be used as the densities predicted by any EOS almost cancel out in (3.8).

Once ε_ρ is calculated and α is obtained by a separate calibration, we can initiate a trial and error procedure by assuming a value for ρ_{fluid} (from EOS) and φ.

We then, can sequentially calculate W_1 from (3.9), W_2 from (3.10), φ_0 from (3.11), ρ_{fluid} from (3.12) and φ from (3.13) until these values converge.

Finally, we can make one-to-one correspondence between corrected and uncorrected density by using the following equation:

$$\rho(\varphi=1,\alpha=1)-\rho_{fluid} = (1-\varphi_0)(\rho_s - \rho_{fluid})-\varepsilon_\rho \frac{\chi_s}{\chi_{s0}}\left(\frac{\rho_s}{\rho_0} - \frac{\rho_{fluid}}{\rho_0}\right)\rho_{fluid} \quad (3.14)$$

We can make a few observations from this equation. First, for a diamagnetic fluid (i.e. χ_s is negative) in a diamagnetic housing (i.e. $1-\varphi_0$ is negative) with the understanding that $\rho_s > \rho_{fluid}$ and ε_ρ has a positive value, the first term on the right hand side is negative while the second term is positive. Therefore, for a diamagnetic fluid the two terms compensate; however, this is not true for a paramagnetic fluid in a diamagnetic housing. Second, the presence of $\rho_s - \rho_{fluid}$ term indicates that the sinker density should be as close to fluid density for better accuracy. For this reason, in a system with a titanium sinker, we should expect better quality data at high density than at low density. Third, the single sinker includes a term proportional to $\chi_s\rho_s$ which takes in to account the different positions of the permanent magnet at measurement point and at zero point.

3.3.3 Force Transmission Error Analysis by a Physical Model

Kuramoto et al. (2004) have developed a more physically realistic model for FTE in single-sinker. The following equation is obtained for the density measurement by the magnetic suspension balance:

$$\rho_{fluid} = \left[C_{housing}\left(K_V\left(W_{V,mp}-W_{V,zp}\right)-K_F\left(W_{F,mp}-W_{F,zp}\right)\right)-C_{liquid}\right]\left[V_s(T,p)\right]^{-1} \quad (3.15)$$

Where, W is the actual balance display, K is the balance sensitivity factor, subscripts v and F refers to conditions when cell is under vacuum and cell is under fluid pressure, respectively. $C_{housing}$ is the magnetic effect of the coupling and housing on the density

measurement and C_{liquid} is the change in the apparent mass of the sinker because of the magnetic properties of the fluid.

Since the position of the permanent magnet is different at measurement position than at zero point position, the total forces acting on the permanent magnet due to the magnetic interaction between the permanent magnet and fluid are not the same. In order to correct this FTE, Kuramoto et al. (2004) calculated the magnetic interaction by using the following equations:

$$H(r) = \frac{q}{4\pi\mu_0} \left[\frac{r - r_+}{(r - r_+)^{3/2}} - \frac{r - r_-}{(r - r_-)^{3/2}} \right]$$ (3.16)

Where, the permanent magnet is assumed to have to two oppositely charged point magnetic charges, $+q$ and $-q$. The two charges are located at r_+ and r_-, respectively, from the top of the measuring cell. The magnetic field at r is $H(r)$ and μ_0 is the magnetic permeability in vacuum. The magnetic moment of the sample liquid of infinitesimal volume dV, at r is given by the equation:

$$M(r) = \chi\mu_0 H(r) dV$$ (3.17)

The potential energy, $U(r)$ in $H(r)$ is calculated as:

$$U(r) = -M(r) \cdot H(r)$$ (3.18)

The force exerted by the permanent magnet on the sample liquid of volume V in the vertical direction, F_z is expressed as:

$$F_z = -\iiint_V \frac{\partial U}{\partial Z} dV$$ (3.19)

Where, F_z is the magnitude of error in force transmission due to fluid magnetic property. This causes change in the apparent mass of the sinker and is represented as:

$$C_{liquid} = \frac{F_{Z,mp} - F_{Z,zp}}{g}$$ (3.20)

Where, $F_{Z,mp}$ and $F_{Z,zp}$ are F_z values at measurement and zero point, respectively and g is the acceleration of gravity.

In order to determine C_{liquid}, first the volume of the sinker coupling and decoupling device is determined from the change in balance reading at the zero point position as the measuring cell which is under vacuum is filled with a reference fluid (such as n-tridecane). Then the ratio of the apparent mass suspended by the electromagnet (i.e. sinker and coupling and decoupling device) at the measuring position for the sample to that of n-tridecane, $\dfrac{R_{sample}}{R_{tridecane}}$ is determined. For this purpose, the density of tridecane could be obtained from literature while for the sample, density data from vibrating tube densimeter could be used. Then $z_{sample,\ mp}$ and $z_{tridecane,\ mp}$ are determined by trial and error method such that the following constraint is satisfied:

$$\frac{F_{Z\ @\ zsample,mp}}{F_{z\ @\ ztridecane,mp}} = \frac{R_{sample}}{R_{tridecane}} \tag{3.21}$$

For mathematical convenience, the sample and tridecane could be kept at exactly at same density so that the ratio is one. In that case, $z_{sample,\ mp}$ and $z_{tridecane,\ mp}$ should be close to each other if their magnetic properties are similar.

Although the distance z_{mp} and z_{zp} are not constant and vary with fluid density, their difference $\Delta z_{zp/mp}$ is considered approximately constant at (5.0 ± 0.5) mm. This constraint is used to calculate z_{zp} for both fluids.

Once these values are known, $F_{z,mp}$ and $F_{z,zp}$ could be calculated both for the sample and for tridecane using equations (3.16)-(3.19). Then C_{liquid} is obtained for both fluids at some density using equation (3.20). The whole process is repeated for different densities so that we have a correlation between C_{liquid} and p,T for both the fluids.

C_{liquid} for the sample could be used as a correction factor in (3.15) to determine corrected fluid density from single-sinker densimeter that takes in to account magnetic properties of housing, coupling and decoupling device and fluid. C_{liquid} for the tridecane could be used similarly in (3.15) to compare densities from single-sinker with tabulated reference values; this will serve to validate the model and the associated assumptions.

4. DEVELOPMENT OF NON- CONTACT FORCE MEASUREMENT SUSPENSION BEARING SYSTEM

4.1 General Principal of Control System

The free suspension of a float or buoy requires measurement of non-contact vertical forces. Holding devices (such as magnets) provide the free suspension that must compensate for force, *F,* on the float resulting from gravity and other vertical forces. The compensating force is transmitted through the wall of the measurement cell to the holding device and must be produced by electrical or magnetic fields. If the float is a magnetic or ferromagnetic material, it could be kept in magnetic suspension when its position is controlled in at least one direction of movement (Lösch, 1987).

The principal of static force transmission for a vertically controlled magnetic suspension bearing appears in figure IV.1.
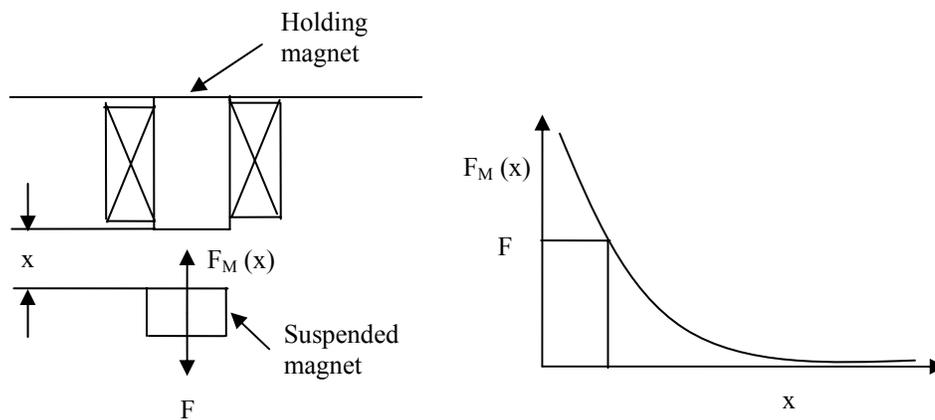
Figure IV.1. Principal of static force transmission for a vertically controlled magnetic suspension bearing (Lösch, 1987).

When the holding magnet generates a constant magnetic field, the suspended magnet experiences a force $F_M(x)$. For a certain distance x_0, this equals force F. For any

small perturbation making $x < x_0$ or $x > x_0$, $F_M(x)$ becomes greater or smaller than F and the suspended magnet accelerates upwards or downwards thus causing an unstable equilibrium (pseudo equilibrium) at distance x_0. To achieve stability, the magnetic field must be controlled in the vertical direction such that a force-distance curve with a positive gradient results in the vicinity of x_0.

The principal of control circuit for the vertical suspension appears in figure IV.2 in its most basic form.
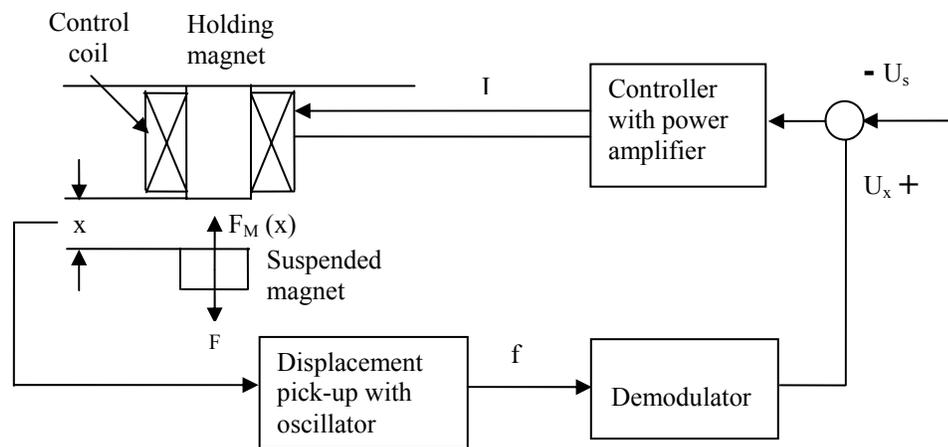
Figure IV.2. Control circuit principal of vertically controlled magnetic suspension bearing for static force transmission (Lösch, 1987).

A non-contact displacement pickup senses the distance between the magnets and transforms it into a direct voltage U_x with the help of an oscillator and a demodulator circuit. The displacement pickup could be capacitive, inductive, or photoelectric. The oscillator circuit, which contains capacitors and inductors among other things, provides an amplified sinusoidal output. The demodulator, which is a rectifier, performs an AC to DC conversion and produces a dc output U_x proportional to the distance.

The demodulator receives a reference AC voltage of the same frequency and with a fixed phase relationship to that of the input AC signal. The demodulator operates by multiplying these signals. If the relative phase shift between the signals is zero

degrees, then the modulator output has the form of a sinusoid at twice the reference frequency, but with a mean or average value that is the DC component. This mean level is proportional to the product of the signal and reference frequency amplitudes and is related to the phase angle between the signal and the reference (www.signalrecovery.com, 2006).

The noise, which has no fixed frequency or phase relationship to the reference, also is multiplied by the demodulator but does not cause any change to the mean DC value. A traditional rectifier makes no distinction between signal and noise and produces error caused by rectified noise components. The noise at the input of the demodulator, however, is not rectified but appears as an AC fluctuation at the output. Thus, the desired signal, now a DC signal, can be separated from the noise and the AC component by a low-pass filter (www.signalrecovery.com, 2006).

The deviation of signal U_x from a nominal voltage U_x is used as an input to the controller, which must have at least proportional-differential characteristics (Clark, 1947). The controller controls the magnetic field in such a way that the suspended magnet is held in suspension at a distance from the holding magnet corresponding to the nominal value. The control action is provided by the control coil whose current is controlled by the power amplifier of the controller.

4.2 Development Stages of Suspension Bearings and Control System

Over the years, different types of suspension bearings have been developed. They differ in their design, means of distance measurement and generation of static fields for the transmission of main force (Lösch, 1987). Instead of a permanent holding magnet, the main force can be generated by a pure electromagnet through which constant current flows. In some cases, ferromagnetic cores are used in electromagnets, which act on ferromagnetic suspended bodies (Hales, 1970). In other cases (Haynes et al., 1976), electromagnets are pure air coils (primary coils) and provide the static force on the suspended permanent magnets. Secondary control windings, which are part of the

holding magnet or control current superimposed on the constant current of the main winding, provide the dynamic forces to maintain the suspended state. On the other hand, a permanent magnet generates the main force for the vertically controlled suspension bearings Gast (1978) and the dynamic forces are generated electrically.

In the system designed by Haynes et al. (1976), a PID controller controls the current in the secondary control windings, which are placed above and below the suspended magnet. The position of the suspended magnet, which is a permanent magnet of barium ferrite, is detected by two sensor coils placed on top and bottom of the cell containing the suspended magnet.   As the suspended magnet moves up and down, the change in inductance is recorded. The primary coil current, being supplied by a precision constant current source, provides the static force that holds the suspended body at an exactly defined position for all densities.

In a small departure from the Haynes method, Masui et al. (1984) have developed a method where both static and dynamic forces are generated in the same winding. The measuring force is no longer determined from coil current but the coil winding is hung directly from the balance. In the de-energized state, no force is transmitted from the air coil to the suspended body, which is a cylindrical permanent magnet. The distance between the magnets is detected capacitatively by two ring electrodes that are fit to the control coil windings above and below the suspended magnet.

In the Gast (1978) method, the holding magnet hangs from the beam of a balance with a knife-edge support. Both the suspended and holding magnets are permanent magnets. Control of the suspended magnet is achieved through control coil in the holding magnet. Flux displacement between sensor coil attached at the lower end of the holding magnet and a copper disc placed at the upper end of the suspended magnet determines the distance between the magnets.

Even for a de-energized control coil, a static force corresponding to the force-distance curve (figure IV.1) is transmitted through the permanent magnet field. The suspended magnet is controlled at a distance x_0 such that transmitted total force F equals

force $F_M(x)$ transmitted to the total magnetic field. Then the control coil provides the dynamic forces, and the current in the control coil is then almost zero on average.

The sample body or float hangs from the suspended magnet; the suspended state is maintained constantly and force changes on the sample body are measured continuously. It is impossible to check the zero point during measurement. For this reason, thermostatic control of the complete system is necessary so that drifting in time of the weighing system remains as small as possible. Finally, the force is determined from the displacement signal from the characteristic force-distance curve (Lösch, 1987).

In order to reach a conclusion regarding the form and shape of any future suspension bearing, Lösch (1987) did a critical analysis of past works including the types of force measurement to be selected. If force is to be measured by measuring current or displacement, very stringent requirements are placed on displacement measurements and on the control of electro-magnetic force with respect to reproducibility and long-term drift. This means that hysteresis (caused by residual magnetism) should be completely avoided; this becomes a problem in an iron-core coil where hysteresis of the magnetization curve can cause the current-force and force-distance-characteristics to shift considerably. Because of these inherent problems, the other type of force measurement technique, i.e. force transmission from the holding magnet to a precision balance, should be a viable option.

The nature of generation of a static magnetic field is another issue for consideration. Purely electrical generation of the static field (i.e. no permanent magnet or iron-core as part of the holding magnet) is attractive in the sense that the coupling force can be switched off completely. When the suspension system is switched off, no force transmission exists and the balance measures only the weight of the suspended magnet assembly. That makes zero-point correction of the balance possible.

The disadvantage of a pure air coil is that higher currents and many coil windings are required to generate enough force. Large size, weight and heat generation limit the range of application of such system as well as accuracy of the force measurement.

An iron-core coil could be used to circumvent this problem. However, the transmission of non-reproducible low-forces, even in the de-energized state, would make the zero-point correction of the balance nearly impossible.

Given all these problems, the concept of static force transmission using a permanent magnet is an acceptable solution. Small magnetic suspension bearings could be used for relatively large force transmission and the holding magnet works with very small power usage. The small size of the iron core means that the hysteresis effect is not very significant.

Finally, the issue of the nature of displacement measurement technique should be resolved. A method similar to Gast (1978) in which the distance between the holding and suspended magnet is detected by a sensor coil is feasible. Figure IV.3 shows the block diagram of the suspension control of such a system using a PI controller (Kleinrahm and Wagner, 1984).
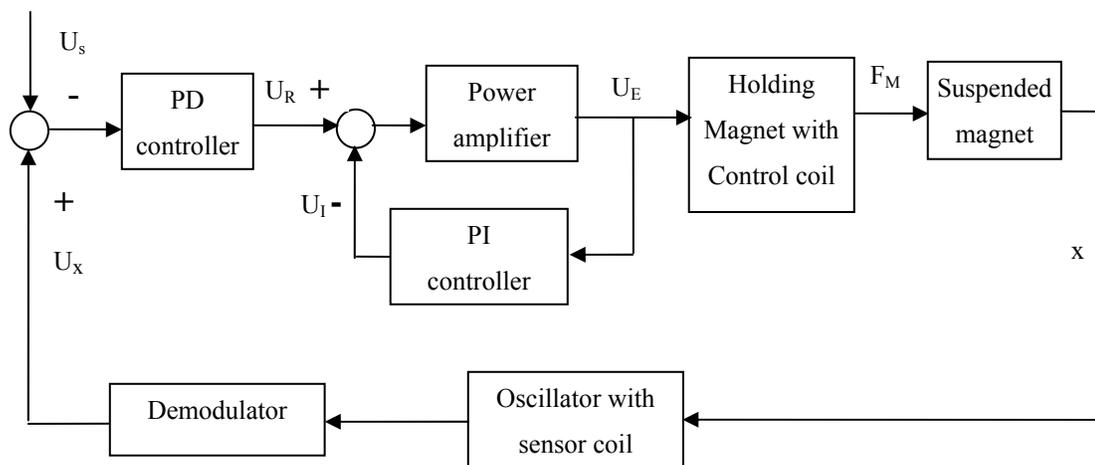
Figure IV.3. Block diagram of suspension control

The distance between the magnets is determined through the flux displacement between the sensor coil placed inside the holding magnet and an aluminum disk inside the suspended magnet. The demodulator converts the displacement into a direct voltage U_x, which is proportional to the distance. After switching on the coupling, a nominal

voltage U_s is preset which corresponds to the initial distance between the magnets. Irrespective of the density of fluid inside the cell, the suspended magnet initially rises to a height corresponding to U_s. The distance can be preset in a manner such that the transmitted force is taken up almost completely by the holding magnet.

As the suspended magnet tries to attain equilibrium, the power amplifier supplies an alternating voltage U_E to the power coil and produces the residual force $F_E(U_E, x)$ such that

$$F_M(x) = F_P(x) + F_E(U_E, x) \qquad (4.1)$$

Where, $F_M(x)$ is total force transmitted by the suspension bearing, $F_P(x)$ is the force transmitted by the permanent magnetic field and $F_E (U_E, x)$ is the force generated by electromagnet.

After switching on, a secondary signal U_I is provided slowly to the power amplifier through the PI controller in the feedback loop such that the position of the suspended magnet changes, the required force is completely transmitted by the permanent magnet, and the direct voltage component of the power coil voltage U_E becomes zero (Kleinrahm and Wagner, 1984).

The main problem of such a technique of measuring distance between the magnets is that the distance measurement falls in the region of force transmission and the criterion of signal separation is not achieved. In addition, the sensitivity and linearity of this method are low because of the large distance between the pick-up and sensor. This affects the quality of measurement because of relatively high control forces and positional fluctuations. This also limits the range of loads that can be measured with the bearing. As a result, a method should be chosen in which the distance between the magnets is no longer measured and controlled; rather the vertical position of the suspended magnet with respect to the suspension-bearing casing is measured and controlled. This technique also ensures the fact that the displacement sensor is not disturbed by the alternating field of the control coil. Finally, inductive sensors rather than capacitive sensors should be used because the actions of the capacitive sensors depend upon the fluid dielectric constant.

5. EXPERIMENTAL METHOD

5.1 Experimental Setup

In our set up for density measurement, a sample cylinder (SC) resides in an explosion proof, heated cylinder container such that the temperature inside is between 60-65 °C, which is higher than the cricondentherms of all the samples measured so far. A Haskel compressor (DC), model AG-303 can increase the pressure up to 39,000 psi. A compressor bypass valve, V2, isolates the compressor when it is not needed for low pressure measurements. For fine adjustment of pressure, a hand - pump (HP1), rated for 30,000 psi from 'High Pressure Company' (HiP) could be used.

The hand pump, the compressor and all the fittings and tubing between T1 and T9 are inside the manifold 1 (figure V.1), which is heated with six or seven 250 W light bulbs. The hand pump has a Teflon 'O'-ring and its temperature should not exceed 65 °C to prevent leakage. All other tubings and fittings not inside the manifold 1 (or 2) are heat-traced to prevent condensation of the natural gas sample. In the figure V.1, 'C' stands for elbows, 'T' for tee-sections and 'S' for crosses. Some ports of the tee-sections and crosses are plugged. Because of the modifications from the initial design, some valves and fittings have become redundant. The valves and fittings, from HiP, are rated for 60,000 psi and the tubing, from the same company is rated for 30,000 psi.

V13, which is closed during density measurement, is open only during calibration of pressure transducers (Paroscientific: 6,000 and 30,000 psi) with a Ruska dead weight gauge (DWG, model # 2450, serial # 19851) and differential pressure indicator (DPI). The DWG is an absolute pressure instrument with which the gas pressure inside the pressure transducer is exactly balanced with calibrated weights placed on a floating piston in a cylinder. The DPI has a diaphragm, which acts as an interface between measured gas on one side (connected through V13) and oil going into DWG on the other side
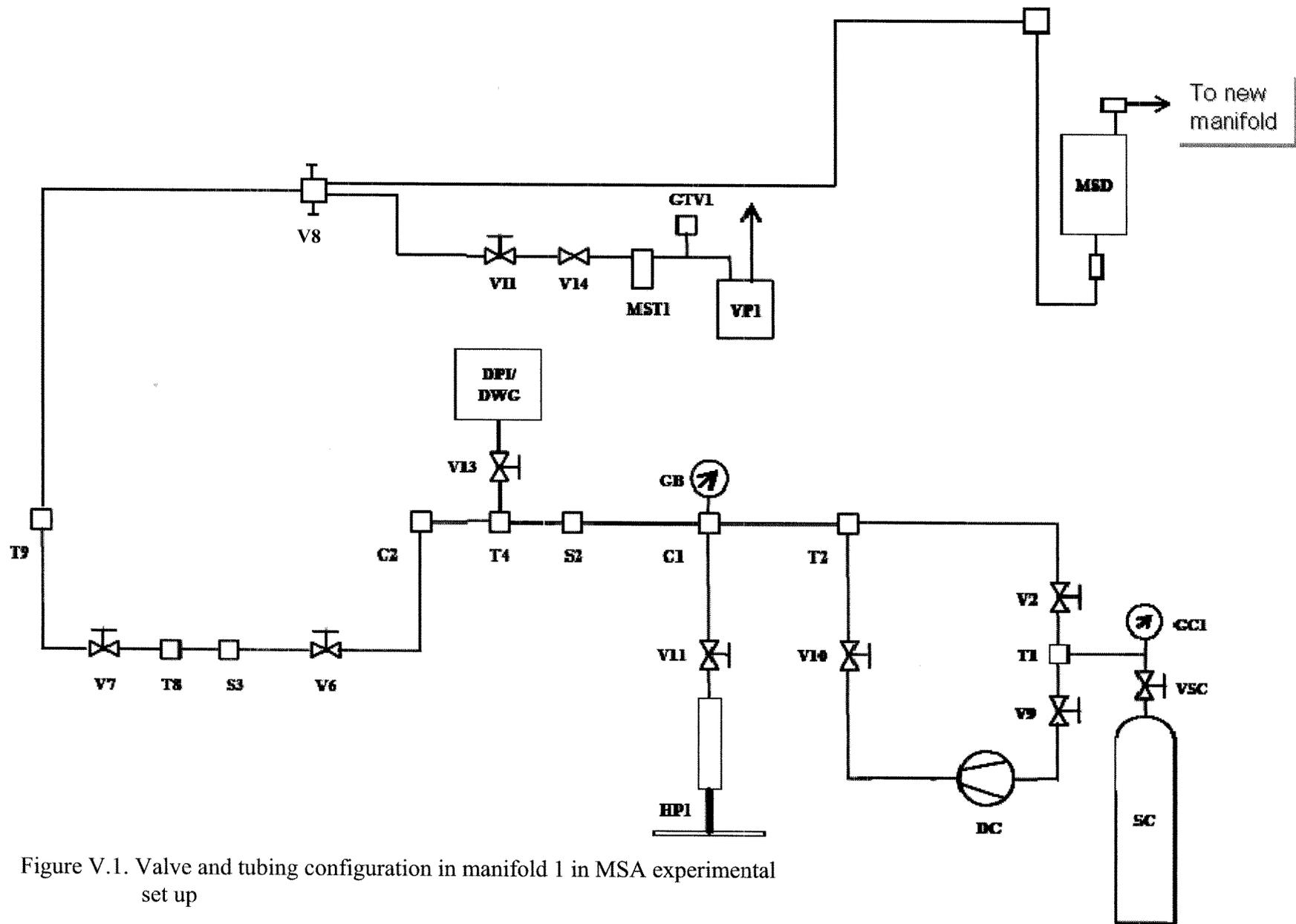
Figure V.1. Valve and tubing configuration in manifold 1 in MSA experimental set up

Performance of the DWG depends upon factors such as elastic distortions of the piston and cylinder, temperature of the piston and cylinder, effects of gravity and buoyancy, hydraulic and gaseous pressure gradients from the DPI reference plane to pressure transducer, liquid surface tension, etc. The null position of the DPI diaphragm should be calibrated once every few years. Once all the corrections have been made, the DWG can make measurements to within 0.001 kg/cm^2 (Ruska, 1977).

Some of the valves have magnetic stems, and we have made certain that none exists within 1 meter of the magnetic suspension assembly (MSA). V8 is a three-way valve, which is closed during measurement to minimize pressure fluctuations inside the MSA cell. A Varian vacuum pump (VP1) evacuates the system. A molecular sieve trap (MST1) between the MSA and VP1 prevents oil or mist flowing from VP1 into the system. The molecular sieve can be re-activated using a heater inside the trap. The frequency of activation depends upon the usage. About one molecular sieve activation every month should be more than sufficient.

Pressure transducers reside inside manifold 2. For measurements below 6,000 psi, we use the 6,000-psi transducer. At pressures above 6,000 psi, we keep this transducer completely isolated by closing VS6K and VG6K. Although these transducers can generally withstand pressure 20% beyond the recommended maximum limit, to minimize hysteresis and to prevent the need for frequent calibration, we never expose it to more than 5500 psi. Manifold 2 is shown in figure V.2.

Both these transducers are thermally compensated. Despite that, we keep them at controlled, constant temperature during measurement and calibration. Experience has shown that this significantly increases the accuracy of measurement. Their temperatures are maintained by Omega controllers and solid-state relays and heaters. The transducers and heaters reside inside heavy, cylindrical, well-insulated aluminum blocks for temperature stability. The maximum allowable temperature for the 6,000 psi transducer is 120 °C, while that of the 30,000 psi instrument is only 50 °C. The transducers should be free from vibration; otherwise they require frequent pressure calibration.
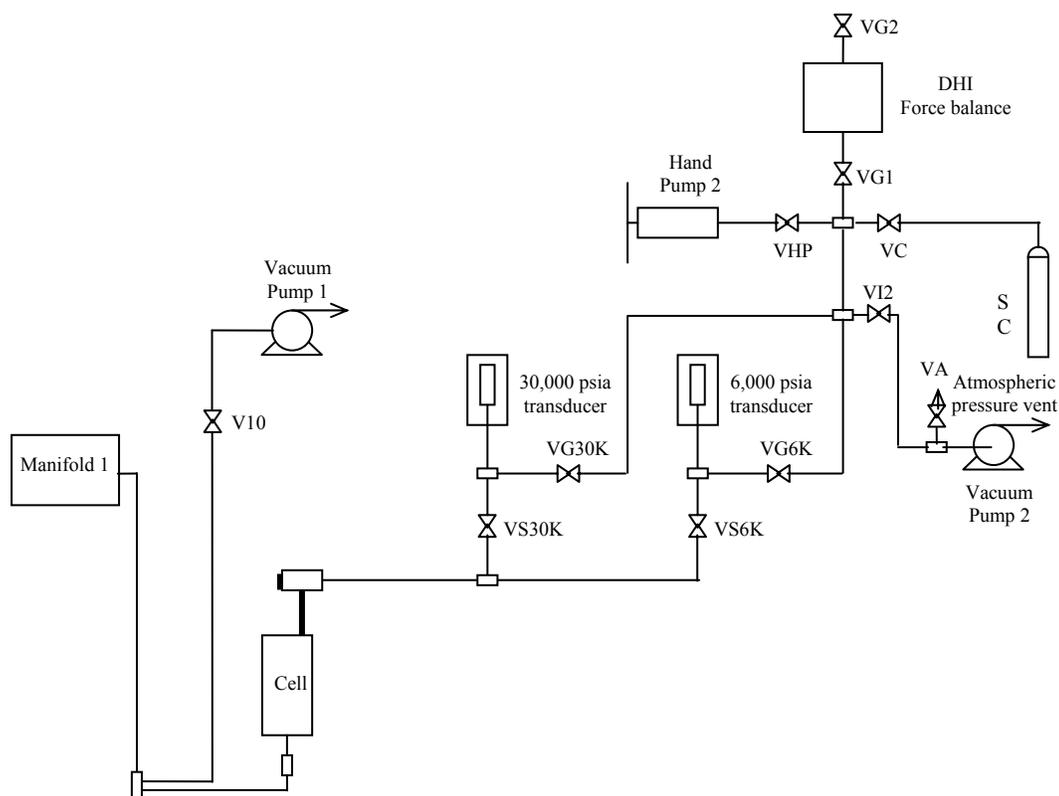
Figure V.2. Valve and tubing configuration in manifold 2 in MSA experimental set up

Manifold 2 also contains a vacuum pump, a hand pump, molecular sieve, and a DHI force balance. A vent to atmosphere allows checks for offsets of the transducers at atmospheric pressure. The DHI force balance can be calibrated against standard weights, and it can be used to calibrate the transducers instead of the DWG. Details of the operations of the valves and the procedures for density measurements appear elsewhere (Patil, 2005).

The vacuum pump in manifold 2 is, for the time being, is connected to the isothermal shields around the MSA cell to provide temperature stability as well as to prevent moisture condensation on PRT. A dry nitrogen blanket is provided to a METTLER analytical balance (to be described below) to prevent condensation around electromagnet and to expel atmospheric air, from the electromagnet vicinity, which is paramagnetic in nature.

5.2 Balance

A METTLER AT 261 electronic balance is used in combination with the magnetic suspension assembly (MSA) for density measurements. The balance has two measuring ranges. The first one (0-62 g) allows a mass measurement accuracy of 0.01 mg, whereas the second one (0-200 g) reduces the accuracy to only 0.1 mg. For our density measurements, we use the first range.

The balance works on the principal of magnetic force compensation. Electric coils, that form an electro-magnet, are attached to a coil support, which in turn is connected to the weighing pan. As weights are placed on the pan, the support rises. A linear variable differential transformer within the balance senses the deviation from the null position when no load is on the pan. This signal is fed to a controller that manipulates the current in the electromagnet such that an active force generated, F, completely balances the weight on the pan, W, and the position sensor returns to the null position

The coils are in a magnetic field generated by a permanent magnet, and the force generated is $F = I/B$, where I is the current flowing through the coils, B is the magnetic field strength, and force F acts in the direction perpendicular to both the magnetic field and the direction of the current. Because the current flowing is proportional to the compensation force generated and that force is equal in magnitude to the weight of the load, a current is generated which is proportional to the load.

Apart from the position sensor and the control system, features like the parallel-motion motion guide system make the balance very stable. It absorbs the shock of a lateral disturbing force and ensures that only the load is transmitted to the balance-weighing cell. Figure V.3 shows the cross section of the balance.

A few factors contribute to the extreme accuracy of the balance. The first is the internal calibration process in which two high precision 100 g weights are weighed one at a time and then together. This dramatically reduces the nonlinearity of the balance. This also takes into account the variation of the acceleration of gravity from location to location.

Second is temperature compensation, which is required because temperature influences the strength of the permanent magnet for magnetic force compensation. A magnetic field becomes weaker at higher temperatures causing higher currents leading to higher, and hence, wrong balance display values.

1 Weighing Pan
2 Hanger
3 Guide of the parallel-motion mechanism
4 Flexible bearing
5 Link
6 Lever to transmit weight force
7 Suspension of lever
8 Compensation coil
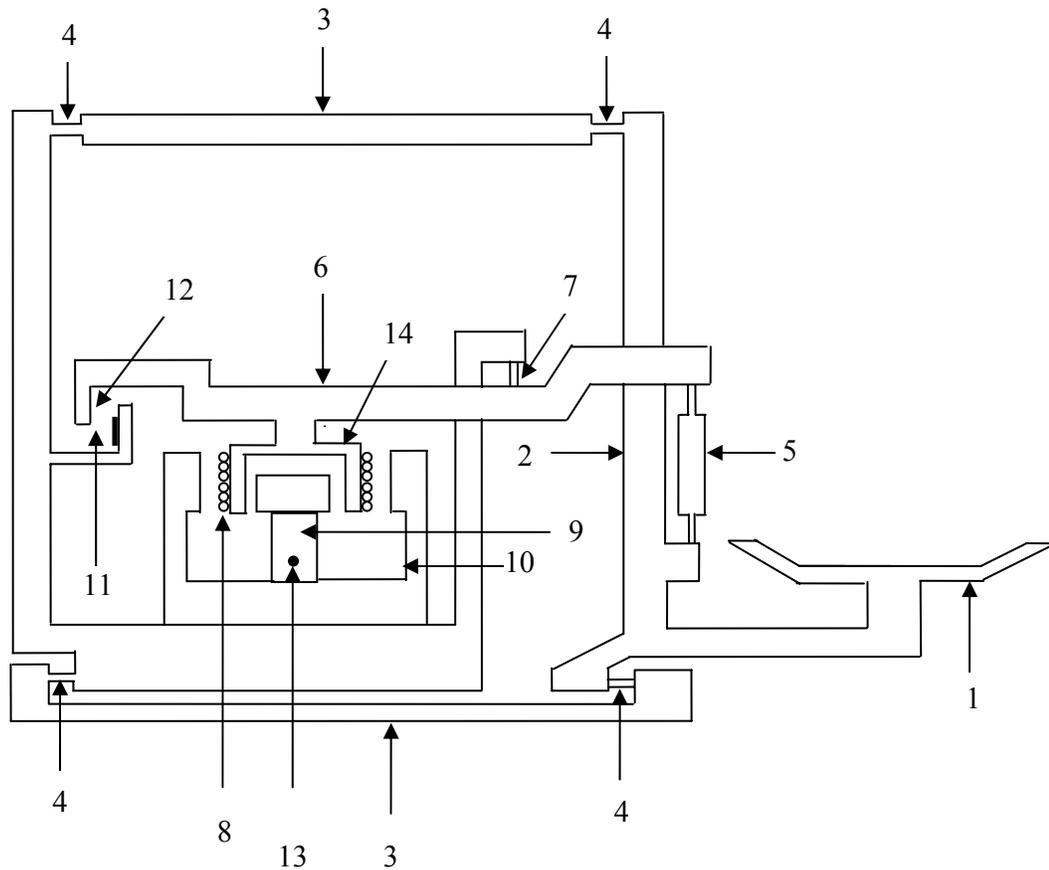
9 Permanent magnet of
   electrodynamic converter
10 Magnetic circuit
11 Position sensor
12 Position indicator
13 Sensor for temperature
   Compensation
14 Coil support

Figure V.3. Schematic cross section of the weighing cell of METTLER AT balance
          (Rutishauser and Reichmuth, 1988)

To compensate the deviation caused by the temperature, a temperature sensor has been built into the balance weighing cell to measure the temperature of the permanent magnet. The balance microprocessor calculates the magnitude of the compensation from the measured temperature value and appends it to every measured value before it is displayed. Finally, analog to digital conversion is made as precise as possible using a 20 bits analog-to-digital (A/D) converter (Rutishauser and Reichmuth, 1988).

5.3 Single-Sinker Magnetic Suspension Assembly

The operation of the two-sinker densimeter, as explained in section 2, is rather complex because of its sinker-changing device that provides the special advantage of high accuracy even at low densities. This advantage is redundant during medium or high-density measurements encountered in many practical applications. In order to extend the instrument measuring range towards higher temperatures and pressures, Wagner et al. (1995) have developed a new type of "single-sinker densimeter". Although the single sinker basic design is much simpler than that of the two-sinker densimeter, it is also possible to perform high accuracy density measurements at relatively low gas densities by applying some of the advantageous features of the two-sinker principal (Goodwin et al., 2003). The single-sinker densimeter also operates based upon Archimedes' principle and the force transmission is provided by the levitation of the sinker in the measuring housing of the high-pressure cell. The density is calculated by measuring m_v, the 'true mass' of the sinker in vacuum, m_a, the 'apparent mass' of the sinker in the presence of fluid and V_s, the volume of the sinker:

$$\rho = \frac{m_v - m_a}{V_s} \tag{5.1}$$

The accuracy of density measurement from a single-sinker densimeter is lower than that from a two-sinker densimeter especially for low densities because it lacks compensation for adsorption. Klimeck et al. (1998) also conclude that the accuracy of density measurements from a single-sinker densimeter is better than that from a Burnett

apparatus because adsorption for an MSA is a point error while that for a Burnett apparatus is a cumulative error.

In our research group at Texas A&M University, we use a compact single-sinker MSA manufactured by Rubotherm Präzisionsmesstechnik GmbH, Germany. The apparatus has an accuracy specification from the manufacturer of ± (0.03% or 0.005 kg/m^3) for densities in the range 0 to 2,000 kg/m^3 over a temperature range of 193.15 to 523.15 K and a pressure range up to 200 MPa with a maximum pressure of 130 MPa at 523.15 K.

The sinker for this work is a titanium cylinder with a volume of 6.74104 ± 0.00013 cm^3 with the uncertainty of ± 0.002 % at the 95% confidence level (2σ) measured at 293.15 K and 1 bar. The sinker mass is 30.39159 g in vacuum. The sinker volume was determined (McLinden, 2005) using a hydrostatic comparison to density standards of single crystal silicon as described by Bowman et al. (1973; 1974).

5.3.1 Operation of Single-Sinker Densimeter

As discussed for the two-sinker apparatus, a considerable difference in volume is required for sinkers of same value of mass to attain high accuracy at low density, which means that one of the sinkers must have a comparatively smaller density. This limits the pressure range of two-sinker densimeters. Although newer versions of two-sinker densimeters are commercially available from Rubotherm Präzisionsmesstechnik for pressures up to 100 MPa and temperatures up to 673 K (Wagner et al., 2003), this may not be enough for many high-pressure applications. The sinker changing device adds to the complication of design, thus making it less attractive in some cases. Therefore, the single-singer densimeter developed by Wagner et al. (1995) particularly for medium and large densities simplifies the sinker design and enlarges the operational pressure and temperature ranges. The single-sinker densimeter also employs differential application of Archimedes' principal and uses a magnetic suspension balance and compensating weights on the balance.

The sinker used for measurements in this work is a titanium cylinder. Its high density ensures a large working range for the MSA. The sinker resides in a cell made of Copper-Beryllium (Cu-Be) which the manufacturer pressure-tested with water to 300 MPa. The sinker can be magnetically coupled to a commercial analytical balance (METTLER AT 261) via a sinker coupling and decoupling device.

The analytical balance stands on a reference plate on which it is fixed and adjusted. A small suspension piece with a threaded joint at the end hangs from the balance pan support through a weighing hook. A shaft connected to the permanent magnet is inserted into this threaded joint and fixed with an M3 screw. Two electronic-grade plugs and sockets, which make the plug-in connection, transfer the electric leads of the control coil from the hanging parts of the electromagnet to the weighing system of the analytical balance. The signal lines, fixed on the weighing system with a parallel guide, are transferred with a $CuBe_2$ spring wire to the balance casing and then to the outside. The plug-in connection is also the disconnection point between the suspension bearing and the balance. For removing the balance, the lower part of the plug-in connection is pulled out, the lower knurled nut of the height adjustment is opened a few turns, the screw loosened, and finally the hanging suspension piece is removed from the weighing hook of the balance. The balance then can be lifted off the reference plate and can function independent of the magnetic suspension assembly.

The magnetic coupling is at the heart of the single-sinker operation. This coupler allows contact-less transmission of force from the pressurized measuring cell to the balance at ambient conditions. The coupling consists of an electromagnet with a soft iron core, a permanent magnet made of Samarium Cobalt ($SmCo_5$), a ferromagnetic sensor core and a control system. The electromagnet is attached to the balance through the hook underneath the balance and the permanent magnet is connected to the sinker in the measuring cell by a sinker coupling-decoupling device. The position sensor core connects to the permanent magnet shaft through a thread. A thin wall separates the two magnets. A PID controller generates gentle vertical movements of the permanent magnet, thus coupling and decoupling the sinker with the permanent magnet through the

sinker coupling-decoupling device. Figure V.4 is a schematic of the MSA and the METTLER balance.
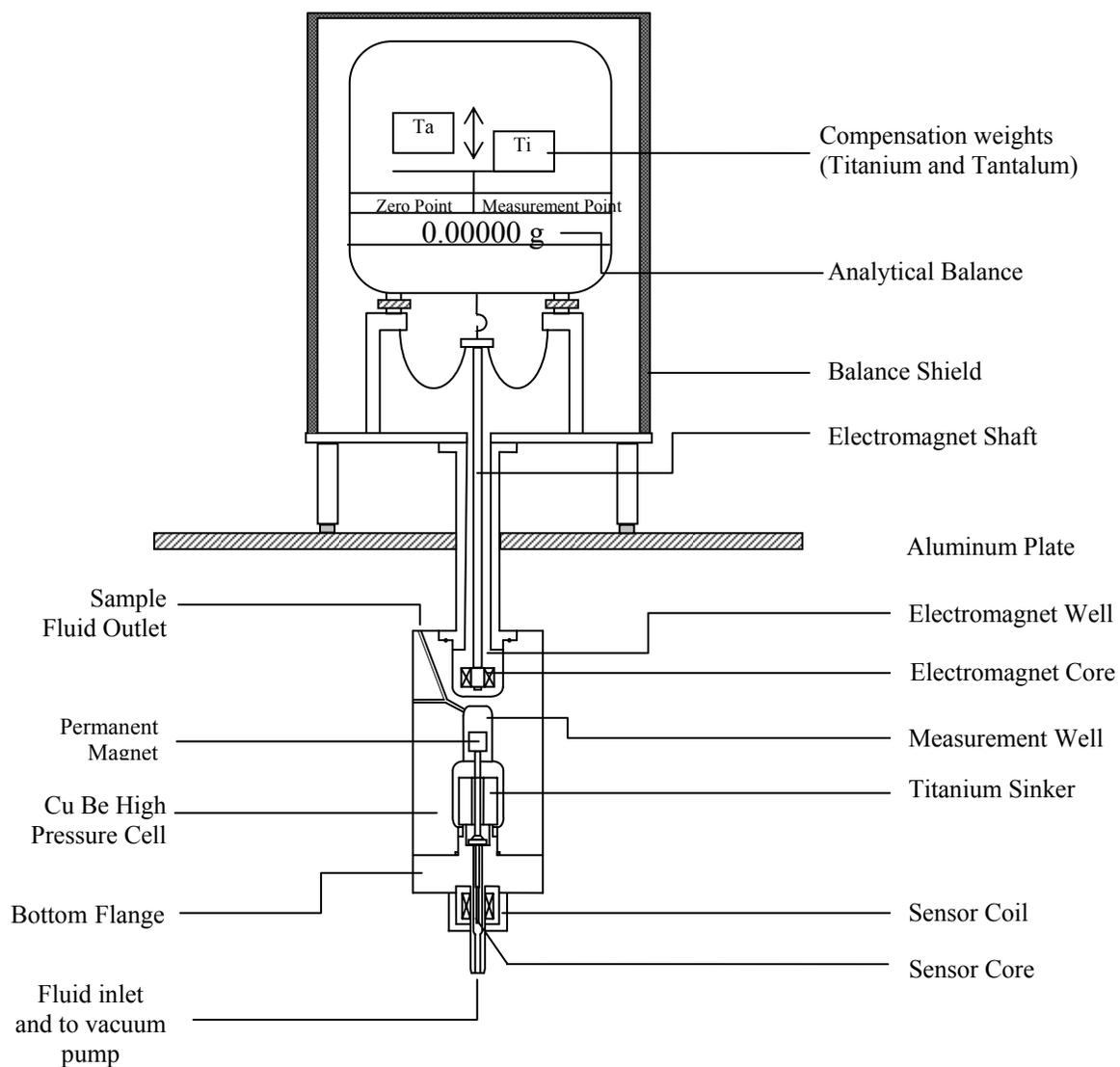
Figure V.4. Schematic of magnetic suspension assembly and METTLER AT balance (Patil, 2005)

The position sensor coil and sensor core are part of the linear variable differential transformer (LVDT). A high frequency alternating voltage is applied to the coil which is inductive in nature; a magnetic field is produced which generates eddy

currents in the sensor. This produces a counter field which partly cancels the original magnetic field (flux displacement); thereby reducing the inductance of the coil. This alters the natural frequency of a resonant circuit which has a unique relationship to the distance i.e. the position of the permanent magnet. The frequency is converted to a direct voltage in a demodulator and then compared to a set point.

In the tare or zero position (ZP), the permanent magnet is raised by only few mm such that it does not couple with the sinker; the balance carrying the weight of the electromagnet and its shaft, the permanent magnet and its shaft and the sensor core, is tared to zero. In the measurement position (MP), the electromagnet is raised such that the sinker is coupled and its net weight can be measured. The distance between the permanent magnet and the top of the inner part of the pressure-cell is about 1 to 3 mm (depending upon gas density) in the measuring position and about 6 mm in the taring position (Wagner and Kleinrahm, 2004; Kuramoto et al., 2004).

To improve the accuracy of the measurement, the balance is operated near its zero point by a load compensation system using cylindrical Tantalum and Titanium weights of equal volume and equal surface area but of different masses, each exposed to ambient conditions (Klimeck et al., 1998). In the zero position, after taring of the balance, the Tantalum weight (mass, $m_{Ta} \approx 41.61804$ g at ambient; volume, $V_{Ta} \approx 2.49$ cm^3; density, $\rho_{Ta} \approx 16700$ kg/m^3) is placed on the balance. Then, the balance is tared, the MSA goes to the measuring position, and using a weight-changing device, the Ta weight is switched with the Ti weight having the same surface area ($m_{Ti} \approx 11.23311$ g at ambient, $V_{Ti} \approx 2.49$ cm^3, $\rho_{Ti} \approx 4500$ kg/m^3). In this measuring position, the sinker also couples with the balance so the total weight is about 41.61 g, when the cell interior is under vacuum.

Because the balance readings are almost identical in both cases, the resultant balance reading at the measurement position is almost zero. Reading of the balance at or near zero reduces the error caused by balance non-linearity, which is the difference between balance actual (true) reading and the balance displayed reading. The whole operation is shown in figure V.5.
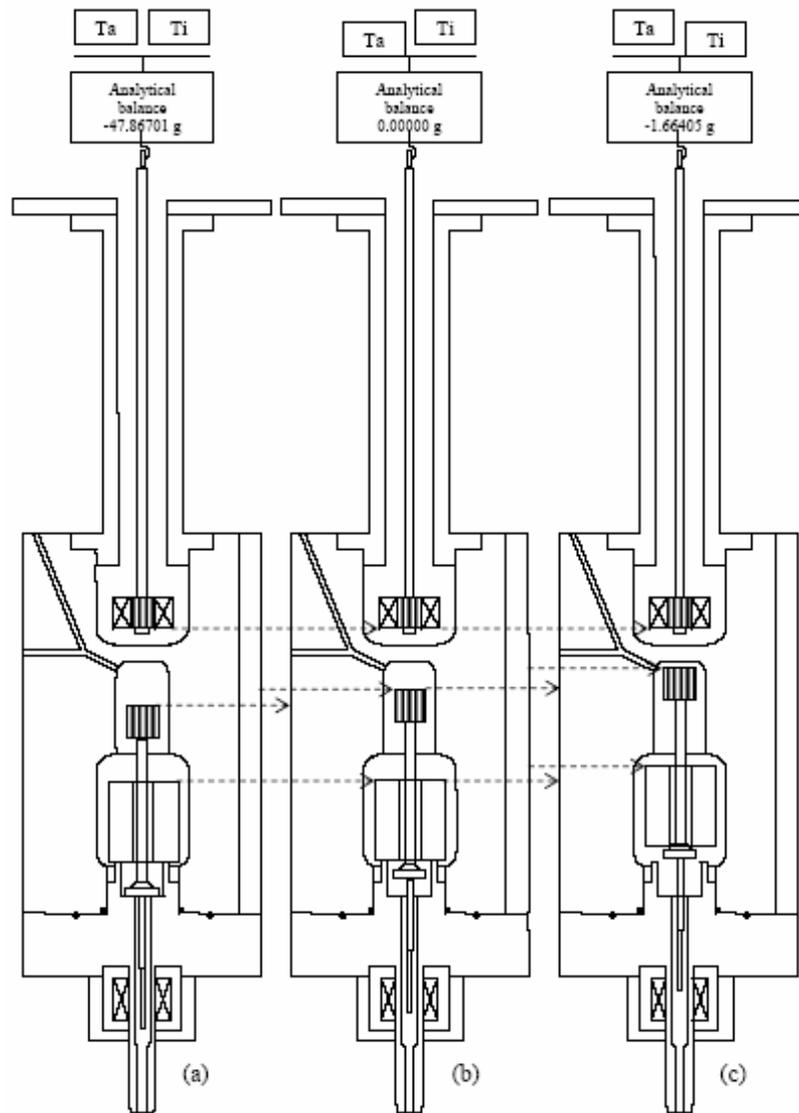
Figure V.5. Operation of the MSA using weight changing device (Patil, 2005)
[(a) suspension control (SC) 'off', Ti and Ta both raised (b) SC 'on'; ZP position, Ta lowered, Ti raised (c) SC 'on'; MP position, Ta raised, Ti lowered]

The process is repeated with the cell under pressure. Based upon the measurement using two external weights, we can re-write equation (5.1):

$$\rho = \frac{(m_v + m_{Ti} - m_{Ta}) - (m_a + m_{Ti} - m_{Ta})}{V_s(T,P)} \qquad (5.2)$$

Where subscripts *v* and *a* stands for conditions under vacuum and at pressure, respectively.

When we increase the gas density, the balance reading moves farther from zero, but even at high density this reading is small compared to the total range of the balance, 62 g. Therefore, application of the two external weights (Ta, Ti) ensures that errors of the balance caused by changes in the slope of the characteristic line or non-linearity are reduced dramatically (Wagner and Kleinrahm, 2004). Error propagation caused by additional mathematical steps also is not significant. Without the external weights, these errors do not cancel between ZP and MP.

As is evident from equation 5.2, because the Ta and Ti weights have the same volume, they have the same buoyancy and the difference between mass of the Ta and Ti weights at ambient equals their difference at vacuum, they cancel. Therefore, the measurement is independent of change of ambient condition in the time interval between vacuum and pressure readings. In addition, the equal surface area of the Ta and Ti weights ensures that adsorption effects cancel. The differential application of Archimedes' principal ensures that most of the side effects, which reduce the accuracy, are eliminated. For the same reason, adsorption on the inner wall, which can be significant, also is eliminated from density calculations (Klimeck et al., 1998).

While using the single-sinker densimeter, we should be conscious of the following three effects, which do not cancel. The first two have been discussed in details in section 2. One is the interaction between the force transmitted and the Cu-Be cell, which is slightly diamagnetic. This means that the sinker mass will not be the same if measured directly at the balance and measured through the coupling under the same condition. This effect of magnetism for the housing introduces a systematic error or force-transmission error (FTE) on the order of 10^{-6} in the density determination (Kuramoto et al., 2004), which persists because of the difference in the vertical height of the permanent magnet at ZP and at MP. Wagner et al. (2004) have suggested a

multiplying factor of ($1 \pm 20 \times 10^{-6}$) to the numerator in equation 5.1

The second effect is the FTE caused by magnetic interaction with the fluids, which might be paramagnetic or diamagnetic. This effect also persists for reasons mentioned in the previous paragraph. Klimeck et al. (1998) have formulated an empirical equation to correct this error that is valid for some diamagnetic pure fluids (methane, ethane, carbon dioxide and nitrogen) for which the relative error in the density measurement is on the order of 40×10^{-6} to 100×10^{-6} (Wagner and Kleinrahm, 2004). Finally, one last effect that remains during gas density measurement is gas adsorption on the sinker surface, which has a decreasing or negative effect on the pressure and a positive effect on buoyancy. However, this is significant only at low densities and in the critical region (Wagner et al., 1995).

The volume of the cell is kept small to generate high pressure. This also allows a lighter cell with a smaller temperature gradient. The smaller gradient is significant while measuring densities near the critical point. Smaller cell volume also ensures relatively smaller thickness of the separator between the permanent and electro magnet, which is about 5 mm (Reza Seif, 2005). Less thickness leads to a smaller force transmission error.

The uncertainty in the volume determination of the titanium sinker at specified temperature and pressure contributes to uncertainty in the density measurement. McLinden (2005) uses single-crystal silicon as a reference material for sinker volume determination by a hydrostatic weighing method. The density determination of the reference material is traceable directly to densities determined by dimensional measurements of near perfect spheres using optical interferometry and mass measurements commencing with the U.S. national mass standards. A optical interferometer can reduce relative uncertainty in volume in a steel sphere to as low as 10^{-11}. The sphere is used instead of a cylinder or a cube because it is less susceptible of damage and spheres of excellent sphericities are available.

For most MSA's, the hydrostatic method using water is used to calibrate sinker volume (Kuramoto et al., 2004). However, McLinden uses fluroether instead of water. Its high density increases the buoyancy force on the submerged objects and thus the

sensitivity of the volume determination. Its surface tension is about 2/9 of water and this reduces the forces on the suspension wire. That and much higher gas solubility relative to water reduce the problems of air bubbles clinging to the solid objects. Low surface tension also means that the liquid surface is less likely to be contaminated. As a result, the buoyancy forces acting on the silicon crystal and titanium sinker are measured with less scattering than with water; thus ensuring a precise volume and density measurement of the solid sample (Fujii, 2004).

5.4 Force Transmission Error Analysis

McLinden et al. (2006) have investigated single-sinker and two-sinker FTE in detail as discussed in section 3. However, his analysis of single-sinker FTE requires two different sinkers with different densities. To overcome this complication, using the same philosophy of McLinden et al. (2006), Hall (2006) has devised an algorithm that requires only one sinker. We use this method for making force transmission correction to our data.

For this purpose, we use equations 3.9 and 3.10 for the measurement point and zero point, respectively, then subtracting:

$$\rho_{fluid} = \frac{\varphi m_s + (m_{c1} - m_{c2}) - (W_1 - W_2)/\ \alpha + \rho_{air}(V_{c2} - V_{c1})}{\varphi V_s} \qquad (5.3)$$

However, $V_{c1} \approx V_{c2}$ and ρ_{air} is small so we can cancel the final term in the numerator:

$$\rho_{fluid} = \rho_s + \frac{(m_{c1} - m_{c2}) - (W_1 - W_2)/\ \alpha}{\varphi V_s} \qquad (5.4)$$

Measurement with vacuum in the cell ($\rho_{fluid} = 0$) gives:

$$\varphi_0 = \frac{-(m_{c1} - m_{c2}) + (W_1 - W_2)_0/\alpha}{m_s} \qquad (3.11)$$

In addition,

$$\varphi = \varphi_0 + \varepsilon_\rho \left(\rho_c \chi \right) \left(\rho_s / \ \rho_c \right) \left(\rho_{fluid} / \ \rho_s \right) \tag{5.5}$$

$$\rho_{fluid} = \rho_s + \frac{\left(m_{c1} - m_{c2} \right) - \left(W_1 - W_2 \right) / \ \alpha}{\left[\varphi_0 + \varepsilon_\rho \left(\rho_c \chi \right) \left(\rho_s / \ \rho_c \right) \left(\rho_{fluid} / \ \rho_s \right) \right] V_s} \tag{5.6}$$

$$\frac{\rho_{fluid}}{\rho_s} = 1 + \frac{\left(m_{c1} - m_{c2} \right) - \left(W_1 - W_2 \right) / \alpha}{m_s \left(\varphi_0 + \varepsilon \chi \rho_{fluid} \right)} \tag{5.7}$$

$$\varphi_0 + \varepsilon \chi \rho_{fluid} = \frac{\left(m_{c1} - m_{c2} \right) - \left(W_1 - W_2 \right) / \alpha}{m_s \left(\rho_{fluid} / \rho_s - 1 \right)} \tag{5.8}$$

$$\varepsilon_\rho = \left(\left(m_{c1} - m_{c2} \right) - \left(W_1 - W_2 \right) / \alpha - \varphi_0 \left(\rho_{fluid} / \rho_s - 1 \right) m_s \right) \frac{\rho_s}{\left(\rho_{fluid} - \rho_s \right) m_s \chi \rho_{fluid}} \tag{5.9}$$

Where, m stands for mass, W for displayed balance reading and V for volume. Among the subscripts, $c1$ and $c2$ stands for external compensation weights (titanium and tantalum, respectively), 1 and 2 are for measurement and zero point respectively when the cell is under pressure, 0 denotes the cell is under vacuum, s stands for sinker and c is critical condition. ε_ρ is an apparatus specific constant independent of the fluid, temperature and pressure.

To evaluate ε_ρ, we do several density measurements on pure methane and observe W_1 and W_2 at various temperatures and pressures including vacuum. At same conditions of temperature and pressure, we calculate density using methane EOS (Setzmann and Wagner; 1991); this should be equal to the corrected density ρ_{fluid}. For each value of temperature and pressure, we obtain one value of ε_ρ using (3.11) and (5.9). All the values of ε_ρ should be more or less same. Once we have ε_ρ, we can calculate ρ_{fluid} using (5.8). Calculation of V_s as a function of temperature and pressure appears in the appendix E.

For our apparatus: $\alpha \approx 1.00015$, $m_{c1} = 41.61804$ g, $m_{c2} = 11.23311$ g. These later two values are at ambient conditions; $m_s = 30.39159$ g at vacuum should be used in the equations. For natural gas mixtures, $\rho_c \chi \approx -2.5 \times 10^{-6}$. Finally ρ_s should be calculated at each temperature and pressure using $\rho_s = \dfrac{m_s (vacuum)}{V_s (T,P)}$. Using high purity nitrogen at 298 K and 350 K, the value of φ_0 was found to be 1.000203935 and average value of $\mathcal{E}_\rho$ was found to be 25 which is equivalent to 25 ppm with respect to Dr. McLinden's derivation (McLinden et al., 2006). This procedure will be carried out for more gases at different temperatures and pressures in future in order to find an optimum universal value.

5.5 Control System

Stable levitation of a permanent magnet by an electromagnet is at the heart of the magnetic suspension system. Because Earnshaw's theorem states that no stationary objects made of charges, magnets and masses in a fixed configuration can be held in stable equilibrium by any combination of static electric, gravitational or magnetic forces (i.e. any forces derivable from a potential satisfying Laplace's equation), stable levitation is not possible (Berry et al., 1997). A PID and a set point controller provide the stable levitation in the vertical direction.

5.5.1 Controller in Vertical Direction

During the controller test phase, a manual controller was used is to optimize the parameters of the PID direct controller (Figure V.6). After using the manual controller, an automatic start-up and shutdown controller (not shown) is used to optimize the values further and ensure swift and smooth start-up and shutdown movements. The suspension assembly can be controlled very well without parameter changes over wide working ranges. During regular operation, when the suspension is turned ON and the second

switch in in the zero position (ZP), the input voltage is 0.6 V (i.e. - $\Delta U_{E,\,set}$). When the second switch is turned to the measuring point position, the nominal voltage initially applied is $\Delta U_{E,\,set}+ U_{E,\,set}(t) \approx 6$ V. Voltage $U_{E,\,set}(t)$, which is used to provide the initial "in-rush" current to lift the suspended magnet (permanent magnet) to the measuring position, falls exponentially to 0 V, so nominal value in the measuring point position is $\Delta U_{E,\,set} = 0.6$ V. Voltage U_s is controlled by a super-imposed set point PI controller such that U_E is zero on average. The direct controller, a PID controller, maintains U_E at zero on average such that U_X is close to U_s. The control circuit also has a limit switch and a protective cutoff (not shown) that has the function of switching off the control unit upon the failure of the controller electronics when U_E is above some adjustable maximum value for an extended period.

U_X is required to anticipate the direction of change of U_E. It is possible to measure density by using U_X only, without using the balance. But then the accuracy of the measurement becomes dependent on the resolution of the MSA controller and very high accuracy can not be obtained.

Samarium cobalt ($SmCo_5$), a rare earth transition metal composite (Wagner and Mirahamdi, 1980) is the permanent magnet material. It has a very high-energy product, an almost linear demagnetization curve and is commercially available. Its only drawback is the relatively low maximum usable temperature of 250 °C. Because the transmission force increases with total stored energy in a magnet, a product of energy density and volume (Kupfermüller, 1968), the transmitted force is optimized by keeping the length of the magnet large. Pressure limitations dictate that the magnet diameter should be as small as possible.

A rigid connection exists between the permanent magnet and the suspension shaft. This has a large effect upon the working range and the control parameters of the magnetic suspension bearing. Such a connection, instead of a fiber connection, ensures a trouble-free control of loads, which can be twenty times the weight of the suspended magnet. The rigid connection also guarantees damping of vertical load movements,

which have a positive effect on the controllability of the suspension bearing (Lösch, 1987).

The holding magnet is connected to the balance through a horizontally acting damper acting on a linkage to the balance. This dampens the oscillating motion of the suspended magnet by working outside the cell.
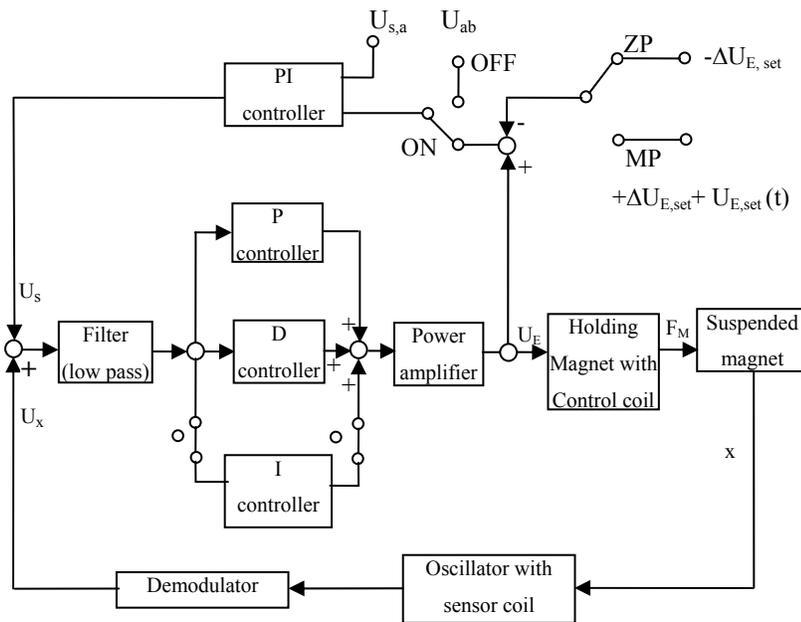
Figure V.6. Block diagram of the single-sinker MSA control system

In the new control principle, the displacement sensor is fitted below the suspended magnet (permanent magnet). It ensures greater flexibility in the suspension bearing casing design and greater stability of the suspension control because of the smaller distance of the displacement sensor from the measuring area (Lösch, 1987).

5.5.2 Control Principal along Horizontal Direction

Earnshaw's theorem does not apply to dimagnets, and stable levitation of a

magnet that is intrinsically unstable, can be achieved by repulsive forces from a feeble diamagnetic material, which is perceived as non-magnetic (Geim et al., 1999). For stable levitation the magnetic force MB'(z) compensates the gravitational force mg (minus buoyancy), where M is the magnetic moment and B (z) and B'(z) are the magnetic field on the axis and its derivative respectively. The total energy of the magnet (permanent magnet in our case) U should have a minimum in the stable region so that $\Delta U > 0$. Close to the equilibrium position (Geim et al., 1999; Berry et al., 1997 and Simon et al., 1997):

$$U \approx U_0 + \left[mg - MB'(z)\right]z + K_v z^2 + K_h r^2 + Cr^2 + \ldots\ldots \tag{5.10}$$

$$K_v (z) = -\frac{MB''(z)}{2} \tag{5.11}$$

$$K_h = - M\frac{\left[B'(z)^2 - 2B(z)B''(z)\right]}{8B(z)} \tag{5.12}$$

K_v and K_h are vertical and horizontal stability functions.

The last term in equation (5.11) signifies diamagnetic repulsion. This causes stable levitation of a permanent magnet in a dimagnetic cylinder. Figure V.7 shows the levitation of a permanent magnet at the axis of a vertical solenoid of radius R and length $\approx$ 2R in a magnetic field created by the solenoid. The levitation is stabilized by the dimagnetic cylinder (Cu-Be in our MSA). We have:
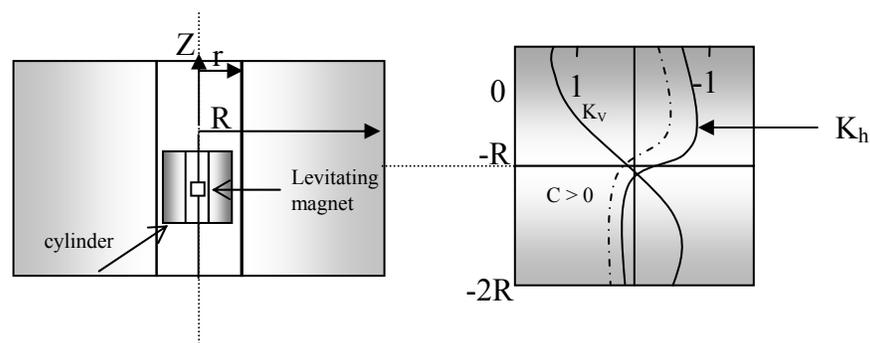
Figure V.7. Levitation of a permanent magnet (Geim et al., 1999)

$$C = \frac{45\,\mu_0\,|\chi|\,M^2}{16D^5} \tag{5.13}$$

Where μ_0 is the permeability of free space, D is the inner diameter of the cylinder and χ is the magnetic susceptibility. Now, for horizontal stability $\left(\frac{\delta^2 U}{\delta r^2}\right)_z > 0$ and for vertical stability $\left(\frac{\delta^2 U}{\delta z^2}\right)_r > 0$, which means $K_h + C > 0$ and $K_v > 0$ for horizontal and vertical stability, respectively when no diamagnetic material is present or D is large and C is zero and both $K_h > 0$ *and* $K_v > 0$. However, looking at stability functions in figure V.7 (solid lines) we see that no region exists in which these two conditions are satisfied. However, by introducing diamagnetic material, the horizontal stability function K_h moves to the left (dashed curve) and a small region of stability arises (Geim et al., 1999). Based upon this principle, the suspension assembly attains horizontal stability of the permanent magnet using diamagnetic material (Cu - Be in our case) as cell material and using a smaller inner diameter of the cell.

5.6 Over View of Data Communication

The computer uses serial ports (RS-232), a General Purpose Interface Bus (GPIB, IEEE-488) and LPT ports for data communication. Serial ports request and receive data from pressure transducers (PT-30K and 2K) and tare, request and receive data from balance. The LPT port simultaneously sends commands to the weight changing device (WCD) and the balance control box for off / ZP/MP transitions. The GPIB requests and receives data from a digital multimeter (DMM). A data acquisition card or DAQ (National Instrument, model: PCI-6527) controls temperature through a National Instrument (NI) connector block. The GPIB and DAQ cards are explained in detail with respect to temperature control. Figure V.8 shows data communication schematic.
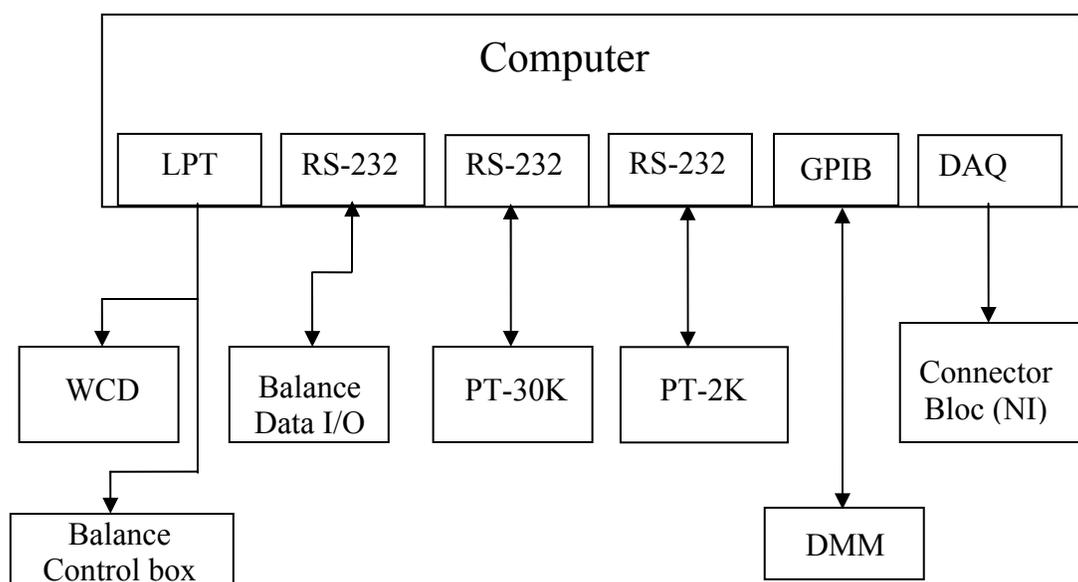
Figure V.8. Overall data communication schematic

5.7 Temperature Control System

The temperature control system in figure V.9 uses two isothermal shields, one radiation shield, one vacuum pump, one circulating bath, cooling tubes welded to the outside of both the isothermal shields and five strip heaters. This includes two strip heaters glued to the outside of the each isothermal shield and one strip heater on cell top. The isothermal shields are made of copper for its large thermal conductivity. The tubes are ¼-inch copper tubes, which carry the temperature control fluids.

Different fluids are used for different temperature ranges. A clean 50/50 ethylene glycol-water mixture could be used to go as low as 255 K and as high as 350 K. For a temperature range of 373 to 473 K, we use Dow-Corning 550 (DC-550), a phenyl methyl siloxane oil. DC-550 has been chosen for its various desirable properties such as high temperature stability, chemical inertness, low flammability and volatility, excellent oxidation resistance, constant heat conductivity over a wide temperature range and unlimited shelf life at room temperature (www.dowcorning.com). A PolyScience
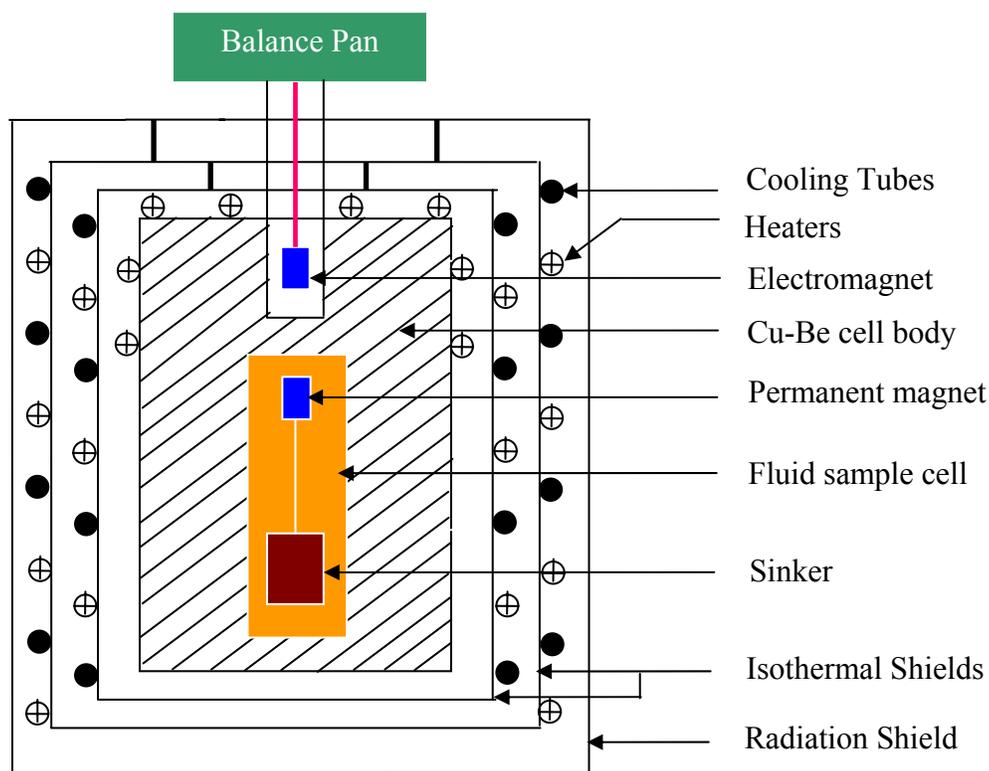
Figure V.9. Temperature control system schematic

circulating bath (model # 9512) circulates these fluids. With the glycol mixture, anti-fungicide chemicals should be used for longer life. Liquid nitrogen is used for measurements below 255 K. Liquid nitrogen is fed from liquid nitrogen tank bypassing the circulating bath, passed through the cooling tubes and vented outside the room.

The clearance between the cell body and the inner shield and between each successive shield varies between 0.75 to 1 inch. Clearance is as small as possible for faster heating or cooling of the sample.

When beginning a heating or cooling stage, the system is kept at ambient pressure and liquid is circulated through both the isothermal shields. Once the desired temperature is reached, the vacuum pump is turned on. This ensures quick heating or cooling initially as well as more stability once temperature equilibrium has been achieved.

After reaching temperature stability, instead of using both isothermal shields as active shields, we could keep either only the inner shield active or only the outer shield active. In the first case, response will be quicker but stability may be sacrificed. In the later case, the reverse should hold true. During measurements, however, we have not seen much of a difference in terms of stability. Generally, we keep both the shields active.

For fine temperature control, two strip heaters are used on each isothermal shield. Each heater carries four high resistance wires. The first two wires are connected in parallel, so are the third and fourth. Then each pair is connected in series. This means that current in wire 1 and 2 flows in one direction, current in 3 and 4 flows in opposite direction, which means that a magnetic field generated by the current is more or less are canceled out.

We use AC power supplies for all heaters. Otherwise, if we had connected heater 1 and 2 on each shield to two different DC power supplies such that for one heater current flows from top to bottom of the shield and for the other one, from bottom to top, additional cancellation of magnetic field would have been possible. The heater action is controlled by LabView using TTL (transistor-transistor logic). Radiation loss becomes significant when a large temperature gradient exists between the cell temperature and room temperature. The radiation shield is made of aluminum (lower emissivity) and its interior is glossy to reduce radiation.

A Platinum Resistance Thermometer (PRT) is inserted into the body of the Cu-Be block to measure the MSA cell temperature, and a silicon oxide paste is used in between the PRT and the bloc for better thermal contact. Vacuum grease is used on the gasket between the aluminum shield and the top support plate for better vacuum. This top plate, also made of aluminum, is very sturdy and carries the weight of the balance and the Cu-Be block without deformation. The radiation shield as well as two circular plates is hung from the top plate; the circular plates support the isothermal shields. Before constructing the temperature control system we ensured that all the materials and components including the stainless steel nuts and screws were non-magnetic.

5.7.1 Temperature Measurement Method and Principal
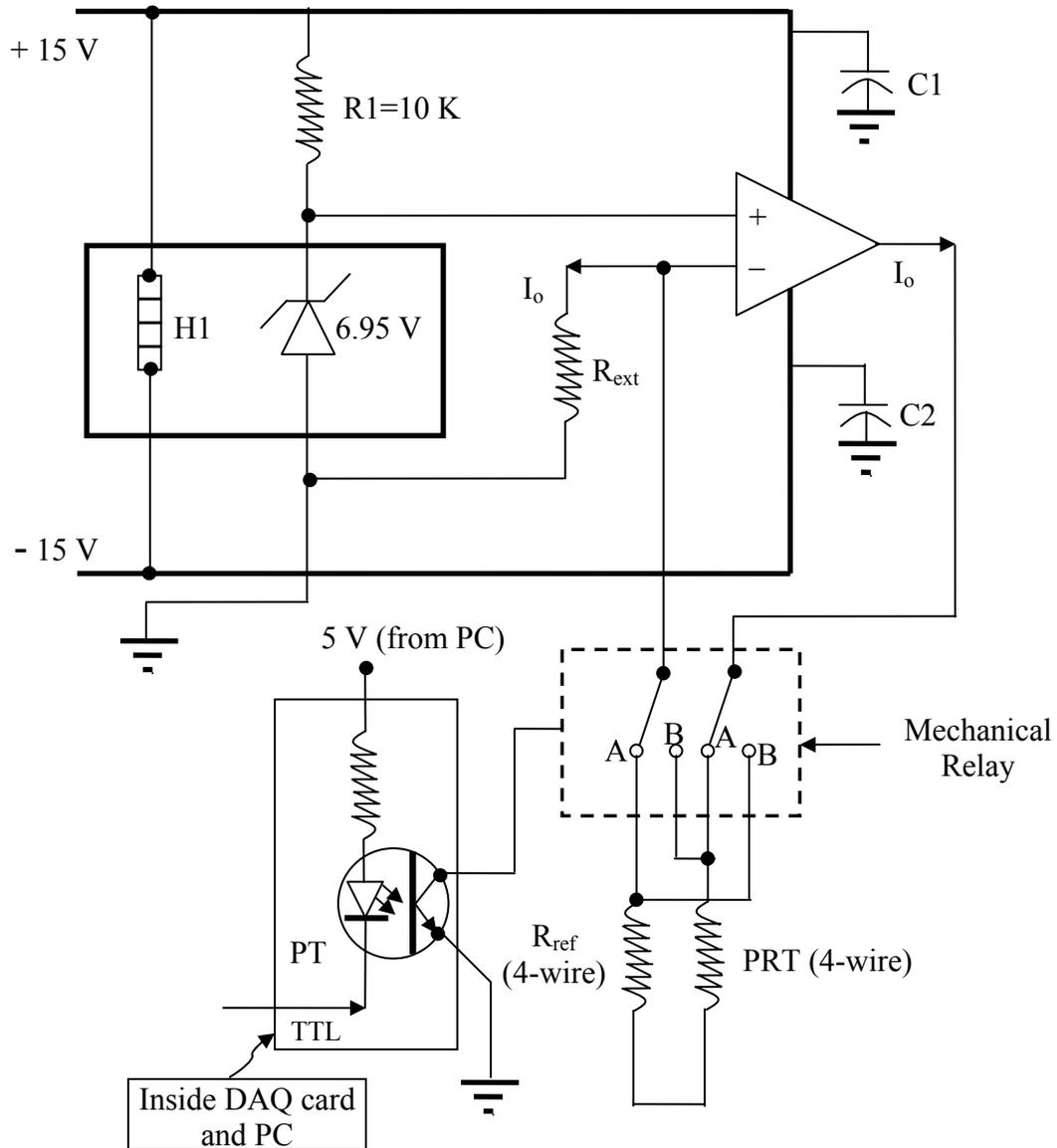
Figure V.10. Constant power supply and automatic relay for current reversal

A constant power supply (figure V.10) is used for temperature measurement. A zener diode maintains a constant voltage of 6.95 V across its terminals. A zener diode is a special diode that can be forward biased or reverse biased. An external voltage of 15 V

is applied, which is larger than the rated breakdown voltage of the reverse biased zener diode. A reverse-biased Zener diode displays a controlled breakdown and lets the current flow to keep the voltage across the zener diode at the zener voltage.

Resistance R1 must be small enough that the current through the zener diode keeps the diode in reverse breakdown. Otherwise, R1 must be large enough that the current through the diode does not destroy the device and power dissipation does not exceed the rated power dissipation.

The constant current can be varied by changing the external resistance R_{ext}. The operational amplifier in the constant power supply is composed of transistors and diodes. Because of the large impedance between the input terminals (+ and -), a negligible current flows between the terminals and both the terminals can be assumed to have same voltage. The output of the constant power supply than is $I_o= 6.95/R_{ext}$ A. We can vary the current from 0.1 to 0.4 mA in 12 stages. Because of the frictionless operation of the op-amps and the presence of heater (H1) that maintains the temperature of the zener diode, its working voltage is very stable, and the power supply is also very stable.

Platinum is used as the temperature sensor material for its high accuracy, good linearity, lack of hysteresis, wide temperature range and excellent repeatability. Hermetically sealed ceramic material is used as a reference resistor because of its stability and low sensitivity to temperature change (low temperature coefficient). For that reason, we think it is sufficient to keep it at ambient temperature rather than immersed in a precisely controlled oil bath.

As shown in figure V.10, constant current I_o flows simultaneously through both the platinum resistance thermometer (PRT) and the reference resistor, which are connected in series. The PRT, with a temperature range of 84.15 to 533.15 K, is manufactured by MINCO and reference resistor is from Julie Research Lab (Tag # CH46T4-100, TXA&M-001). Both were calibrated using procedures followed by National Institute of Standard and Technology (NIST); PRT by MINCO and reference resistor by Process Instruments Inc. in June 2005. The PRT calibration was checked by Dr. M. McLinden of NIST in July 2005 using a water triple-point cell and it differed by

2 mk. The calibrations are traceable to NIST and calibration information appears in appendix E. Current I_0 produces a voltage drop on each resistor that is proportional to their respective resistances. These voltages are measured with an amplifier and analog-to-digital converter (ADC) inside a Keithley Digital Multimeter (DMM, Model 2000-20). Because one voltage can be measured at a time, a scanner card at the back of the multimeter sends voltage signals to different channels of the Multimeter and reads channels at different times.

For the PRT, we do not use the two-wire method because the voltage drop in the two-lead wires as well as junction resistance between wires erroneously propagates to the temperature measurements. The PRT has four wires, one pair of leads carries the constant current to the sensor and back, the other pair measures the voltage drop across the sensing element. Because of the high impedance of the ADC, the current in the voltage sensing lead is very small. As a result, the voltage drop caused by lead wire resistance and junction resistance is negligible.

Two other methods, a two-wire bridge circuit and a three-wire bridge circuit, are as good as or better than the four-wire method with respect to lead-wire resistance (Bateson, 1999). In our arrangement, however, differential application of voltage measurement has eliminated the even negligible lead wire and contact resistance, which are function of temperature and are constant. This has made our measurements as good as the three-wire bridge circuit method.

The voltage on each resistor is measured twice, once with the current in one direction and then with the current in the opposite direction. It is absolutely essential that the current be exactly the same in both cases (i.e. during one cycle). The reversal of current direction takes place because of the TTL sent by a LabView program controlling the temperature to the opto-coupler (photo- transistor, PT). Optocoupler operations are explained in terms of transistor operations in section 5.7.3.

Each ratio measurement requires four voltage measurements: forward and reverse current for PRT sensor ($V_{PRT, F}$ and $V_{PRT, R}$, respectively), forward and reverse current for reference sensor ($V_{Ref, F}$ and $V_{Ref, R}$, respectively). The ratio of the sensor

resistance to reference resistance is obtained by subtracting and dividing the voltage samples:

$$R_{PRT} = R_{Ref} \frac{V_{PRT,F} - V_{PRT,R}}{V_{Ref,F} - V_{Ref,R}}$$

(5.14)

The differential application not only eliminates lead wire and contact resistance errors, but also eliminates errors caused by driving current imprecision and drift of the driving current, amplifier bias current, amplifier offset voltage, amplifier gain, ADC offset and ADC scale because they all affect the voltage samples equally (Hart Scientific, 2002).

Nonlinearity, which is the curvature in the graph of the relationship between the actual resistance ratio and the resistance ratio measured by the experimental method, is also minimized. Because samples of opposite polarity are subtracted, zeroth order errors (offsets), second-order errors, and all higher even-order components of nonlinearity cancel. Third order and higher odd-order components remain, but they diminish greatly in magnitude the higher the order (Hart Scientific, 2002).

Noise can be reduced by grounding and shielding of cables and digital filtering by the computer. It can be further reduced by using an ADC with better resolution, i.e. instead of using 6-bits as now; we could use an ADC with 24-bits.

Problems like electrical leakage, reactance and eddy currents are minimized by using direct current (DC) circuitry instead of alternating current. Finally, self-heating error, caused by power dissipation in the PRT that raises the temperature of the element itself, should be considered. The size of self-heating error depends upon the magnitude of the current, the thermal resistance of the PRT and the thermal resistance of the film between the probe and the surrounding fluid (Bateson, 1999). In our arrangement, the self-heating error has been minimized by keeping I_o between 0.1 to 0.14 mA. The self-heating error can be calculated from:

$$\text{Self - heating error} = \frac{I_o{}^2 R_{PRT}}{P_{diss}}, {}^0C$$

(5.15)

Where P_{diss} is the dissipation constant.

A thermopile, a combination of five copper/constantan thermocouples ('T' type) in series, measures the temperature difference ΔT between the cell top and bottom, where $\Delta T = T_{top} - T_{bottom}$. A voltage (called the Seebeck effect) is generated between the measuring junction and the reference junction; this voltage difference is proportional to the temperature difference and is measured at a channel in a Keithley multimeter. As we require only the temperature difference and not the temperature itself, cold junction compensation is not required. The temperature difference is only required to control the heater at the cell top (so that ΔT is minimized). Therefore, quality control of the thermopile output by signal conditioning or thermal electromotive force compensation is not essential. Thermopile signal conditioning has been discussed in detail by Bateson (1999). The cell top heater, which receives ΔT signal as feedback, is active only when measurements are above ambient temperature. Below ambient, we need a similar heater at the cell bottom to minimize ΔT; this is not possible in our apparatus because of the cell flange containing the sensor coil.

5.7.2 Temperature Data Acquisition and Control

The computer, through a DAQ card and a Labview program, sends TTL to control the on/off action of solid-state relays (SSR) and one mechanical relay. SSR control the on/off action of heaters while mechanical relay performs the current reversal. The voltage signals from the PRT and thermocouple (TC) are fed to the digital multimeter (DMM) where they are digitized and the PRT signal is converted to resistance. The signals are sent to the PC through the GPIB card, in which a LabView program converts them to temperature or temperature difference. International Temperature Scale of 1990 (ITS-90) is used to convert the resistance signal to temperature signal. Known Seebeck coefficients for the thermocouple are used to convert voltage into temperature difference. The temperature data acquisition and control schematic are shown in figure V.11.
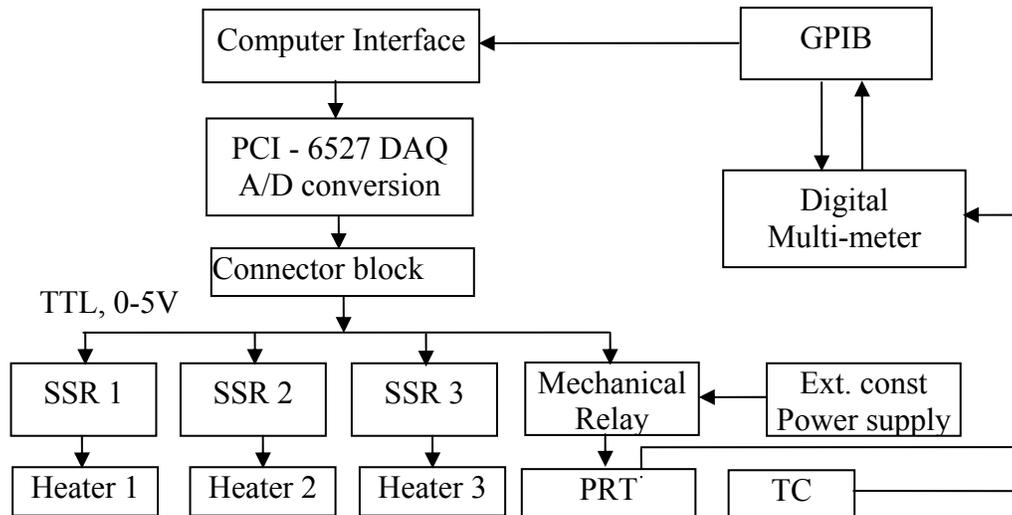
Figure V.11. Temperature data acquisition and control schematic

5.7.3 Transistor Principal and Operation

Transistors are necessary for current reversal and heater operation. The transistor consists of an emitter (E), a base (B) and a collector (C). The emitter and collector (both N-type for an NPN transistor) are made by doping a semi-conductor material like silicon or germanium (no free electrons) with an N-type penta-valent material like antimony, arsenic or phosphorous (free electrons as charge carriers in their conduction bands). Similarly, the base (a P-type for an NPN transistor) is made by doping the substrate with a P-type trivalent material: boron, aluminum or gallium. Therefore, although E, B and C are individually electron neutral; E and C are rich in conduction electrons, but B is electron deficient with its outer shell electrons in its valence band.

When E and B are combined, an electron-hole recombination occurs at the junction (i.e. conduction electrons from E fall into the valence band in B) and a potential barrier between E and B occurs that prevents flow of charge. Now, B has become electron rich and E, electron deficient. Next, an external voltage is applied (biasing) with the positive electrode connected to B and E connected to ground. This external field

works against the potential barrier, thus shrinking it in size and strength. This is forward biasing (FB) of the E-B potential barrier that enables flow of charge. Thus, the barrier becomes a "proportional switch" controlled by V_B.

On the other hand, the potential barrier between B and C is reverse-biased ($V_C > V_B$) and it enlarges and strengthens the barrier between B and C. Once electrons in the base cross the barrier B-C, they are pulled towards the collector because of reverse-biasing. The reverse-biasing cannot change the current I_c. Thus, the transistor acts as a switch and a constant current power supply.

The base area is small. That causes less electron-hole recombination in the base and makes the base current (or leakage current) very small.

In our experiment, the computer sends a TTL (transistor-transistor logic) in response to the command sent by a LabView program controlling the temperature. A TTL is created by a combination of transistors or diodes using logic gates such as AND, NAND, OR, etc. The input to the logic gates are 5 V, the output is either LOW (i.e. FALSE, generally 0 V) or HIGH (TRUE, generally 5 V).

Opto-couplers such as photo transistors are used for digital isolation. They are used when a voltage differential exists between the data acquisition system and external equipment. Large voltage differences could lead to measurement problems or equipment failure. In the event of equipment failure, the internal voltage of the external equipment can damage the data acquisition system.

In figure V.12, when TTL is 0 V, the light emitting diode (LED) in the phototransistor (PT1) is forward-biased. Because the diode cut-off voltage is less than the voltage difference of 5 V, the diode acts like a switch and emits infrared light. This additional photon energy forward-biases the barrier between the base and emitter in the transistor inside the phototransistor, so current flows between its collector and emitter, i.e. contact between S-S "closes". S-S are connector ports 67 and 68 in the National Instrument DAQ card (installed in the PC) for heater 1. Similarly, the same is true for ports 71 and 72 for heater 2, ports 75 and 76 for external polarity control (for current reversal), and ports 79 and 80 for heater 3 (see section 5.7.4).
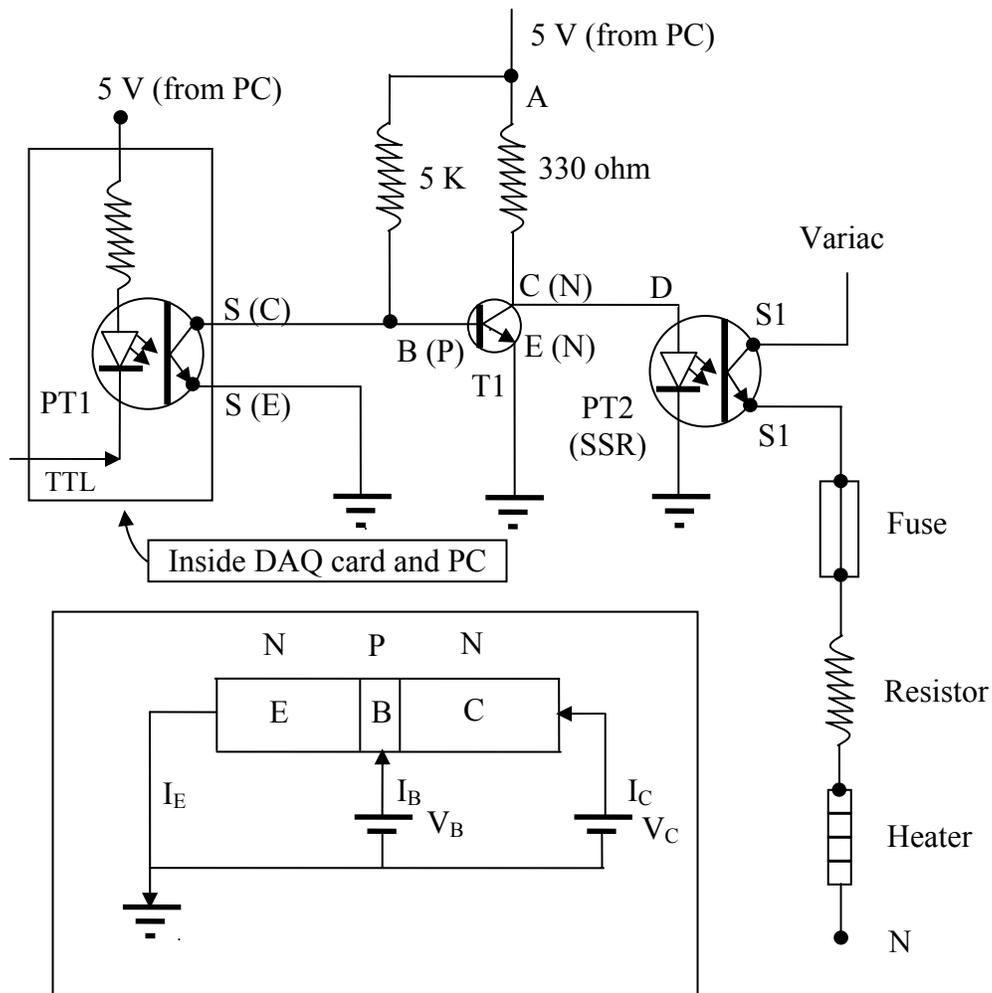
Figure V.12. Control action of heaters driven by TTL. (Inset is a common-emitter NPN transistor in which the emitter is grounded. This is part of the photo-transistor PT1 or PT2.)

This makes the base of the transistor T1 grounded. The emitter also is grounded. Then the junction B-C is reverse-biased and the transistor is "open" (off). No current flows between C and E in transistor T1. A small current flows between A and D, and V_D is more than the cut-off voltage of the LED inside PT2. PT2 is the second phototransistor, inside a solid-state relay (SSR) that works as just described. So, the LED conducts, and that closes contact between S1-S1 (i.e. the transistor is conducting) and the heater receives power.

On the other hand, when TTL is 5V, contact S-S is open. Therefore, the B-E junction is

forward-biased and current flows between C and E in T1. There is a larger voltage drop in the 330-ohm resistor than before and V_D is less than the cut-off voltage of the LED. Then S1-S1 is open and the heater does not receive power.

5.7.4 DAQ Card and Connector Bloc

The National Instrument DAQ card (model # 6527) is embedded in the computer. Its pins are short-circuited with the pins of the NI connector bloc located outside the PC,. as shown in figure V.13. Because the DAQ card has 100 pins and the bloc has only 50 pins, pins 51, 52,…67, 68, …71, 72,…75, 76,…79, 80,...99, 100 in the DAQ card are externally short-circuited with pins 01, 02, … 17, 18, … 21, 22, …25, 26, …29, 30, … 49, 50 in the connector bloc, respectively by connecting a ribbon cable between the DAQ card and the connector bloc. Pins 99 and 100 in the DAQ card (i.e. pins 49 and 50 in the bloc) are power supply (+ 5V) and ground, respectively.

Instead of using the pins 51….100 in the DAQ card, we could have used pins 1….50. This DAQ card can handle only digital input and digital output. The designation of DAQ card pins in the LabView temperature control program in terms of channel and line numbers appears in the appendix G. The reader should consult the DAQ 6527 User Manual for further clarification (www.ni.com).

Based upon the TTL from PC, Pins 17 and 18 in the connector bloc drive SSR1 (a photo-transistor) for turning heater 1 on or off. R1 is 5 K ohm and R2 is 330 ohm. Similarly, pins 21, 22 and pins 29, 30 are used to drive heater 2 and heater 3, respectively. Heaters 1 and 2 are for the inner isothermal shield and heater 3 is on the cell top. The powers of the heaters come from variable AC voltage supplies (Variacs). Two more relays (SSR4 and SSR5) and their circuits (not shown) can control the two heater operations on the outer isothermal shield.
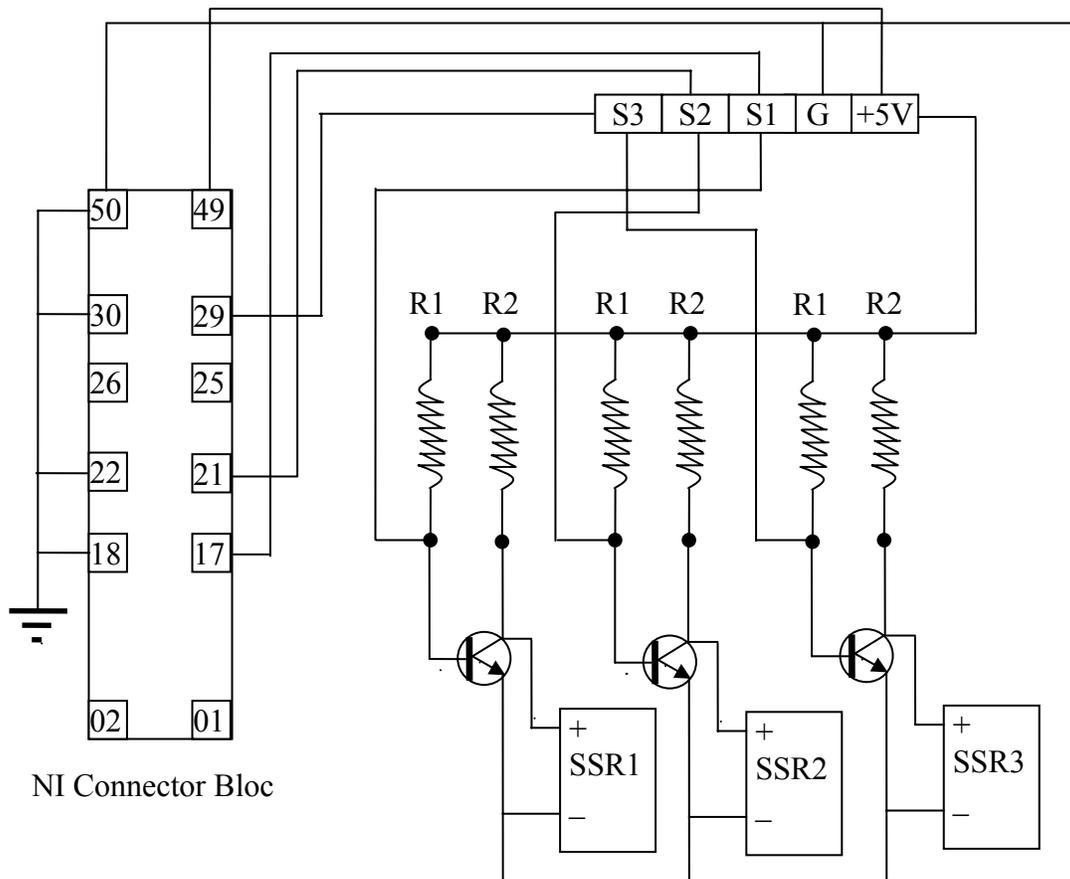
Figure V.13. Physical connections in connector bloc and temperature control box

Pins 25 and 26 are connected to the constant power supply box for current reversal in PRT resistance measurement. When the TTL is 0 V, contact between pins 75 and 76 on the DAQ card closes, and power supplied from the computer creates a magnetic field. This brings the mechanical contact, a single-pole double-throw type, from position A-A to position B-B (figure V.10). When the TTL 5 V, there is no power supply and the relay goes back to position A-A.

Use of multiple ground points at different potentials can lead to measurement error and generation of ground loops. Ground loops can result in current flows through circuit common or cable shields. This can lead to measurements being degraded through noise or suffering from reduced signal input range. To overcome this problem, all digital

grounds and the grounds of solid state relays have been connected to the DAQ card ground reference.

5.7.5 Propane Cooling System

Presently we use Liquid N_2 (LN) for cooling below 255 K. A few problems are present with LN cooling. If the LN dewar pressure is too low, the flow rate is too small for cooling. On the other hand, if the dewar pressure is too high, then vapor-liquid equilibrium shifts to higher temperature and also produces less cooling. LN heat capacity is comparatively low, about 57 J/ (mole-K) at its normal boiling point of 77 K. Because of the large length of copper tube between the LN dewar and the isothermal shields, its temperature increases quickly. At the same time, LN has comparatively less cooling effect because of low heat of vaporization; at its normal boiling point, liquid nitrogen has a heat of vaporization of 5.57 kJ/mole, which is more than an order of magnitude less than that of water. So, some of LN evaporates even before it reaches the shields. This two phase flow of nitrogen leads to temperature instability in the density measurement as well as inefficient cooling. The heat capacity of nitrogen gas at constant pressure is also very low, about 28.87 J/ (mole-K) at atmospheric pressure and at 298.15 K. Therefore, for better low-temperature control and stability, we wish to replace LN with a liquid propane system. Propane cooling system is shown in figures V.14 and V.15.

Liquid propane has physical properties that makes it more desirable as a cooling fluid. Its relatively low vapor pressure, relatively high heat capacity of 119.6 J/ (mole-K) at 300 K, high heat of vaporization of 18.774 kJ/mole at normal boiling point of 231.04 K and gas heat capacity at const pressure of 73.6 J/ (mole-K) at atmospheric pressure and at 298.15 K make it nearly ideal as a low temperature cooling medium.
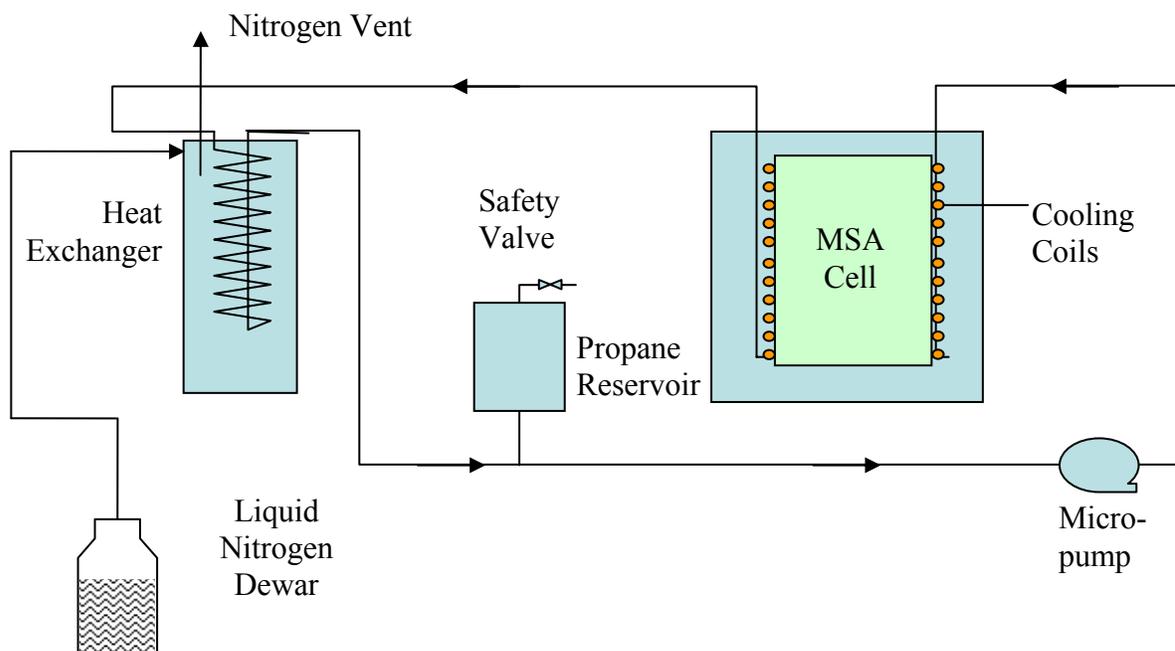
Figure V.14. Schematic diagram of the propane cooling system
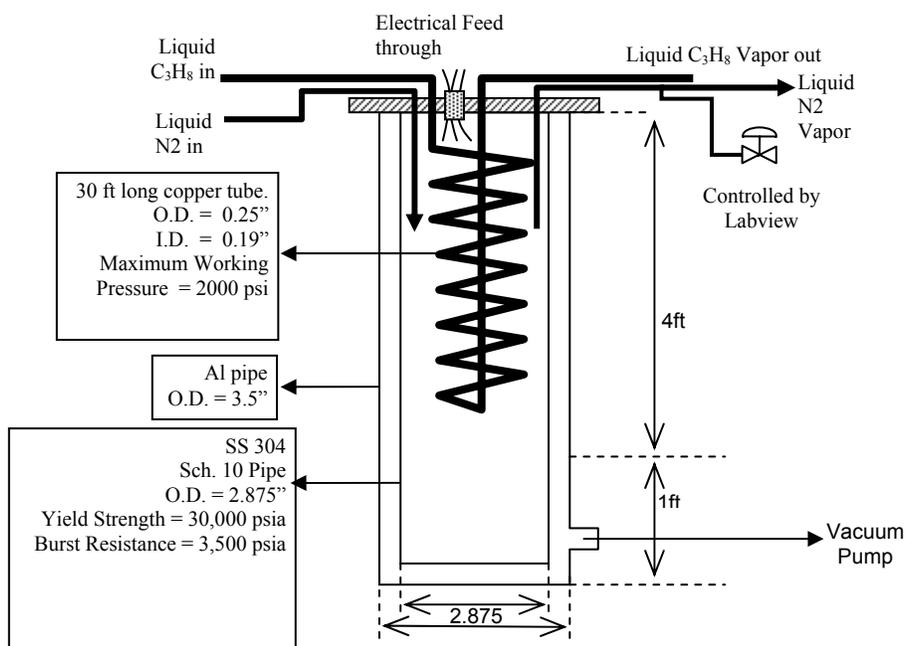
Figure V.15. Schematic diagram of propane heat exchanger

The newly built propane cooling system consists of a liquid propane reservoir, a propane tank with a heat exchanger inside, a gear pump, cooling tubes glued to the two isothermal shields and a liquid nitrogen dewar. LN cools propane in a cylindrical heat exchanger, and the propane in turn cools the cell inside the isothermal shield.

The heat exchanger is a ¼-inch outer diameter copper tube coiled inside a 2.875-inch outer diameter SS-304 pipe. This pipe is inside a 3.5-inch outer diameter aluminum pipe; these two are isolated by vacuum. Nitrogen boiling point is -196 °C while the freezing point of propane is around -188 °C.

Therefore, to avoid freezing propane, the clearance between the bottoms of the tube and the SS pipe is kept at one foot, so the tube is never submerged in LN. Propane flows through the heat exchanger tube with an area of about 3600 cm^2 whereas LN flows into the pipe and exits as vapor through a venting hood into the atmosphere.

An inert helium atmosphere maintains the pressure inside the liquid propane reservoir. This ensures that the pump has enough net positive suction head. Three level indicators in the reservoir change color upon contact with propane. The reservoir also has a pressure safety valve. No insulation is placed around the reservoir.

A temperature data acquisition and control program, similar to that described previously is used. The only difference is that the temperature signal, which is read from the tube inside the pipe, is sent to a solenoid on/off valve instead of a heater. When the temperature of the propane is too low or approaching its freezing point, the solenoid valve in the LN outlet in the heat exchanger opens to the atmosphere to reduce the height of LN in the tube by letting nitrogen escape to the atmosphere.

5.8 Pressure Transducers

For accurate, reliable and stable pressure-measurement even under difficult conditions, we use Digiquartz Paroscientific digital pressure transducers as secondary pressure measuring devices. The excellent performance is achieved with precision quartz crystal resonators. Quartz is a polarized material whose molecules align themselves in

response to applied electric fields. This alignment of molecules results in induced dipoles causing the material to change dimensions and generate stress. Conversely, in response to applied mechanical stress, it generates a voltage (proportional to frequency of oscillation) that varies with pressure-induced stress; the voltage varies with temperature to some extent, too.

Remarkable repeatability, low hysteresis, high resolution and excellent stability have made the quartz crystals very attractive as sensing elements. The load sensitive resonator is a double-ended tuning fork consisting of two identical parallel beams placed between two mounting pads. The beams are driven piezoelectrically in 180° phase opposition by a very low power oscillator circuit such that very little energy is transmitted to the mounting pads.

Pressure transducers employ Bourdon tubes as the pressure-to-load generators. Pressure applied to the Bourdon tube generates an uncoiling force that applies tension to the quartz crystal to increase its resonant frequency. The transducers are evacuated and hermetically sealed to reduce air damping and maximize the "Q" factor of the resonators. The vacuum also acts as a reference for the absolute pressure transducers in our apparatus.

To compensate the calculated pressure thermally and achieve high accuracy over a wide range of temperatures, the transducer has a temperature sensor inside that consists of piezoelectrically driven, dual torsionally oscillating tines whose resonant frequency is a function of temperature only. This sensor is kept in vacuum and never exposed to any mechanical stress or applied pressure.

The working equation of the pressure transducer can be obtained from the well known force-frequency (F-f) effect of a flexture beam (pressure resonator in our case) in axial tension or compression (Albert, 1984; Albert, 1982):

$$f = f_0 \sqrt{1 + SF}$$

$$f_0 = a_0 \frac{t}{L^2} \sqrt{\frac{E}{\rho_b}} \tag{5.16}$$

$$S = a_s \frac{L^2}{Ebt^3}$$

Where beam dimensions L, b and t are length, width and thickness, respectively, E and ρ_b are elastic modules and density of the beam material, respectively and dimensionless constants a_0 and a_s are known from conditions of fundamental vibration mode and fixed-fixed boundary conditions.

Substituting $\tau = 1/f$, $\tau_0 = 1/f_0$ and $F = -PA_e$ in the previous equations and solving, where τ is the vibration period of the pressure resonator, τ_0 is the vibration period at the fundamental vibration mode of the pressure resonator, F is the force, P is the pressure, A_e is the effective bourdon tube area and the minus sign for beam compression, we get:

$$P = \frac{1}{SA_e} \left[1 - \tau_0^2 / \tau^2 \right] \tag{5.17}$$

Letting $1/SA_e = C$ and including an additional empirical term results in the following characterization equation:

$$P = C \left\{ \left[1 - \tau_0^2 / \tau^2 \right] - D \left[1 - \tau_0^2 / \tau^2 \right]^2 \right\} \tag{5.18}$$

By calibrating the transducer over a number of temperature points while measuring the pressure output, τ_0 and parameter U of the imbedded temperature sensor, coefficients C, D and τ_0 can be expressed as a function of temperature to provide a thermally compensated transfer function so that pressure readout becomes a function of temperature:

$$C = C_1 + C_2 U + C_3 U^2 \tag{5.19}$$

$$D = D_1 + D_2 U \tag{5.20}$$

$$\tau_0 = T_1 + T_2 U + T_3 U^2 + T_4 U^3 + T_5 U^4 \tag{5.21}$$

$$U = X - U_0 \tag{5.22}$$

And X is vibration period of the temperature resonator and U_0 is vibration period of the temperature resonator at some reference temperature (25 °C).

Finally, temperature, T of the transducer can be calculated from:

$$T = Y_1U + Y_2U^2 + Y_3U^3 \qquad (5.23)$$

The units of vibration periods, pressure and temperature are μsec, psia and deg C, respectively.

Because coefficients C, D and τ_0 have been expressed as a function of U and the coefficients C_1, C_2, D_1, D_2, T_1, $T2$, T_3 T_4 and T_5 have been determined from linear regression, the indicated pressure as calculated by this "thermal model", which is also the displayed pressure, agrees with the true applied pressure with a typical absolute accuracy of ± 0.01 percent of the transducer full scale at all temperatures and pressures in the operational range (www.paroscientific.com, www.pressuresystems.com).

5.9 LabView Temperature and Balance Programs

The LabView program MSA_main_1.vi was initially developed by Jingjun Zhou (Zhou, 2005) for data acquisition and control in his isochoric apparatus. It was later modified for use in the magnetic suspension densimeter. As explained previously, the temperature program measures voltage across a PRT and a reference resistor for both forward and reverse direction of current and calculates the resistance of the PRT using the calibrated resistance of the reference resistor. This resistance is converted to temperature by using international temperature scale (ITS-90) and using coefficients determined during calibration of the PRT.

The program calculates instantaneous temperature as well as average and standard deviation of temperature. The values of last 40 readings are taken into account for average and standard deviation calculations. Once the program starts, random numbers are used to fill in the data points during the first 40 points; so the correct temperature average and standard deviation result only after the initial 40 temperature points have been collected.

The sub vi (virtual instrument or sub-program), 'Meas-Temp_MSA.vi' does the current reversals and measures voltage drop across the resistors one at a time. The sub vi has eight sequence structures (SS). In the first sequence structure (SS-0), the configuration of the Keithley DMM takes place. A maximum value of NPLC = 10 means that the data collection rate is slowest but readings are most accurate (least noise). A minimum value of NPLC is 0.1, where the reverse is true. Presently, we use a NPLC value of 5, which is accurate, stable and relatively quick.

The second sequence structure (SS-1) has case structures that are activated based upon boolean logic (TRUE or FALSE) connected to the input terminals. Inside the case structure, there is a 'write to digital line.vi', which receives a TRUE logic (5 V) which means that the LED in the optocoupler is reverse-biased, so the transistor inside the optocoupler is open between collector to emitter and no current flows between them in the transistor (figure V.12). The connector in this case is connected to pin 75 on the DAQ card (i.e. 25 on the connector bloc) and the emitter is connected to ground (pin 76 in DAQ card). In the 'write to digital line.vi', device 2 means the DAQ card, channel 4 and line 3 means the pin 75 on the DAQ card (see appendix 1). So, the TRUE logic makes sure that the contact between pins 75 and 76 is open and the mechanical switch moves back from position B-B to its natural position A-A (figure V.10).

In SS-2, voltage across a secondary resistor is measured and read in channel 12 of the Keithley DMM. Similarly, in SS-3, voltage across the PRT is measured and read in channel 6. The DMM channels are different from DAQ card channels and should not be confused with each other.

In SS-4, a FALSE logic is sent to 'write to digital line.vi'. So, this time the contact closes between pins 75 and 76 on the DAQ card as the transistor in the optocoupler conducts current between collector and emitter. This causes the mechanical switch to change position from A-A to energized position B-B. This reverses the direction of current through the resistors.

SS-5 has a timer to prevent data overflow. SS-6 is similar to SS-2 and SS-7 is similar to SS-3 except that now the current direction is reversed. In SS-8, the voltage

difference across the thermopile is read in DMM channel 9. After that, based on all the measurements during the cycle, PRT resistance is calculated and then the whole cycle is repeated again.

The Keithley DMM is connected to the PC through GPIB cable, so in the program various vi's such as 'GPIB write.vi', 'GPIB read.vi' etc. have been used. The commands in these vi's have been taken from the Keithley Model 2000 Multimeter User's Manual.

Once the resistance of the PRT is known, it is sent to 'Resis_Temp_N560_Isochoric.vi' where resistance is converted to temperature using ITS-90 scale. Two different formulas are used depending upon if the measured resistance is greater or smaller than the PRT resistance at the triple point of water.

To calculate the cell temperature differential, the thermopile voltage difference from 'Meas-Temp_MSA.vi' and temperature from 'Resis_Temp_N560_Isochoric.vi' is sent to 'voltage_Temp_MSA.vi' where ΔT is calculated using Siebeck coefficients for copper-constantan thermopiles.

The temperature output is also sent to 'PID.vi's' which triggers PID control action on the heater. There are three 'PID.vi's which act independently on three heaters; heater 1 and 2 on inner isothermal shield and heater 3 on cell top. The output of each vi varies between 0 to 5 V. This output, proportional to the difference between set point temperature and actual temperature, determines what fraction of time, out of total 3 seconds (as of now) the heater will be turned on or off. Heater on/off action results from sending FALSE/TRUE logic to 'write to digital line.vi'. The DAQ card channels and lines in these vi's could be explained, as before, with the help of appendix G.

We use 'MSAautobalance_final_1.vi' for magnetic suspension operations and balance data collections. Balance data is collected through a computer serial port (com 4) and MSA operations such as changing off position, zero point position and measurement position using a computer LPT port. Initially the balance is configured through the serial port with the following settings: bits per second - 9600, data bit - 7, parity - even, stop bits - 1, flow control - none, hand shake – hardware, end of line – CR.

After that, from whatever its initial position is, the MSA goes to ZP. The address for the LPT port is 888 and the binary command to the LPT port for the ZP is 100101. Then it goes to the off position. After that it starts a forerun between ZP and MP. The binary commands for zero position and MP are 0 and 10100110, respectively. The number of foreruns can be changed from the front panel of the program.

After the forerun, the MSA goes to ZP and tares the balance. Then zero point data are collected using 'readZP1.vi'. This vi includes 'VISA write.vi' which upon receiving a command 'SI' immediately reads data from the balance. These balance commands are available in the 'METTLER Bidirectional Data interface' manual. Then the MSA goes to MP and the balance sends data using 'readMP1.vi'. After that MSA goes to ZP again, and again the balance sends data. This is the end of one cycle. Then the cycle is repeated. The number of cycles, forerun ZP and MP time, number of zero points and measurement points in each cycle, ZP and MP stability time, etc can be controlled from the front panel. Apart from that, a number of time delays have been inserted into the program to give balance enough time to attain stability. The frequency of data collection is controlled from within the program.

Because of the balance drift, a correction factor must be applied to the MP data:

Corrected MP value = Uncorrected MP value- $ZP_{average,\ initial} - n*d$ (5.24)

Where n = 0, 1, 2, N-1 and N = total number of readings

$d = (ZP_{average,\ final} - ZP_{average,\ initial})/ (N-1)$ (5.25)

The relationship provides a linear correction. $ZP_{average,\ initial}$ is the average of all the ZP data in that cycle before the MP run, and $ZP_{average,\ final}$ is the average of all the ZP data in that cycle after the MP run.

6. PURE COMPONENTS AND SYNTHETIC NATURAL GAS MIXTURES DENSITY MEASUREMENTS

6.1 Pure Component Density Measurements

Densities of pure methane, carbon dioxide and nitrogen were measured to justify correct operation of the magnetic suspension assembly and also to find the magnitude and sign of the systematic bias error of the apparatus, which varies from laboratory to laboratory. These data were compared with equation of states developed with high quality density data of these components. EOS for methane, carbon dioxide and nitrogen were developed from the works of Setzmann and Wagner (1991), Span and Wagner (1996) and Span et al. (2000), respectively. Relative deviations of the measured densities from this work as well from previous work (Patil, 2005) from these EOS's would give the systematic bias error of the apparatus.

The pure components were measured at different times in between 2005 and 2007, generally before and after natural gas measurements. Nitrogen was measured in March, 05; December, 05, April-May, 06 and February-March, 07. Methane and carbon dioxide were measured between December, 05 and January, 06. Table VI.1 shows the purity of the components, the impurities (where available) and the sources of the cylinders. The compositions of these gases were never analyzed in the lab before or after the measurements; rather the compositional analysis provided by the manufacturers were used for theoretical density calculations.

Nitrogen densities were measured in the pressure range of 1,000 psia to about 24,000 psi in the temperature range of 250 to 340 K; carbon dioxide densities were measured in the pressure range of 1,000 to 5,000 psi at 309 and 338.35 K; methane densities were measured at 305 and 338 K in the pressure range of 1,000 to 5,000 psi.

Table V1.1. Pure component compositions

Pure Gas	Cylinder Label	Purity	Impurities	Supplier
		mole %		
Nitrogen	N2 2	99.9995	CO < 1 ppm CO_2 < 1 ppm THC < 0.5 ppm H_2O < 2 ppm O_2 < 0.5 ppm	Scott Specialty Gas
CO_2		99.99	unknown	Matheson Tri Gas
Methane		99.99	unknown	Matheson Tri Gas

Paroscientific pressure transducers, 6 K and 30 K were used for measurement under 6,000 psi and over 6,000 psi, respectively. The term 'xxx K' indicates the isotherm temperature. The average values of temperature and pressure over a period of 10 to 15 minutes as well as the standard deviations of pressure, temperature and balance readings are provided; standard deviation is a measure of the measurement instability as well as uncertainty.

Pressure transducers were frequently calibrated against Ruska dead weight gage. The transducers are temperature compensating, i.e. even if the body temperature of the transducers change, the pressure display should still agree with the true pressure within a certified accuracy. But despite that, for better performance the transducers are kept at constant temperature in thermally insulated aluminum blocks and both the calibrations and measurements are done at this constant temperature. The standard deviation of the aluminum block temperature is generally below 5 mK.

The experimental densities were compared with the values calculated by NIST-12 software, which among other things uses reference EOS's by Span et al. (2000) for nitrogen, Setzmann and Wagner (1991) for methane and Span and Wagner (1996) for carbon dioxide. The percentage relative deviation between experimental and theoretical values is defined as:

$$\Delta\rho\big/\rho = \left(\rho_{\text{exp}t} - \rho_{theo}\right)\big/\rho_{theo} \times 100 \qquad\qquad (6.1)$$

The uncertainty in density of the equation of state for nitrogen ranges from 0.02% at pressures up to 30 MPa (4,350 psia) to 0.6% at very high pressures (200 MPa or 29,000 psia); except in the range from 270 to 350 K at pressures less than 12 MPa (1,740 psia) where the uncertainty in density is 0.01%. The uncertainty is expressed at 95% confidence level. The equation is valid from the triple point temperature to temperatures of 1,000 K and up to pressures of 200 MPa. From 1,000 to 1,800 K, the equation was validated with data of limited accuracy. For calibration purposes, the equation is supplemented by a simple but accurate formulation, valid only for supercritical nitrogen between 250 and 350 K at pressures up to 30 MPa (Span et al., 2000).

This nitrogen reference equation of state has been formulated using the Helmholtz energy as the fundamental property with independent variables of density and temperature. Thermal and caloric properties of nitrogen such as pressure, compressibility, internal energy, enthalpy, entropy, Gibbs energy, isochoric heat capacity, isobaric heat capacity, and the speed of sound can be calculated. The equation can be used to predict vapor-liquid and solid-liquid coexistence properties such as critical point, triple point, vapor pressure, saturation densities, melting pressure.

The new equation of state describes the thermal properties in the critical region very accurately; therefore it can also provide good predictions on isobaric heat capacities as isobaric heat capacity depends mainly on derivatives of thermal properties in the critical region. However, as the equation is purely analytic in nature, the predicted values for the isochoric heat capacity and for the speed of sound do not agree with theoretical expectations close to the critical point (Span et al., 2000).

The new reference equation for methane (Setzmann and Wagner, 1991) is generally valid in the temperature range of 90 to 620 K for pressures up to 100 MPa (14,500 psia). For the density, uncertainties of ± 0.03% for pressures below 12 MPa (1,740 psia) and temperatures below 350 K and ± 0.03% to ± 0.15% for higher pressures

and temperatures are estimated. The equation, which is explicit in the Helmholtz free energy, can calculate the thermal and caloric values as well as properties in the single phase, two-phase, super critical and near critical region. The equation is also able to provide saturated vapor densities which are much more reliable than those calculated from the original saturated vapor density equation of Kleinrahm and Wagner (1986).

Table VI.2 shows the measured density for each pure component at different isotherms.

Table V1.2. Pure component measured density data

Temperature Average K	Nitrogen Pressure Average psi	March & December, 2005 Density		Relative Deviation
		Experimental kg/m^3	NIST-12 kg/m^3	%
289.99	1000.75	80.686	80.707	-0.026
289.98	1998.62	158.124	158.204	-0.050
290.01	2999.03	227.709	227.840	-0.057
305.19	1001.34	76.184	76.155	0.039
305.18	2000.67	148.912	148.831	0.055
305.19	3000.54	214.527	214.400	0.059
305.20	4002.39	271.564	271.408	0.058
305.16	4999.50	320.132	319.934	0.062
340.05	1000.21	67.488	67.458	0.044
339.97	1999.53	131.314	131.251	0.048
339.97	2998.85	189.378	189.303	0.040
339.96	3999.97	241.001	240.906	0.039
339.99	4999.80	286.186	286.045	0.049

Table V1.2. (continued)

Methane		December, 2005		
Temperature	Pressure	Density		Relative Deviation
Average	Average	Experimental	NIST-12	
K	psi	kg/m^3	kg/m^3	%
305.25	1002.80	48.616	48.566	0.103
305.29	3000.25	155.059	154.916	0.093
305.27	4994.37	223.460	223.256	0.092
338.14	1001.30	42.086	42.060	0.060
338.05	2997.91	130.190	130.062	0.098
338.05	5000.47	195.644	195.466	0.091
338.25	1001.25	42.058	42.040	0.043

Table VI.2. (continued)

Carbon dioxide		January, 2006		
Temperature	Pressure	Density		Relative Deviation
Average	Average	Experimental	NIST-12	
K	psi	kg/m^3	kg/m^3	%
309.22	1000.16	207.047	206.809	0.115
309.29	3005.29	866.500	865.846	0.076
309.26	5005.92	946.752	946.311	0.047
338.35	1001.33	146.053	145.979	0.050
338.38	3005.21	703.175	702.799	0.054
338.36	5002.95	840.914	840.527	0.046

Table V1.2. (continued)

Temperature Average	Pressure Average	Nitrogen	April-May, 2006	Relative Deviation
		Density		
		Experimental	NIST-12	
K	psi	kg/m^3	kg/m^3	%
250.36	2179.52	208.007	208.000	0.003
250.34	2898.69	267.532	267.450	0.031
250.34	4351.07	362.278	362.180	0.027
250.37	7253.14	481.930	481.810	0.025
250.33	10000.03	552.896	552.780	0.021
250.36	14504.96	630.931	630.910	0.003
250.37	18117.95	676.079	676.290	-0.031
250.37	21724.46	712.413	712.930	-0.073
250.40	23920.21	731.498	732.270	-0.105
290.07	1001.21	80.625	80.719	-0.116
290.06	2998.78	227.717	227.770	-0.023
290.08	5001.93	337.659	337.629	0.009
293.23	2173.95	168.772	168.760	0.007
293.18	2903.04	218.736	218.670	0.030
293.21	4350.10	302.408	302.310	0.032
293.26	7250.67	420.117	420.038	0.019
293.22	9991.51	494.556	494.407	0.030
293.25	14502.57	578.417	578.405	0.002
293.34	18116.05	627.145	627.271	-0.020
293.24	21737.62	666.615	666.968	-0.053
293.21	23898.79	687.001	687.475	-0.069
340.16	2176.40	141.906	141.895	0.008
340.09	2900.98	183.841	183.829	0.007
340.12	4354.42	257.591	257.488	0.040
340.20	7252.71	368.487	368.199	0.078
340.23	10003.50	443.072	442.830	0.055
340.13	14495.49	529.545	529.516	0.006
340.14	18129.72	580.828	581.231	-0.069
340.12	21752.43	621.977	623.020	-0.167
340.14	23918.84	643.745	644.667	-0.143

Table V1.2. (continued)

Temperature Average K	Pressure Average psi	Density Experimental kg/m^3	NIST-12 kg/m^3	Relative Deviation %
	Nitrogen	**January-March, 2007**		
264.81	140.73	12.333	12.409	-0.616
264.81	281.28	24.848	24.918	-0.281
264.81	570.05	50.835	50.896	-0.121
264.83	869.53	77.966	78.031	-0.083
264.80	1157.56	104.064	104.100	-0.035
264.83	1425.93	128.069	128.110	-0.032
264.80	2175.78	192.394	192.380	0.007
264.81	2901.11	248.422	248.370	0.021
264.82	3625.31	297.269	297.180	0.030
264.83	4347.92	339.279	339.160	0.035
264.78	5086.98	376.320	376.220	0.027
264.81	7249.29	459.283	459.130	0.033
264.82	10847.85	549.946	549.740	0.037
264.82	14567.06	613.512	613.210	0.049
293.15	140.54	11.111	11.161	-0.448
293.15	281.01	22.309	22.347	-0.172
293.15	569.74	45.362	45.408	-0.101
293.15	869.33	69.258	69.287	-0.042
293.15	1157.17	92.006	92.021	-0.016
293.15	1425.61	112.917	112.930	-0.011
293.15	2158.54	167.720	167.710	0.006
293.15	2899.35	218.488	218.450	0.017
293.15	3620.87	262.794	262.730	0.024
293.14	4348.95	302.420	302.340	0.027
293.15	5077.10	337.417	337.310	0.032
293.15	5793.21	367.897	367.790	0.029
293.15	7276.03	421.122	420.990	0.031
293.15	10878.82	514.098	513.930	0.033
293.17	14503.10	578.711	578.510	0.035
293.16	18219.08	628.968	628.700	0.043
293.15	21907.81	669.071	668.750	0.048
298.14	1451.85	112.643	112.660	-0.015
298.17	4354.14	297.020	296.940	0.027
298.15	7226.56	413.310	413.170	0.034
298.17	10876.10	508.053	507.870	0.036
298.14	14520.46	573.430	573.200	0.040
298.15	18092.21	622.188	621.900	0.046
298.16	21914.31	664.169	663.820	0.053

Table V1.2. (continued)

| Temperature Average K | Nitrogen Pressure Average psi | January-March, 2007 Density | | Relative Deviation % |
		Experimental kg/m^3	NIST-12 kg/m^3	
350.01	141.93	9.361	9.412	-0.539
350.00	431.79	28.460	28.518	-0.204
349.99	713.67	46.861	46.927	-0.141
350.00	866.60	56.756	56.808	-0.091
349.99	1085.48	70.761	70.817	-0.079
350.00	1446.46	93.481	93.497	-0.017
349.99	1999.90	127.050	127.070	-0.016
350.01	2499.57	155.931	155.930	0.000
350.00	2999.34	183.325	183.310	0.008
349.99	3500.23	209.254	209.210	0.021
349.99	4000.55	233.559	233.540	0.008
350.00	4329.56	248.751	248.710	0.017
350.00	5031.51	279.083	279.020	0.023
350.05	7244.18	358.852	358.680	0.048
349.99	10875.20	453.089	452.950	0.031
350.01	14500.55	520.476	520.320	0.030
350.00	18050.35	571.501	571.320	0.032
350.00	21803.18	615.187	615.000	0.030

The relative deviations of density measurements for pure compounds as shown in table VI.2 exist due to random and systematic bias error of the apparatus. For nitrogen, it is between 0.04 to 0.08, for methane it is about 0.1 % and for carbon dioxide, it is about 0.05 on average. Patil (2005) drew conclusions based on extensive density measurements of pure components such as argon, nitrogen and methane that the bias error is inversely related to molecular weight and suggested a tentative equation for correcting the bias error by using the molecular weight. He also suggested that additional density measurement data for fluids with molar mass lower than methane and higher than argon are required to validate the dependence of the relative density deviation or the apparatus bias error on the molar mass. This temperature independent bias error

correction was assumed to apply equally for natural gas mixtures including four gas mixtures measured between 2003 and 2006. They contain 78, 88, 91 and 94 % methane, respectively. The first two samples, measured as a part of this research have not been presented in this dissertation because of reasons of confidentiality while the last two samples have been published elsewhere (Patil, 2005).

In the wake of moving into a new lab in Jack E. Brown building and appearance of new articles shedding light into force transmission error due to magnetic properties of the fluids and surroundings, this kind of molecular based bias error calculation is no longer valid or necessary. A detailed investigation is being carried out in our group right now with the objective of determining apparatus and fluid specific force transmission correction parameters; eventually they will be applied to the pure component 'uncorrected' data presented in this section. No force transmission error analysis has been done on natural gas mixtures in our group or any other group.

The uncertainty of the data comes from temperature and pressure measurements, from the balance readings, from the sinker volume determination and for the mixtures, from the compositions as well. Temperature and pressure uncertainties have been assumed to contribute to random error only; sinker volume and force transmission error uncertainty contribute to systematic or bias error. Random errors are statistical fluctuations in either direction in the measured data caused by the precision limitations of the measurement devices. Bias errors are reproducible inaccuracies that are consistently in the same direction. The combined maximum uncertainty for temperature and pressure up to 5000 psi and in the temperature range of 270 to 340 K is about 0.03 % at 1σ. The total uncertainty, which is a function of temperature and pressure, is dominated by compositional uncertainty. The detailed uncertainty methodology and uncertainty analysis appear in appendix B.
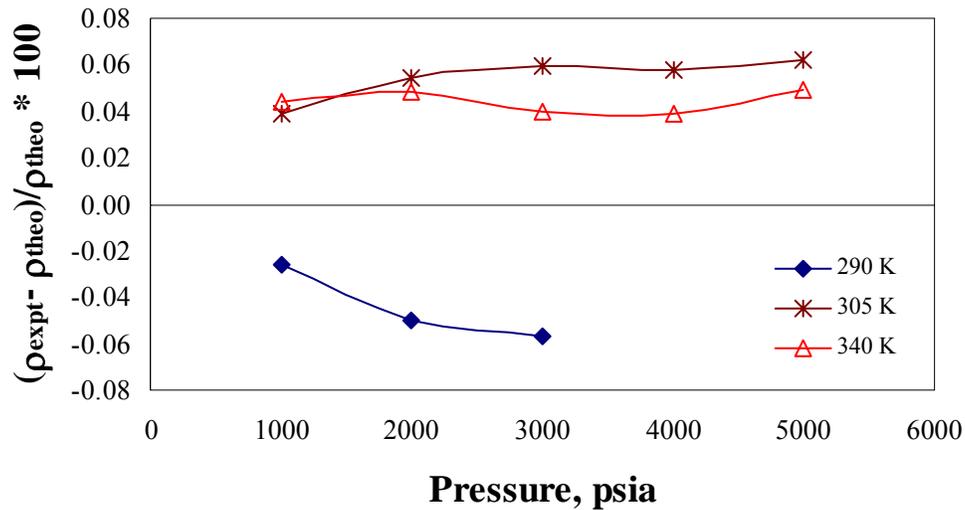
Figure V1.1. Percentage deviation of measured nitrogen densities from NIST-12 measured in 2005
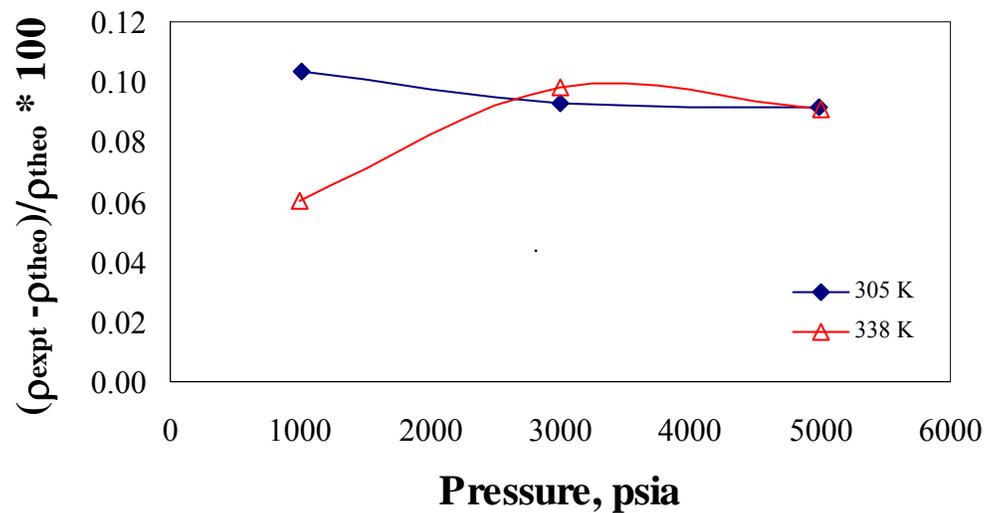

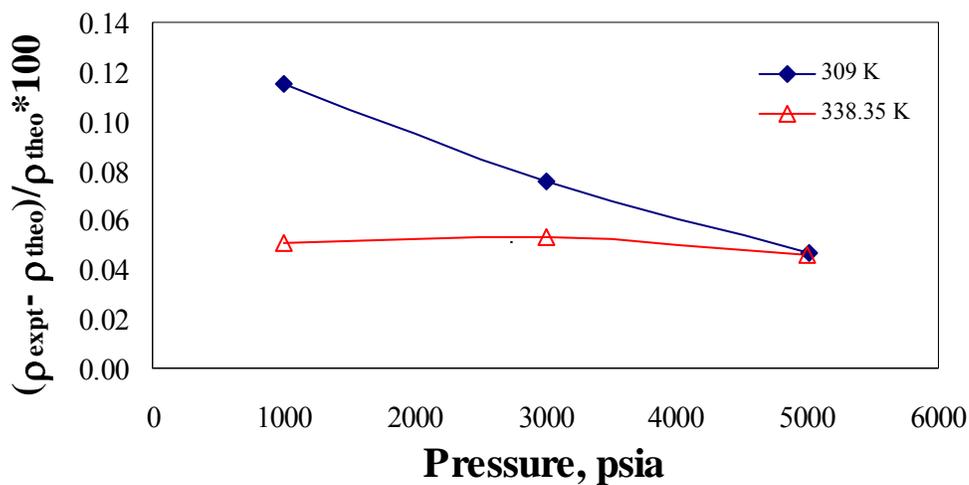Figure V1.2. Percentage deviation of measured methane densities from NIST-12 measured in 2005

Figure V1.3. Percentage deviation of measured carbon dioxide densities from NIST-12 measured in 2006
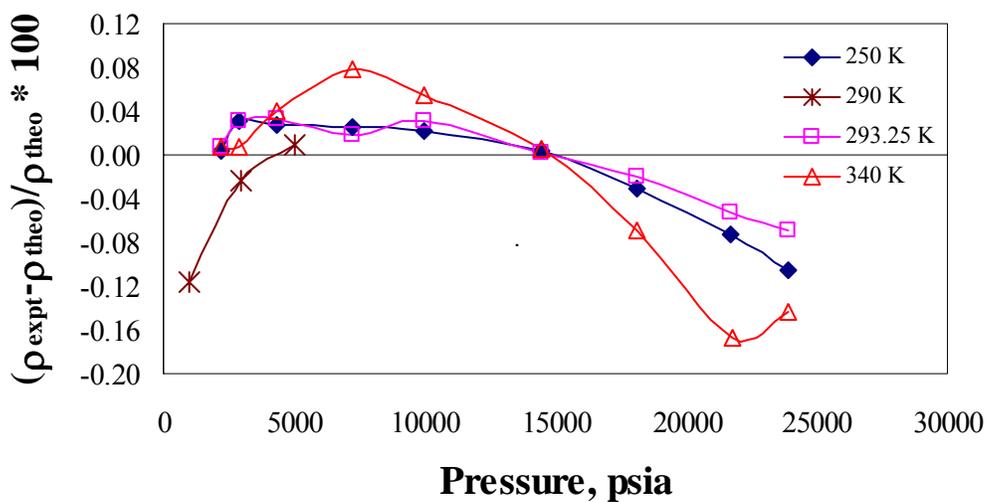
Figure V1.4. Percentage deviation of measured nitrogen densities from NIST-12 measured in 2006
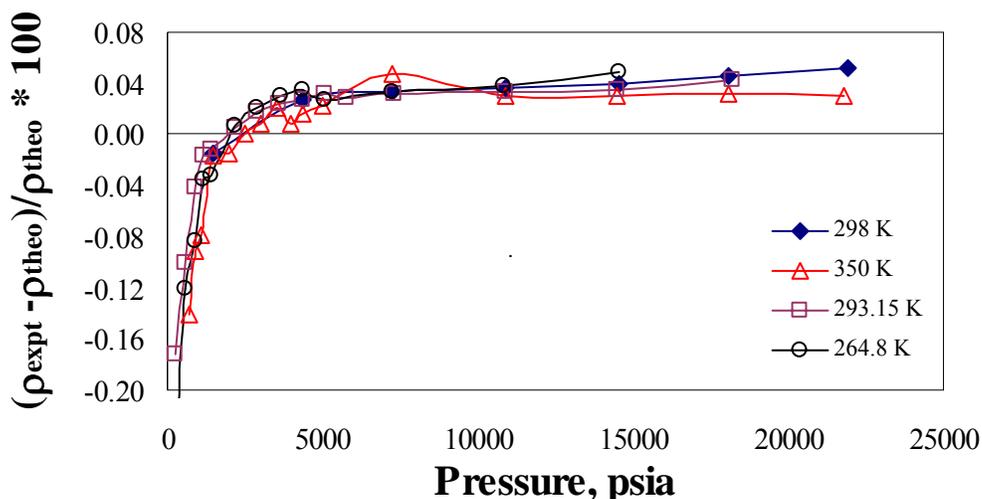
Figure V1.5. Percentage deviation of measured nitrogen densities from NIST-12
measured in 2007

Figures VI.1 to VI.5 show the relative density deviations of density measurements for pure compounds namely nitrogen, carbon dioxide and methane measured between 2005 and 2007.

6.2 Comparison with Pure Component Density from Literature

The pure component densities measured with the magnetic suspension assembly were compared with the literature data available on nitrogen and methane by looking at their deviations from NIST-12 predictions. A close match between our and their data should certify the quality of our work.

Literature data on components with purity of 99.99 mole percent or better were chosen. The data with relatively low uncertainty were favored and most of the data were collected recently; some of those were used to develop the EOS's for nitrogen and methane based on work by Span et al. (2000) and by Setzmann and Wagner (1991), respectively. Where applicable, the temperatures measured with the International Practical Temperature Scale of 1968 (IPTS-68) were converted to the ITS-90 scale using the difference table given by Preston-Thomas (1990).

The literature data on nitrogen include measurements done by Klimeck et al. (1998) using a single-sinker MSA, Nowak et al. (1997 a; 1997 b) using a two-sinker MSA, Pieperbeck et al. (1991) using a two-sinker MSA, and Duschek et al. (1988) using a two-sinker MSA. Jacobson and Stewart (1973) collected data from different sources.

The total experimental uncertainty due to temperature and pressure for pure components in our laboratory is the order of ± 0.03 % as discussed in appendix B. this is generally larger than those measured at Ruhr University in Germany. This is due to the type and range of MSA used in their laboratories. Klimeck et al. (1998) measured nitrogen densities with a single-sinker MSA with a range of 4,350 psia. Nowak et al. (1997 a; 1997 b) used a two-sinker MSA with a range of 1,740 psia for nitrogen measurements, while Kleinrahm et al. (1988) used a two-sinker MSA with a range of 1,160 psia for methane measurements. Pieperbeck et al. (1991) also measured nitrogen and methane densities with a two-sinker MSA with a range of 1,740 psia.

The deviations of the nitrogen data are generally smaller than our data, especially those done by two-sinker methods. Because of the fact that a difference in volume and a difference in mass is used in density calculations as well as the fact that the relative positions of the sinker at measurement and zero point position are almost same, the two sinker method shows superior performance specially at low density. For single sinker densimeter, the deviations at low pressure are high which is evident from the low pressure region in figure VI.5; this is due to low buoyancy force at low density.

The systematic deviations of our data could be improved once we apply the force transmission error. The remaining off set could be attributed to various other factors, as discussed during uncertainty analysis in appendix B.

The systematic shift $\Delta\rho$ is also a function of sinker density, as evident from the following equation (McLinden et al., 2006):

$$\Delta\rho = \left(1 - \varphi\right)\left(\rho_s - \rho_{fluid}\right) \tag{6.1}$$

Where ρ_s is the sinker density and φ is the coupling factor, as discussed in section 3. Instead of using a titanium sinker as used presently, if we could have used a quartz-glass

sinker with the same mass but half the density, the systematic error would have been reduced by half, as evident from equation (6.1). But, as this will require a sinker with twice the present volume, this scenario is not possible to implement because of fixed cell volume. Also, with quartz-glass sinker, the systematic shift will be small only at low fluid densities when fluid and sinker densities are close but not at a large density.

On the other hand, we could use quartz-glass sinker with the same volume as titanium sinker but about half the mass and density. This should reduce the systematic error by 1/2 as well. But low mass of the quartz sinker will limit the operational range of the densimeter at higher fluid density.

The deviations of the nitrogen data are shown in figures VI.6 to VI.8.
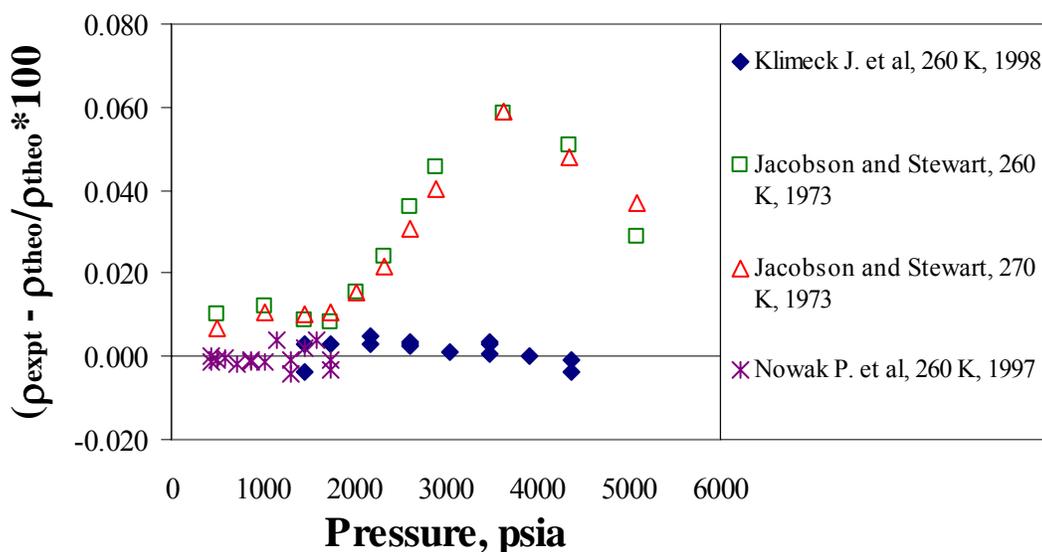
Figure V1.6. Percentage deviation of measured nitrogen densities from NIST-12 by other workers between 260 to 270 K

Equation 6.1 and 2.8 can also be used to explain molecular weight dependant biased error. The closer the density of the gas to the sinker, smaller is the error. So, provided that magnetic properties are similar, gas with larger molecular weight should show smaller error at same temperature and pressure. This conclusion could also be explained by the fact that when fluid density is very close to sinker density, the MSA is

exerting less and less control on the electromagnet by generating less current. Which means less self heating of the electromagnet causing more stability of the balance as well as smaller magnetic fields between electromagnet and permanent magnet leading to less FTE.
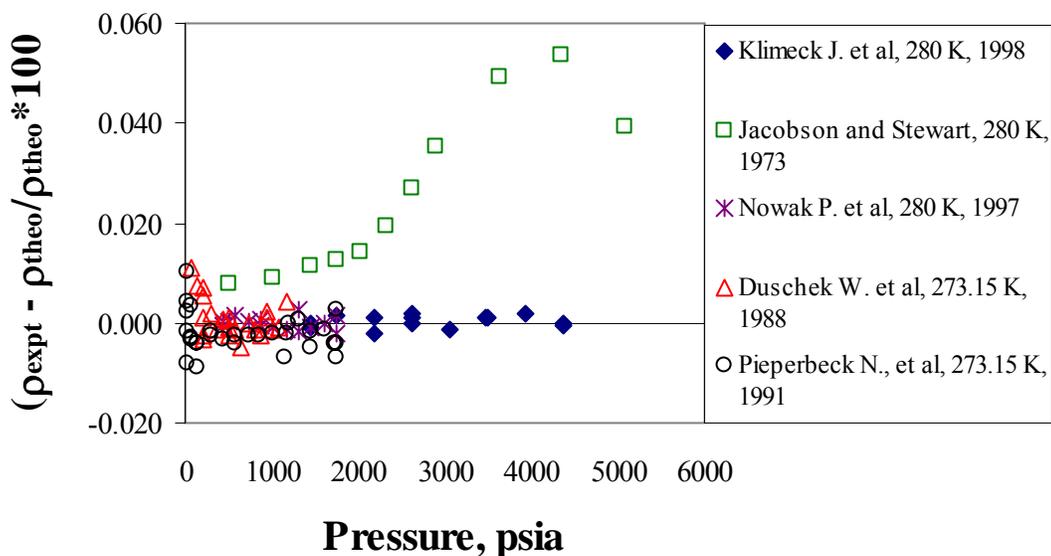
Figure V1.7. Percentage deviation of measured nitrogen densities from NIST-12 by other workers between 273.15 to 280 K

The literature data on methane include measurements done by Händel et al. (1992) using a two-sinker MSA, Pieperbeck et al. (1991) using a two-sinker MSA, Kleinrahm et al. (1988) using a two-sinker MSA, Achtermann et al. (1986) using the refractive index method, Trappeniers et al. (1979) using a piezometer, Douslin et al. (1964) using a pycnometer and Schamp et al. (1958) using the piezometer method. The deviations of the methane data are shown in figures VI.9 to VI.11. Again, a better agreement than our data is observed which can be explained as before.

Figure VI.8. Percentage deviation of measured nitrogen densities from NIST-12 by other workers between 330 to 350 K

Figure VI.9. Percentage deviation of measured methane densities from NIST- 12 by other workers at 260 and 263.15 K

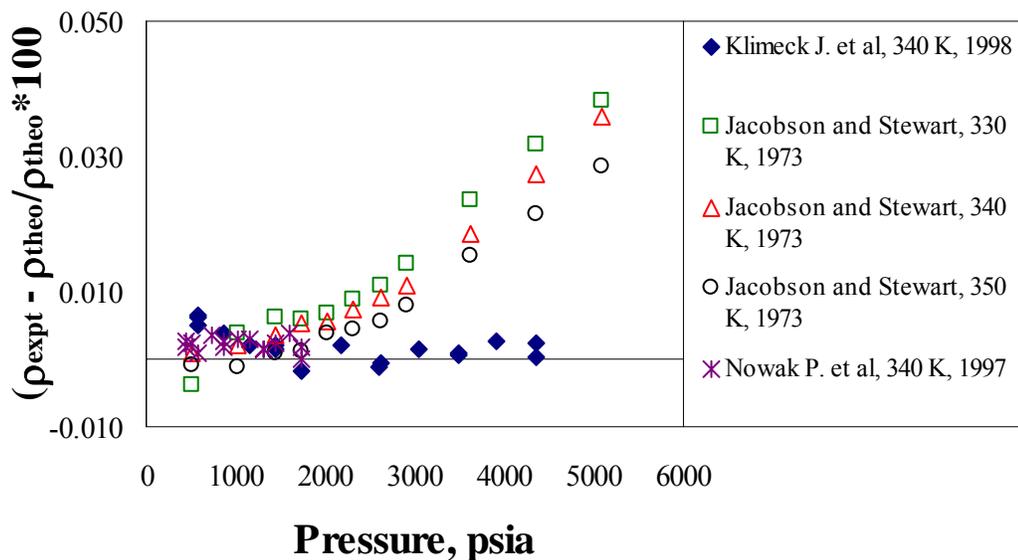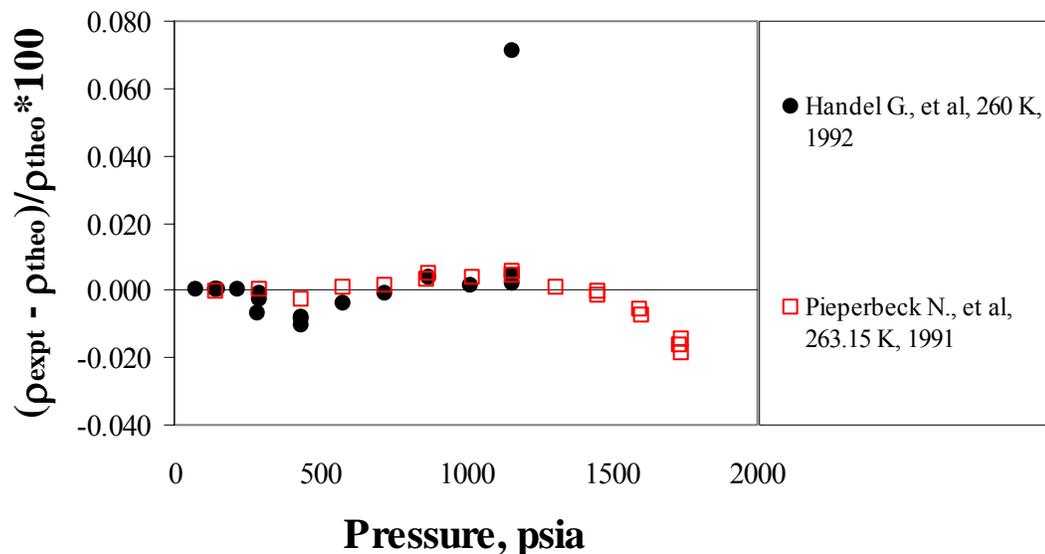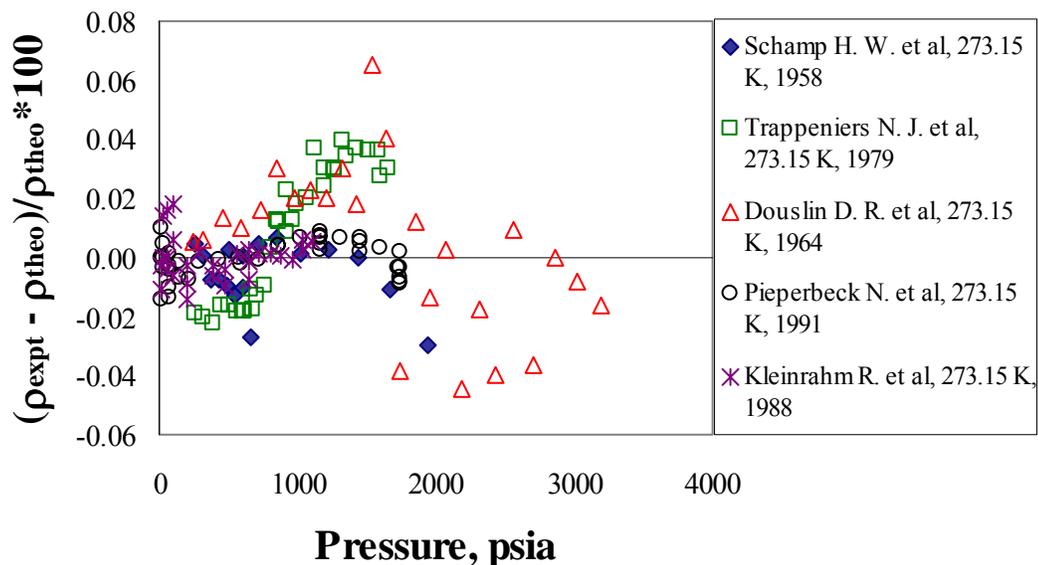Figure VI.10. Percentage deviation of measured methane densities from NIST-12 by other workers at 273.15 K
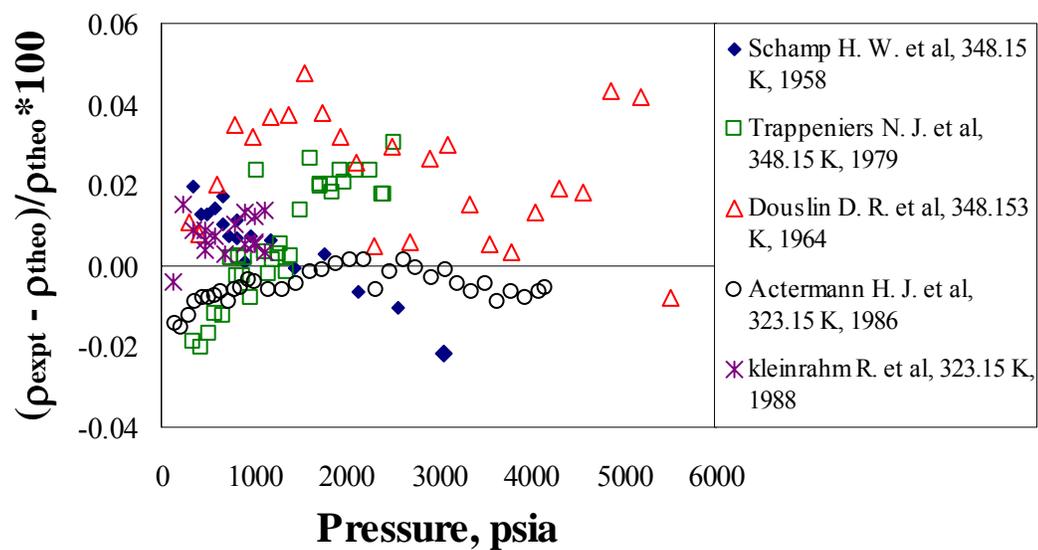
Figure VI.11. Percentage deviation of measured methane densities from NIST-12 by other workers between 323.15 to 348.15 K

6.3 Density Measurements of Natural Gas Mixtures

Density measurements of two synthetic natural gas like mixtures, SNG3 and SNG5 have been presented in this section. The measurements are done to simulate reservoir conditions and this kind of density data is not available in literature.

While filling gas, precautions were taken in order to avoid passing through the two phase region of the sample by keeping temperature of the cell under vacuum above the cricondentherm. Then gas was put into the system and pressure increased above the cricondenbar. Once far way from the two phase region, pressure was decreased by reducing the temperature. Generally we are above 150 psi and 10 deg C from any point on the phase envelope during actual measurements or at any other time. For the same reason, tubes and manifolds are heated all the time. Like pure components, compositions were never checked before or after the measurements.

6.3.1 Density Measurements of SNG3 Natural Gas Mixture

The densities of SNG3 were measured at three different isotherms, 250, 350 and 450 K in the pressure range of 10 to 165 MPa, i.e. from about 1,450 psia to about 23,925 psia. The data were compared with both AGA8-DC92 EOS and GERG02 EOS calculated by REFPROP program. SNG3 have compositions that can be classified as falling under the 'normal range' as defined by the AGA8-DC92 EOS report (American Gas Association, 1992) where the C_{6+} fraction is lower than 0.2%.

The AGA8-DC92 EOS is hybrid in nature; i.e. it combines a virial equation of state for low-density conditions and exponential functions for high-density conditions. It provides high accuracy, broad temperature-pressure-composition application range and derived thermodynamic property capabilities (AGA, 1992).

In AGA8-DC92 EOS, the targeted uncertainty for natural gas compressibility factors using the detail characterization method can be divided in to four regions. In region 1 that spans over the range 265 to 335 K up to 1,740 psia, the relative density

deviations from the AGA8-DC92 EOS predictions were expected to be lower than ±0.1% for SNG3. In region 2 that covers the range of 211 to 394 K and 1,740 to 2,465 psia, the relative density deviations from the AGA8-DC92 EOS predictions were

expected to be lower than ± 0.3. In region 3 between the range of 144 to 477 K and 2465 to 10,150 psia, the density deviations should be less 0.5 %. In region 4 between the range of 144 to 477 K and above 10,150 psia, the density deviations should be less 1.0 %. The normal range of composition gives range of gas characteristics for which the average expected uncertainty corresponds to the uncertainties just discussed. The composition and phase envelop for SNG3 appear in table VI.3 and figure VI.12, respectively.

Table VI.3. SNG3 gas mixture composition

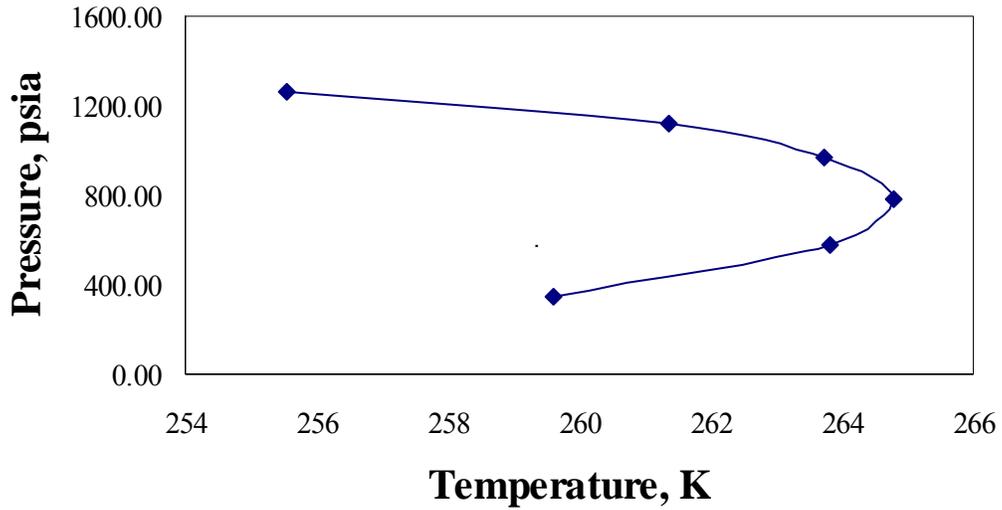| Component	Concentration %
Methane	89.982
Ethane	3.009
Propane	1.506
i-Butane	0.752
n-Butane	0.753
i-Pentane	0.3
n-Pentane	0.3
Nitrogen	1.697
Carbon Dioxide	1.701

Figure VI.12. Phase envelope of SNG3 gas mixture (Martinez, 2006)
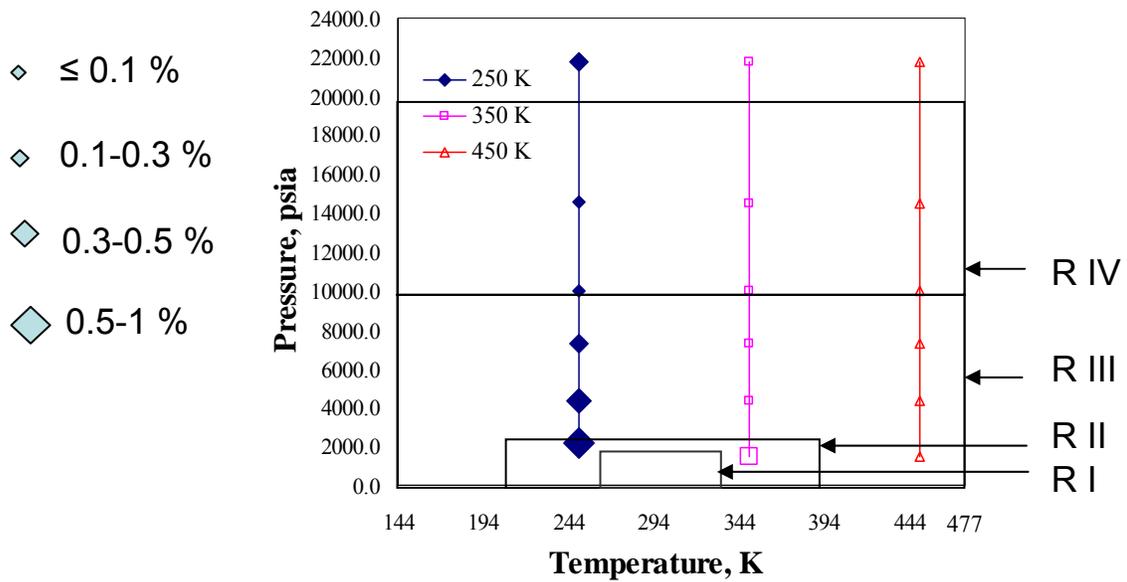

Figure VI.13. Evaluation of SNG3 gas mixture data w.r.t. AGA8-DC92

Figure VI.13 shows the relative performance of SNG3 density measurement with respect to AGA8 EOS. Based on temperature and pressure, the lowest pressure point at 250 K should lie in region 2. However, as the % deviation is in between 0.5 to 1.0 %, it is actually in region 4. Except for this point, all other points either meet the minimum % deviation criteria or exceed it. This is something to be expected as SNG3 is a 'lean mixture', i.e. the composition falls in the 'normal range'. The first point, which lays out side the expected region, is at 250 K and at 2174.88 psi. At this pressure, the MSA should perform well and condensation can easily be ruled out. This might indicate that at low temperature and pressure, AGA8 might need more reliable and exhaustive data to modify its parameters.

The data were also compared with GERG02 EOS. This equation for natural gas is the first accurate equation that can be used to calculate thermal and caloric properties in the gas, liquid and super critical region as well vapor-liquid phase equilibrium calculations. This equation was developed based on multi fluid approximation; i.e. pure substance equation for each component and experimental data for binary mixtures were used. As a result, the representation of multi component mixture is predictive. It has been claimed that the results calculated with this equation for thermal and caloric properties of natural gas mixtures have shown improvements over AGA8-DC92 EOS (Jaeschke et al. 2003). The major drawback of this equation is that it is based on limited set of data as well as the fact that no natural gas mixtures were used as a data base. Generally, AGA-8 has performed better than GERG02 for SNG3 predictions.

Equations of state for each of the main components of natural gas, namely methane, ethane, nitrogen, carbon dioxide etc have been developed. The equations for methane, ethane and nitrogen have an identical structure of 24 terms while the equation for carbon dioxide consists of 22 terms. Typical deviations of calculated densities from experimental data are approximately ± 0.03% for gas and supercritical fluids and ± 0.05% for liquids. Simple equations of states with 12 terms are used for secondary and minor components such as propane, n-butane and isobutane, n-pentane and isopentane, argon and oxygen. The deviations are about ± 0.1% for secondary components and ±

0.1% to ± 0.2% for minor components, for gas, supercritical and liquid regions. The natural gas reference equation is explicit in the reduced Helmholtz energy. The uncertainty in density of typical natural gases is less than ± 0.1% for temperatures from 250 to 350 K and pressure up to 30 MPa (4,350 psia). Outside this range at lower temperature, the thermodynamic properties are calculated within the experimental uncertainty of the best available data. On the other hand, AGA8-DC92 can not accurately describe the data at the lowest temperature especially for nitrogen rich gases, where deviations of -0.2% can occur (Jaeschke et al., 2003).

For LNG like mixtures, the GERG02 equation can reproduce experimental liquid saturated densities to within ± 0.2% where widely used Peng-Robinson EOS can deviate by more than 10%. Gas densities were also calculated for gas mixtures containing high fractions of ethane (up to 20%), propane (up to 14%) and butane (up to 6%). Gas densities measured in the temperature range of 310 to 360 K and pressures up to 30 MPa and at lower temperatures below the two phase regime are calculated by the GERG02 EOS within ± 0.1% to ± 0.2%. The AGA8-DC92 equation does not accurately predict the densities of these gas mixtures.

This new equation is able to describe accurately hythane mixtures, i.e. natural gas mixtures containing a high fraction of hydrogen. For natural gases containing a large fraction of hydrogen (10% hydrogen) or for methane-hydrogen binary mixtures containing up to 75% hydrogen, the equation predicts densities which are accurate within ± 0.1% in the temperature range of 270 to 350 K and pressures up to 30 MPa. For the special gas mixtures containing high fractions of hydrogen, nitrogen and carbon monoxide, the equation is in agreement within ± 0.1% whereas the AGA8-DC92 equation can deviate by 0.3% to 0.7%.

The experimental density data for SNG3 are presented in table VI.4, the comparisons with AGA8 and GERG02 EOS are shown in the same table.

Table VI.4. Measured density data of SNG3 gas mixture

Temperature Average K	Pressure Average psi	SNG3 Experimental kg/m^3	June, 2006 Density AGA8-DC92 kg/m^3	GERG kg/m^3	Relative Deviation AGA8-DC92 %	GERG %
249.99	2174.88	231.579	233.666	231.820	-0.893	-0.104
250.03	4350.94	316.531	317.639	315.320	-0.349	0.384
250.06	7250.89	361.487	362.148	360.190	-0.183	0.360
249.99	10003.48	387.768	388.049	386.520	-0.073	0.323
250.00	14535.32	417.775	417.549	416.600	0.054	0.282
249.97	21734.63	450.514	449.693	449.510	0.183	0.223
349.98	1450.09	70.377	70.457	70.423	-0.113	-0.065
350.02	4349.42	200.129	200.080	199.81	0.024	0.160
350.03	7250.28	270.002	269.967	269.32	0.013	0.253
349.99	9999.05	309.537	309.553	308.76	-0.005	0.252
350.03	14496.16	351.821	351.843	350.98	-0.006	0.240
350.01	21742.86	395.616	395.580	394.76	0.009	0.217
449.99	1449.54	50.366	50.411	50.392	-0.090	-0.052
450.00	4347.65	142.400	142.361	142.29	0.027	0.077
450.00	7249.07	208.003	207.870	207.71	0.064	0.141
450.00	9999.50	251.034	251.014	250.66	0.008	0.149
449.99	14498.93	299.531	299.580	299.07	-0.016	0.154
450.00	21740.93	350.208	350.155	349.72	0.015	0.140

The relative deviations of experimental density values for SNG3 from AGA8-DC92 and GERG02 EOS are shown in figures VI.14 to VI.16.
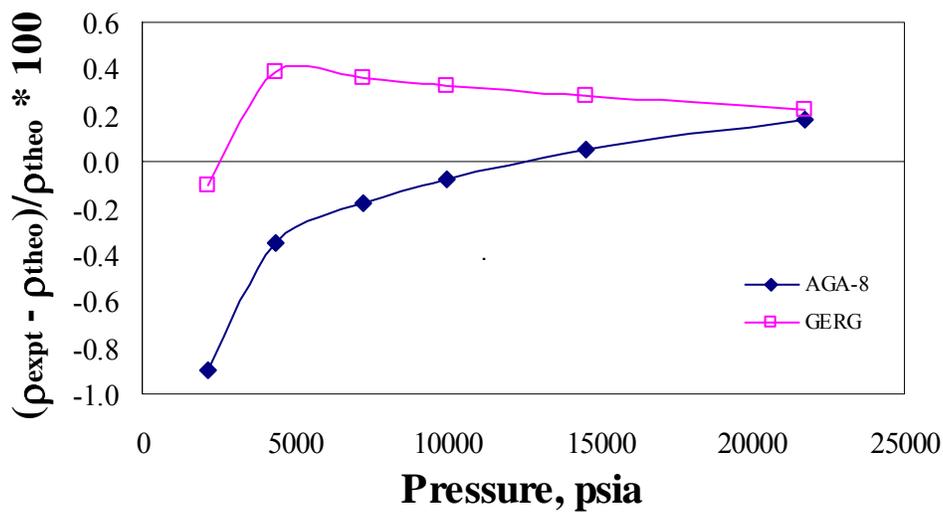
Figure VI.14. Percentage deviation of SNG3 measured densities from AGA8-DC92 and GERG02 EOS at 250 K

Figure VI.15. Percentage deviation of SNG3 measured densities from AGA8- DC92 and GERG02 EOS at 350 K
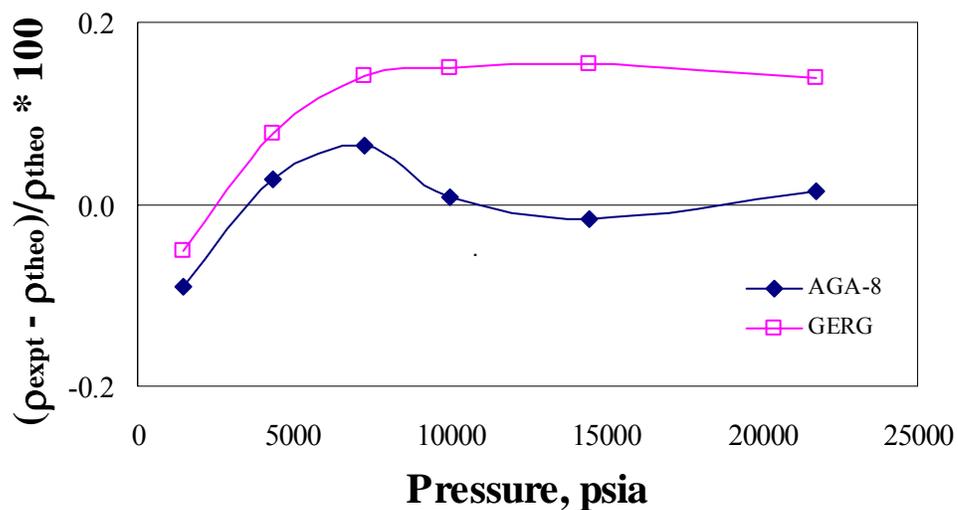
Figure VI.16. Percentage deviation of SNG3 measured densities from AGA8-DC92 and GERG02 EOS at 450 K

6.3.2 Density Measurements of SNG5 Natural Gas Mixture

Table VI.5. SNG5 gas mixture composition

Component	Concentration %
Methane	89.975
Ethane	2.885
Propane	1.427
i-Butane	0.709
n-Butane	0.722
i-Pentane	0.45
n-Pentane	0.45
Nitrogen	1.713
Carbon Dioxide	1.669

Similar to SNG3, the densities of SNG5 were measured at three different isotherms, 250, 350 and 450 K in the pressure range of 10 to 165 MPa, i.e. from about 1,450 psia to about 23,925 psia. Likewise, the data were compared with both AGA8-

DC92 EOS and GERG02 EOS calculated by REFPROP program. SNG5 also have compositions that can be classified as falling under the 'normal range'.

Table VI.5 shows the compositions of SNG5 while figure VI.17 shows the phase envelop of the mixture.
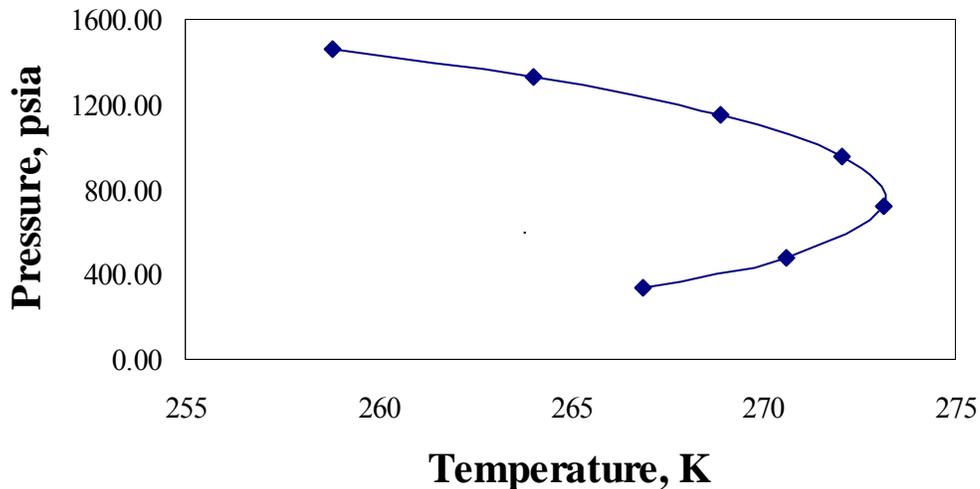
Figure VI.17. Phase envelope of SNG5 gas mixture (Martinez, 2006)
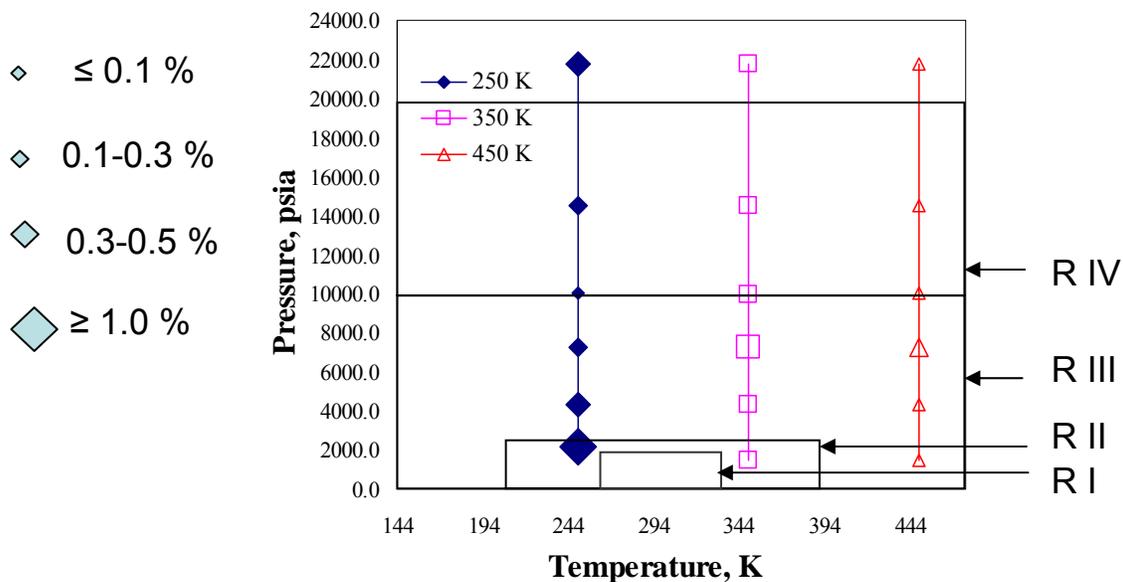
Figure VI.18. Evaluation of SNG5 gas mixture data w.r.t. AGA8-DC92

SNG3 and SNG5 have similar compositions but SNG3 has 0.6 mole % pentane while SNG5 has 0.9 mole percent pentane. This has a dramatic effect on the phase envelopes. The cricondenbar (CB) of SNG3 is 1263 psi at 255.5 K and cricondentherm (CT) is 265.8 K at 780 psi. Whereas for SNG5, CB is 1460 psi at 259 K and CT is 273.15 K at 719 psi

Figure VI.18 shows the relative performance of SNG5 density measurement with respect to AGA8 EOS. Again, except for the lowest pressure point at 250 K, all other points either meet the minimum % deviation criteria or exceed it.

Table VI.6. Measured density data of SNG5 gas mixture

Temperature Average	Pressure Average	SNG5 June, 2006 Experimental	Density AGA8-DC92	GERG	Relative Deviation AGA8-DC92	GERG
K	psi	kg/m^3	kg/m^3	kg/m^3	%	%
249.95	2171.46	232.906	235.762	233.470	-1.211	-0.241
249.95	4346.16	317.745	319.286	316.280	-0.483	0.463
250.02	7251.64	363.004	363.597	360.910	-0.163	0.580
250.03	10002.65	389.228	389.329	387.060	-0.026	0.560
249.95	14485.79	419.218	418.553	416.840	0.159	0.571
250.01	21749.30	452.432	450.973	449.950	0.323	0.552
349.95	1448.59	70.740	70.828	70.793	-0.125	-0.075
349.98	4350.72	201.849	201.293	200.890	0.276	0.477
350.01	7250.20	272.370	271.174	270.210	0.441	0.799
349.98	9990.35	311.091	310.641	309.430	0.145	0.537
349.98	14487.59	353.832	352.966	351.570	0.245	0.643
350.01	21739.28	398.053	397.520	395.260	0.134	0.707
449.99	1450.93	50.688	50.727	50.710	-0.076	-0.043
449.99	4347.65	143.202	143.103	142.990	0.069	0.148
450.00	7248.72	209.053	208.803	208.500	0.120	0.265
450.03	9998.38	252.160	251.994	251.410	0.066	0.298
449.99	14497.71	300.704	300.617	299.760	0.029	0.315
450.00	21744.76	351.438	350.340	350.340	0.036	0.313

Measured data of SNG5 appear in table VI.6. The lowest pressure point (2171.458 psi) at 250 K is badly predicted by AGA8-DC92, as was the case in SNG3. Both the samples have similar compositions; however there is a slight difference in heptane composition. This causes a significant difference in density as well as phase behavior as evident from figures VI.12 and VI.17.

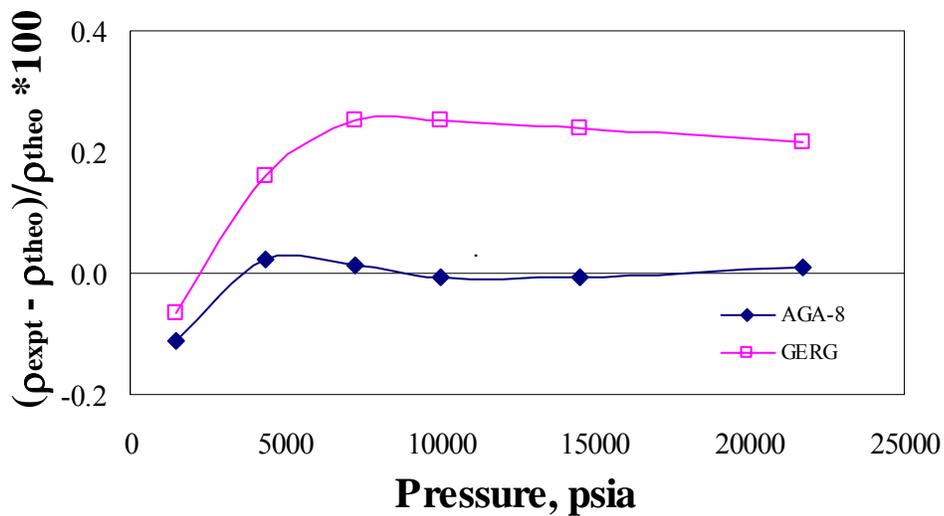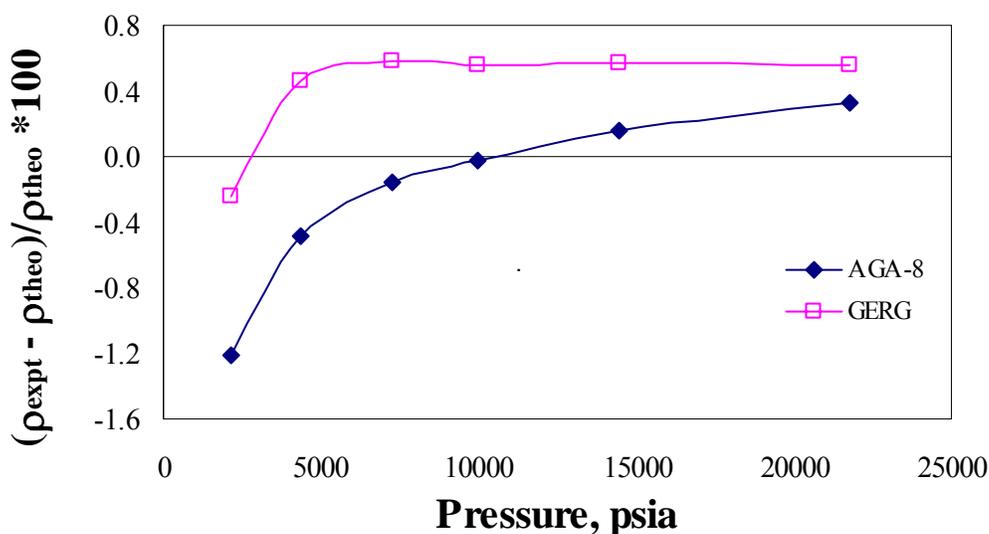Figure VI.19. Percentage deviation of SNG5 measured densities from AGA8-DC92 and GERG02 EOS at 250 K

The relative deviations of experimental density values for SNG5 from AGA8-DC92 and GERG02 EOS are shown in figures VI.19 to VI.21.

The % deviation profiles with respect to both the EOS's are very similar for both the samples at 250 K and 450 K. However, at 450 K for SNG5, % deviations for GERG02 is much larger than in the case of SNG3; which may be due to the limited volume of reference data used to develop GERG02 EOS.

For both the samples, even though almost all the points are within their regions of uncertainty (wrt AGA8), at some temperatures, significant % density deviations are observed near the pressures of custody transfer; this may render AGA8 unsuitable for
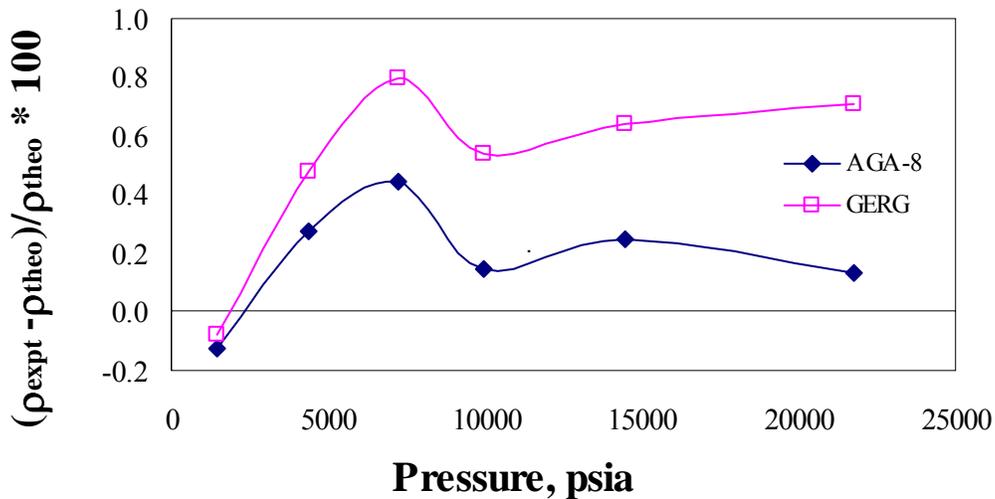
Figure VI.20. Percentage deviation of SNG5 measured densities from AGA8-DC92
and GERG02 EOS at 350 K
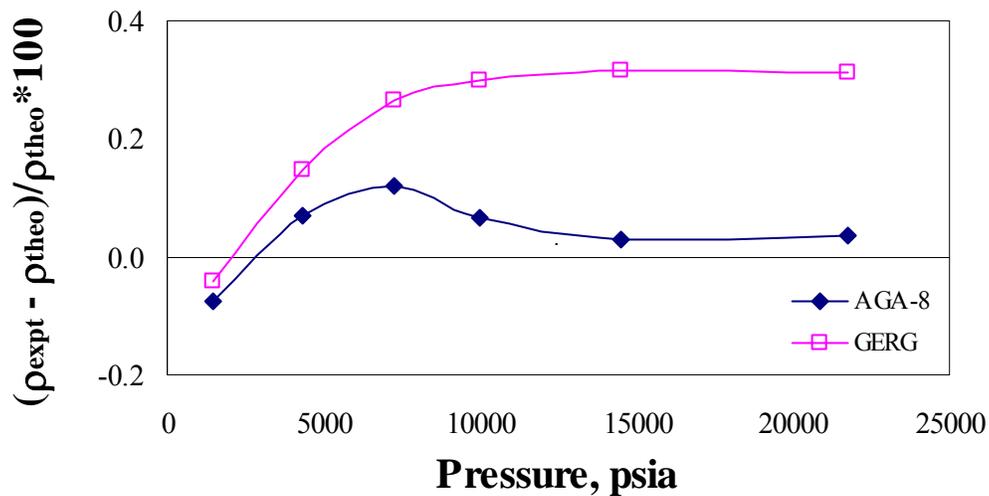
Figure VI.21. Percentage deviation of SNG5 measured densities from AGA8-DC92
and GERG02 EOS at 450 K

custody transfer in some cases. On the other hand, AGA-8 has performed better than
GERG02 for SNG5 predictions as was the case for SNG3.

7. CONCLUSIONS AND RECOMMENDATIONS

7.1 Conclusions

(1)   An experimental set up capable of measuring gas density in the temperature range of 200 to 523 K and in the pressure range of 0 to 30,000 psia has been set up. The heart of this set up is a magnetic suspension densimeter built by Rubotherm Präzisionsmesstechnik . This has been used to measure pure component densities like nitrogen, methane, carbon dioxide and argon for calibration purposes as well as Gulf of Mexico gases such as M88C1 and M78C1 for the purpose of gas custody transfer. These densities have been measured in the temperature range of 270 to 340 K and in the pressure range of 500 to 5,000 psia. For reasons of confidentiality, these data are not appearing in the dissertation. Pure component density (nitrogen) has been used for calculating force transmission error and uncertainty in sinker volume.

(2)   Pure component densities were compared with NIST-12 program and they generally agree within $\pm$ 0.05 to 0.1 % which shows the reliability of the data.

(3)   Densities of four synthetic natural gas mixtures (SNG3, SNG4, SNG5, and SNG6) were measured in the temperature range of 250 to 450 K and in the pressure range of 1450 to 21,750 psi. The objective is to simulate reservoir conditions and build a data base for future development of an EOS with a wide temperature and pressure range. SNG3 and SNG5 data are presented in the dissertation.

(4)   These synthetic mixtures (SNG3, SNG5) with compositions in the 'normal range' of the American Gas Association (1992) show less than expected deviations predicted by AGA8-DC92 EOS in region 2, 3 and 4 except at low temperature in region 2. Small numbers of points were collected in region 2 and no points in region 1. More data are required to validate the previous observations (Patil, 2005) where larger than the expected deviations of $\pm$ 0.1% and $\pm$ 0.3% from the AGA8-DC92 EOS predictions were observed in regions 1

and 2 respectively, for light mixture. These regions cover the most relevant ranges of pressure and temperature for natural gas custody transfer.

(5)   For the synthetic gas mixtures, AGA8 showed better predictions than GERG02 EOS. GERG02 is generally based on low pressure data with high accuracy ensured only up to 35 MPa or 5,075 psi. Also, the volume of the data base is relatively small and it contains data only on pure and binary mixtures. Compared to GERG02 EOS, AGA8-DC92 EOS used vast number of real samples with a wider range of compositions.

(6)   Force transmission error for the apparatus, using only nitrogen, was calculated to be 25 ppm.

(7)   The maximum total uncertainty in the density measurement has been estimated to be 0.11%. It has been observed that compositional uncertainty dominates the total uncertainty

7.2 Recommendations

(1)   Because of the uncertainty associated with AGA8 EOS, more high quality density data is required to validate, modify or altogether replace AGA8 EOS. AGA8 EOS is a semi-empirical virial type EOS whose parameters are determined from statistical fit of data. Parameters determined for one region of temperature and pressure may not be valid in a different region. Binary interaction parameters between one particular component and other similar components sometimes do not show any trend. Some binary interaction parameters such as that between methane and ethane is non existent. Binary interaction of components such as oxygen, carbon monoxide with other components is hardly accounted for. These problems as well as physically unrealistic interaction parameters and presence of heavy fractions limit the accuracy as well range of AGA8 EOS.

Measurements should be made with compositions both in 'normal range' as well as in 'expanded range'. Binary mixtures of similar hydrocarbons and dissimilar

hydrocarbons as well as binary mixtures containing hydrocarbons and oxygen, carbon monoxide, nitrogen, hydrogen sulfide and carbon dioxide should be measured to determine binary parameters some of which are yet to be determined. Three body interaction parameters should also be measured to make the AGA8 work near critical region. Multi component mixtures should also be measured to extend its applicability over a wider range of compositions. The same data base could be used to develop an entirely new EOS that is more accurate than the AGA8-DC92 EOS over wider ranges of temperature, pressure and composition.

(2) Extensive density measurements of air, oxygen, methane and other fluids should be done to determine fluid specific force transmission error. These data should also be used to confirm the apparatus force transmission error already determined with nitrogen. This apparatus error should be independent of temperature, pressure and composition. Methods should be investigated to apply the fluid specific error to mixtures.

(3) As evident from uncertainty analysis, the uncertainty in composition contributes most to the overall uncertainty. A mixing apparatus in the lab could be put to use to produce gas mixtures in the lab. Composition should also be measured after density measurement as suggested by Dr. McLinden of NIST.

(4) The optimum values of the volume expansivity and isothermal compressibility factors of the isochoric apparatus should be determined by combining isochoric and magnetic suspension densimeter data to check whether they match with literature data. Through investigation should be done to determine whether these values are functions of pressure, temperature and cell geometry.

(5) The single sinker densimeter data should be compared with two-sinker densimeter data from NIST. This will help us to calibrate single sinker at low density region where the inaccuracies are larger compared to high density region. This will also give us some idea about the force transmission error which is very small for two-sinker densimeter.

(6)   Sinker volume uncertainty as a function of temperature should be determined using the concept of density-ratio gas thermometer discussed in the appendix D. Low pressure density measurements should be done at various isotherms for different gases for the purpose of verification.

(7)   More low pressure data (up to 3,000 psi) at smaller temperature- intervals, near and away from the phase boundary, are required for synthetic light mixtures to check the consistency between the magnetic suspension densimeter data and isochoric apparatus data.

(8)   The system can be fully automated by modifying the system for automatic filling of the cell. A very high pressure vessel could be installed upstream of the cell. Initially the vessel should be filled with compressed gas by the operator. A solenoid valve, placed in between the vessel and the cell could be opened by transistor-transistor logic. The logic could be sent once a balance stability criterion has been achieved or a time-out has occurred. Once the desired pressure has been reached, the solenoid will close. The pressure and balance Labview programs need to be combined into a one big program for this purpose.

Rupturing of the vessel is the only factor that might pose a safety concern. Use of double walled vessel might alleviate the concern.

LITERATURE CITED

Achtermann, H. J., T. Bose, H. Rogener, and J. M. St-Arnaud, "Precise determination of the compressibility factor of methane, nitrogen, and their mixtures from refractive index measurements," *International Journal of Thermophysics*, **7 (3),** 709-720 (May 1986).

Albert, W. C., "Vibrating Quartz Crystal Beam Accelerometer," *28th International Instrumentation Symposium,* Las Vegas, NV, 28, 1, 33-44 (1982).

Albert, W. C., "Force Sensing Using Quartz Crystal Flexure Resonators," *Proceedings of the 38th Frequency Control Symposium*, Philadelphia, PA, 233-239 (1984).

American Gas Association (AGA), "Compressibility Factors of Natural Gas and Other Related Hydrocarbon Gases" Transmission Measurement Committee Report No 8 (1992).

Ando, T., Y. Isobe, D. Sunohara, Y. Daisho, and J. Kusaka, "Homogeneous Charge Compression Ignition and Combustion Characteristics of Natural Gas Mixtures: The Visualization and Analysis of Combustion" Society of Automotive Engineers of Japan Review, **24**, 33-40 (2003).

Bateson, R. N., *Introduction to Control System Technology*, Sixth Edition Prentice-Hall, Inc., Upper Saddle River, NJ, 281-294 (1999).

Beams, J. W., and A. M. Clarke, "Magnetic Suspension Balance Method for Determining Densities and Partial Specific Volumes," *The Review of Scientific Instruments*, **33** (7), 750-753 (July 1962).

Berry, M.V., and A.K. Geim, "Of Flying Frogs and Levitrons," *European Journal of Physics,* 18, 307 (1997).

Beyer R.V., Bolland O., "Coal Power Generation", Compendium for the course SIO7005 "Energi & Miljø" (Energy & Environment), Norwegian University of Science and Technology, (December 1998).

Bignell, Noel, "Magnetic Flotation in Densimetry," *Measurement Science and Technology*, **17,** (10), 2574-2580 (2006).

Blanke W., G. Klingenberg, and R. Weiss, "PVT Measurements on Tetrafluoroethane (R134a) along the Vapor-Liquid Equilibrium Boundary between 288 and 373 K and

in the Liquid State from the Triple Point to 265 K," *International Journal of Thermophysics*, **16 (5)**, 1143-1153 (September 1995).

Blanke W., G. Klingenberg, and R. Weiss, "PVT Measurements on 1-Chloro-1-2-2-2-Tetrafluoroethane (R124) along the Gas-Liquid Boundary Curve between 293 K and 395 K and in the Liquid State from 120 K to 268 K," *Journal of Chemical and Engineering Data,* **41** (3), 576-580 (1996).

Booras, G. S., and S. C. Smelser, "An Engineering and Economic Evaluation of CO_2 Removal from Fossil Fuel-Fired Power Plants," *Energy*, **16**, 1295-1305 (1991).

BP, "BP Statistical Review of World Energy," available at http://www.bp.com (June 2006).

BP web site, http://www.bp.com/sectiongenericarticle (November 2006).

Canfield, F. B., T. W. Leland, and R. Kobayashi, "Compressibility Factors for Helium-Nitrogen Mixtures," *Journal of Chemical and Engineering Data*, **10**, 92-96 (1965).

Claus P., R. Kleinrahm, and W. Wagner, 'Measurements of The (P, P, T) Relation Of Ethylene, Ethane, and Sulphur Hexafluoride in the Temperature Range from 235 K to 520 K at Pressures up to 30 MPa Using an Accurate Single-Sinker Densimeter", *The Journal of Chemical Thermodynamics*, **35**, 159-175 (2003).

Cockett, A. H., K. Goldman, and N. G. Scrase, "The Density of Liquid Nitrogen from 85 to 120 deg K and from the Saturation Boundary to 200 atm," Proceedings of the Second International Cryogenic Engineering Conference: Brighton, England, 276-280 (1968).

Crain, R. W. Jr., and R. E. Sonntag, *Advanced Cryogenic Engineering,* **11**, 379-391 (1966).

Daridon, J. L., A. Lagrabette, and B. Lagourette, "Speed of Sound, Density, and Compressibilities of Heavy Synthetic Cuts from Ultrasonic Measurements under Pressure," *The Journal of Chemical Thermodynamics*, **30**, 607-623 (1998).

Davis, L. A., and R. B. Gordon, "Compression of Mercury at High Pressure," *The Journal of Chemical Physics*, 46 (7), 2650-2660 (April 1967).

Dow Corning, Dow Corning 550 Fluid, http://www.dowcorning.com (accessed on January 2007).

Eubank, P. T., L. L. Joffrion, M. R. Patel, and W. Warowny, "Experimental Densities and Virial Coefficients for Steam from 348 to 498 K with Correction for Adsorption Effects," *The Journal of Chemical Thermodynamics,* 20, 1009-1034 (1988).

European Carbon Dioxide Network, "Capturing and Storing Carbon Dioxide: Technical Lessons Learned," September 2004, http://www.co2net.com/infocentre/reports.

Exxon Mobil, "Tomorrow's Energy: A Perspective on Energy Trends, Greenhouse Gas Emissions and Future Energy Options," http://www.exxonmobil.com (accessed on February 2006).

Friedman, A. S., "Pressure-Volume-Temperature Relationships of Gaseous Hydrogen, Nitrogen and a Hydrogen-Nitrogen Mixture," PhD Dissertation, Ohio State University, Columbus, OH (1950).

Fujii, K., M. Takenaka and K. Nara, "New Densimeter for Cryogenic Fluids by Magnetic Levitation of a High-T_c Superconductor," *The Review of Scientific Instruments*, **59** (12), 2539-2543 (December1988).

Fujii, K., "Present State of The Solid and Liquid Density Standards," *Metrologia*, 41, S1 (2004).

Gast, T., "A New Magnetic Coupling for the Separation of Microbalance and Reaction Vessel in Experiments with Controlled Atmospheres," *Thermochimica Acta*, **24,** 247- 250 (1978).

Geim, A. K., M.D. Simon, M.I. Boamfa, and L.O. Heflinger, "Magnet Levitation at Your Fingertips," *Nature*, 400, 323 (1999).

Hales, J. L., "An Apparatus for Accurate Measurement of Liquid Densities Over an Extended Temperature Range," *Journal of Physics*, E 3, 855-861 (1970).

Hart Scientific manual, published by Hart Scientific Inc., American Fork, UT (2002).

Haynes, W. M., M. J. Hiza, and N V. Frederick, "Magnetic Suspension Densimeter for Measurements on Fluids of Cryogenic Interest," *The Review of Scientific Instruments*, **47** (10), 1237-1250 (October 1976).

International Energy Agency, "World Energy Outlook 2004 Edition," 2004, http://www.worldenergyoutlook.org (accessed on October 2006).

Iwagai K, T. Masuda, H. Sato, and K. Watanabe, *Proceedings of 20th Japan Symposium on Thermophysical Properties, Japan Society of Thermophysical Properties, Tokyo, Japan*, 197-200 (1999).

Jacobsen, R. T., R. B. Stewart, and J. Jahangiri, *J. Phys. Chem. Reference Data*, **15**, 735-909 (1986).

Jaeschke, M., H.-M. Hinze, H. J. Achtermann, and G. Magnus, "PVT data from Burnett and Refractive Index Measurements for the Nitrogen—Hydrogen System from 270 to 353 K and Pressures to 30 Mpa," *Fluid Phase Equilibria*, **62** (1-2), 115-139 (1991).

Jaeschke, M., A. Benito, A. Fredheim, J. M. Henault, B. Viglietti, P. Van Wesenbeeck, R. Klimeck, O. Kunz, and W. Wagner, "GERG02 Project: Wide-Range Reference Equation of State for Natural Gases," *Gas - und Wasserfach. Gas – Erdgas*, 144 (7), 430-435 (2003).

Judkins, R. R., W. Fulkerson, and M. K. Sanghvi, "The Dilemma of Fossil Fuel Use and Global Climate Change," *Energy & Fuels*, **7,** 14-22 (1993).

Keller, G. E., and M. M. Bhasin, "Synthesis of Ethylene via Oxidative Coupling of Methane: I. Determination of Active Catalysts", *Journal of Catalysis*, 73 (1), 9-19 (1982).

Kinoshita M., and K. Fujii, *Proceedings of 20th Japan Symposium on Thermophysical Properties, Japan Society of Thermophysical Properties, Tokyo, Japan*, 555-559 (1999).

Kleinrahm, R., and W. Wagner, "Development and Construction of a Density Measurement Apparatus for Measurement of Boiling and Dew Densities of Pure Fluids over the Complete Phase Boundary Curve," *Progress Reports of the VDI Journals*, 3 (92) (1984).

Kleinrahm, R., and W. Wagner, "Measurement and Correlation of the Equilibrium Liquid and Vapour Densities and the Vapor Pressure along the Coexistence Curve of Methane," *Journal of Chemical Thermodynamics*, **18**, 739-760 (1986).

Klimeck J., *Dissertation*, Ruhr-Universität, Bochum, Germany (1997).

Klimeck, J, R. Kleinrahm, and W. Wagner, "An Accurate Single-sinker Densimeter and Measurements of the (p, ρ, T) Relation of Argon and Nitrogen in the Temperature Range from (235 to 520) K at Pressures up to 30 MPa," *Journal of Chemical Thermodynamics*, **30**, 1571-1588 (1998).

Klimeck J., R. Kleinrahm, and W. Wagner, "Measurements of the (p, ρ, T) Relation of Methane and Carbon Dioxide in the Temperature Range from (240 to 520) K at Pressures up to 30 MPa Using a New Accurate Single-Sinker Densimeter," *The Journal of Chemical Thermodynamics*, **33**, 251-267 (2001).

Kreyszig, E., "Advanced Engineering Mathematics," 8th international edition, John Wiley & Sons, New York, 832-836 (2004).

Kupfermüller, K, "Introduction to Theoretical Electrical Engineering," 9th edition, Springer-Verlag, Berlin (1968).

Kuramoto N., and K. Fujii, *Proceedings of 22nd Japan Symposium on Thermophysical Properties,* Japan Society of Thermophysical Properties, Sendai, Japan, 341-343 (2001).

Kuramoto N., K Fujii, and A. Waseda, "Accurate Density Measurements of Reference Liquids by a Magnetic Suspension Balance," *Metrologia,* **41**, S84-S94 (2004).

Lau, W. R., C. A. Hwang, H. B. Brugge, G. A. Iglesias-Silva, H. A. Duarte-Garza, W. J. Rogers, K. R. Hall, J. C. Holste, B. E. Gammon, and K. N. Marsh, "A Continuously Weighed Pycnometer for Measuring Fluid Properties," *Journal of Chemical and Engineering Data*, **42 (4)**, 738-744 (July 1997).

Lösch, H.W., "Development and Design of New Magnetic Suspension Balances for Non-Contact Measurements of Vertical Forces," VDI Progress Report, Series 3, No. 138, Düsseldorf, Germany (1987).

Majer, V. and A. A. H. Pádua, "Measurement of Density with Vibrating Bodies," *Measurement of the Thermodynamic Properties of Single Phases, Experimental Thermodynamics vol* VI, IUPAC Elsevier Science, 1st edition, Amsterdam, The Netherlands, 149 (2003).

Mallet, C., M. Aho, J. Hamalainen, J. P. Rouan, and J. R. Richard, "Formation of NO, NO_2, and N_2O from Gardanne Lignite and Its Char under Pressurized Conditions," *Energy & Fuels*, **11,** 792-800 (1997).

Martinez, S. A., Personal Communication, Dept. of Chemistry, University of Burgos, Spain (2006).

Masui, R., W. M. Haynes, R. F. Chang, H. A. Davis, and J. M. H. L. Sengers, "Densimetry in Compressed Fluids by Combining Hydrostatic Weighing and Magnetic Levitation," *The Review of Scientific Instruments*, **55** (7), 1132-1142 (July 1984).

McLinden, M. O., Personal Communication, Physical and Chemical Properties Division, National Institute of Standard and Technology, Boulder, CO 80305, USA (2005)

McLinden, M. O., "Densimetry for Primary Temperature Metrology and a Method   for

the *in Situ* Determination of Densimeter Sinker Volumes," *Measurement of Science and Technology*, **17,** 2597-2612 (2006).

McLinden, M. O., R. Kleinrahm, and W. Wagner, "Force Transmission Errors in Magnetic Suspension Densimeters," *Presented at Sixteenth Symposium on Thermophysical Properties,* Boulder, CO 80305, USA (2006).

McLinden, M. O., and C. Lösch-Will, "Apparatus for Wide-Ranging, High-Accuracy Fluid p-ρ-T Measurements Based on a Compact Two-Sinker Densimeter," Submitted for Publications (2006).

Mehta, A., J. Walsh, and S. Lorimer, "Hydrate Challenges in Deep Water Production and Operation," http://www.blackwell-synergy.com (accessed on November 2006).

Mirzaeian, M., and P. J. Hall, "The Interactions of Coal with CO_2 and Its Effects on Coal Structure," *Energy & Fuels*, **20,** 2022-2027 (2006).

National Instruments, DAQ 6527 User Manual, http://www.ni.com (accessed on January 2007).

Nowak, P., R. Kleinrahm, and W. Wagner, "Measurement and Correlation of the (p, ρ, T) Relation of Nitrogen I. The Homogeneous Gas and Liquid Regions in the Temperature Range from 66 K to 340 K at Pressures up to 12 MPa," *The Journal of Chemical Thermodynamics*, **29** (10), 1137-1156 (October, 1997 a).

Nowak, P., R. Kleinrahm, and W. Wagner, "Measurement and Correlation of the (p, ρ, T) Relation of Nitrogen II. Saturated-liquid and Saturated-Vapor Densities and Vapor Pressures along the entire coexistence Curve," *The Journal of Chemical Thermodynamics*, **29** (10), 1157-1174 (October, 1997 b).

Oldenburg, C. M., and S. M. Benson, "Carbon Sequestration with Enhanced Gas Recovery: Identifying Candidate Sites for Pilot Study," First National Conference on Carbon Sequestration; Washington, DC (May 2001).

Pádua, A. A. H, J. M. N. A. Fareleira, J C. G. Calado, and W. A. Wakeham, "Electrochemical Model for Vibrating-Wire Instruments," *The Review of Scientific Instruments*, 69 (6), 2392-2399 (June 1998).

Parkyns, N. D., C. I. Warburton, and J. D. Wilson, "Natural Gas Conversion to Liquid Fuels and Chemicals: Where does it Stand?" *Catalysis Today*, **18**, 385-442 (1993).

Paroscientific Incorporated, Model number 735 Intelligent Display User's Manual, http://www.paroscientific.com (accessed on January 2007).

Patil, P. V., "Commissioning of a Magnetic Suspension Densitometer for High-accuracy Density Measurements of Natural Gas Mixtures," PhD Dissertation, Texas A&M University, College Station, TX (May 2005).

Peters, W. A., and M. A. Serio, "Symposium on Environmental and Health Effects of Fuel Choice: An Introduction," *Energy & Fuels*, **7,** 2-3 (1993*)*.

Pieperbeck, N., R. Kleinrahm, W. Wagner, and M. Jaeschke, "Results of (pressure, density, temperature) Measurements on Methane and on Nitrogen in the Temperature Range from 273.15 K to 323.15 K at Pressures up to 12 Mpa Using a New Apparatus for Accurate Gas-Density Measurements" *The Journal of Chemical Thermodynamics*, **23** (2), 175-194 (February 1991).

Pressure Systems, Model 960 Pressure Standard, www.pressuresystems.com (2006).

Renesme, G., J. Saint-Just, and Y. Muller, "Transportation Fuels and Chemicals Directly from Natural Gas: How Expensive?" *Catalysis Today*, **13**, 371-380 (1992).

Richardson, G. E., L. S. French, R. D. Baud, R. H. Peterson, C. D. Rorark, T. M. Montgomery, E. G. Kazanis, G. M. Conner, and M. P. Gravois, "Deepwater Gulf of Mexico 2004: America's Expanding Frontier," U.S. Department of the Interior, Mineral Management Service, Gulf of Mexico OCS Region, OCS Report MMS 2004-021, New Orleans, LA (May 2004).

Ruska Instrument Corporation (Presently GE Ruska), Dead Weight Gauge Operating Manual, Houston, TX (1977).

Rutishauser, H, and A. Reichmuth, *The New METTLER AT Analytical Balance*, METTLER Instruments AG, Greifensee , Switzerland (1988).

Saleh B., and M. Wendland, " Measurement of Vapor Pressures and Saturated Liquid Densities of Pure Fluids with a New Apparatus," *Journal of Chemical and Engineering Data*, **50**, 429-437 (2005).

Sauer, S. R., and J. Wiseman, "Commissioning and Startup of the Caesar and Cleopatra Mardi Grass Deepwater Pipelines," Paper presented at Offshore Technology Conference, Houston, TX, USA (May 2006).

Schlumberger, Oilfield Glossary, http://www.glossary.oilfield.slb.com (October 2006).

Seif, R., Personal Communications, Director Engineering, Rubotherm Präzisionsmess-technik GmbH, Bochum, Germany (2005).

Setzmann, U., and W. Wagner, "A New Equation of State and Tables of the Thermodynamic Properties for Methane Covering the Range from the Melting Line to 625 K at Pressures up to 1000 Mpa," *Journal of Physical and Chemical Reference Data*, 20, 1061-1155 (1991).

Shine, K. P., R. G. Derwent, D. J. Wuebbles, and J. J. Morcrette, "Radiative Forcing of Climate," *Climate Change: The IPCC Scientific Assessment*; J. T. Houghton, G. J. Jenkins and J. J. Ephraums; Cambridge University Press, Cambridge, UK (1990).

Signal Recovery Inc., Technical Note TN 1000, 2000, http://www.signalrecovery.com

Simon, M.D., L.O. Heflinger, and S.L. Ridgway, "Spin Stabilized Magnetic Levitation," *American Journal of Physics*, 65, 286 (1997).

Smith, I. M., and K. V. Thambimuthu, "Greenhouse Gas Emissions, Abatement and Control: The Role of Coal," *Energy & Fuels*, **7**, 7-13 (1993).

Span, R. and W. Wagner, "A New Equation of State for Carbon Dioxide Covering the Fluid Region from the Triple-Point Temperature to 1100 K at Pressures up to 800 MPa," *Journal of Physical and Chemical Reference Data,* 25 (6), 1509-1596 (1996).

Span, R., E.W. Lemmon, R.T. Jacobsen, W. Wagner and A. Yokozeki, "A Reference Equation of State for the Thermodynamic Properties of Nitrogen for Temperatures from 63.151 to 1000 K and Pressures to 2200 MPa," *Journal of Physical and Chemical Reference Data*, **29**(6), 1361 (2000).

Straty, G. C., and D. E. Diller, "(p, V, T) of Saturated and Compressed Fluid Nitrogen ," *The Journal of Chemical Thermodynamics*, **12** (10), 927-936 (October 1980).

Tan, X., and K. Li, "Oxydative Coupling of Methane in a Perovskite Hollow-Fiber Membrane Reactor," *Ind. Eng. Chem. Res.*, **45**, 142-149 (2006).

Tillner-Roth, R., and H. D. Baehr, "Burnett Measurements and Correlation of Gas-Phase *(P, P, T)* of 1, 1, 1, 2-Tetrafluoroethane (R134a) and of 1, 1-Difluoroethane (R 152a)," *The Journal of Chemical Thermodynamics*, **24,** 413-424 (1992).

U.S. EPA, "Inventory of U.S. Greenhouse Gas Emissions and Sinks: 1990-1998," U.S. Environmental Protection Agency, Washington, DC 20460 (2000).

Villamañán M. A., and C. R. Chamorro, *17th Thermodynamics Conference on Thermodynamics and Statistical Mechanics with Industrial Applications.* School of Chemistry, University of Bristol (2001).

Wagner, F. E, and A. Mirahamdi, "Non-Wearing Magnetic Bearings with Rare Earth/Cobalt Magnets for Use in Electricity Meters," *Thyssen Edelstahl*, Techn. Ber. 6, 33-52 (1980).

Wagner, W., K. Brachthäuser, R. Kleinrahm, and H.W. Losch, "A New, Accurate Single-Sinker Densimeter for Temperatures from 233 to 523 K at Pressures up to 30 MPa," *International Journal Thermophys.*, **16** (2), 399-411 (1995).

Wagner, W., R. Kleinrahm, H.W. Lösch, and J.T.R. Watson, "Hydrostatic Balance Densimeters with Magnetic Suspension Couplings," *Measurement of the Thermodynamic Properties of Single Phases*, *Experimental Thermodynamics,* 1st edition, vol VI, IUPAC Elsevier Science, Amsterdam, 127-149 (2003).

Wagner, W., and R. Kleinrahm, "Densimeters for Very Accurate Density Measurements of Fluids Over Large Ranges of Temperature, Pressure and Density," *Metrologia,* **41**, S24-S39 (2004).

Warowny, W., and P. T. Eubank, "Generalized Equations of the Burnett P - V - T Methods for Adsorbing Gases," *Fluid Phase Equilibria*, **103** (1), 77-95 (1995).

Watson J. T. R., and B. Millington, "The Density of Rich Natural Gas Mixtures. A joint Industrial Project," Project No DRG001, Report No 110/97, National Engineering Laboratory, 1998, East Kilbride, Glasgow, Scotland.

Watson, R. T., H. Rodhe, H. Oeschger, and U. Siegenthaler, "Greenhouse Gases and Aerosols," *Climate Change: The IPCC Scientific Assessment*; Cambridge University Press, Cambridge, UK (1990).

Westbrook, C. K., "The Internal Combustion Engine at Work," Lawrence Livermore National Laboratory, University of California, 1999, available at: http://www.llnl.gov/ str/Westbrook.html (accessed on October 2006).

World Bank, "World Development Indicators," Published by the World Bank, Washington, DC (2004).

Zhou, J., "Automatic Isochoric Apparatus for PVT and Phase Equilibrium Studies of Natural Gas mixtures," PhD Dissertation, Texas A&M University, College Station, TX (May 2005).

APPENDIX A

CONSISTENCY BETWEEN ISOCHORIC APPARARTUS AND MSA
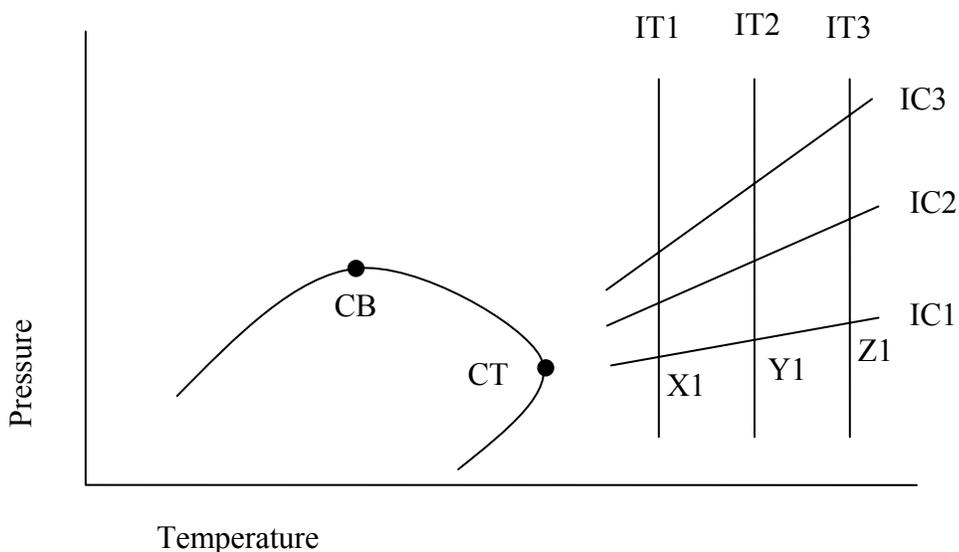
Figure A.1. Crossing of isochoric and isothermal data

Consistency of the MSA density data can be checked by isochoric data with the MSA isothermal data.

MSA experimental densities, at or close to isotherm IT1 (in figure A.1) are first converted to densities corresponding to IT1 temperature by using any equation of state, even perfect gas law should work. IT1 is expressed in a functional polynomial form: $\rho = \rho(P)$. The coefficients of this polynomial can be calculated from a non- linear regression fit of the P-ρ data at this isotherm.

IC1, an iso-mole line, can be expressed in a functional polynomial form: $P = P(T)$, where the coefficients can be obtained from non-linear regression fit of isochoric data at constant mass.

Therefore, at the intersection point X1, we know the temperature because at this temperature, isothermal measurements were done by the MSA. From that, we can calculate the pressure using the second polynomial. Knowing the pressure, we can calculate the density at X1, ρ_{X1} by using the first polynomial equation.

The density along IC1 is not constant because of change in isochoric cell and tubing volume due to temperature and pressure effect. By using ρ_{X1} as base density, we can calculate the density at Y1, ρ_{Y1} from the following relation:

$$\frac{V_{Y1}}{V_{X1}} = \frac{\rho_{X1}}{\rho_{Y1}} = 1 + \alpha(T_{Y1} - T_{X1}) + \kappa(P_{Y1} - P_{X1}) \tag{A.1}$$

Where, α is the linear thermal expansion coefficient and κ is the pressure distortion coefficient of the isochoric apparatus cell material.

ρ_{Y1} can also be calculated from the intersection of IT2 and IC1, just as ρ_{X1} was calculated previously from the intersection of IT1 and IC1. If the two densities at Y1 are within the experimental error of each other, we can assume that the MSA data is consistent with the isochoric apparatus data.

This method, besides checking consistency, could be used to calculate densities of intermediate points. For IC1, we can calculate pressure for each temperature point between X1 and Z1 by using $P = P(T)$. So, using X1 (or Y1) as reference and using equation similar to (1), we can calculate the densities ρ (T, P) at these points.

APPENDIX B

UNCERTAINTY ANALYSIS FOR GAS MIXTURES

The total error in density measurements is a combination of random errors and systematic error. Uncertainty in pressure and temperature measurement, molar compositional analysis (in case of a mixture), and measurement of sinker mass under vacuum and at pressure contribute to random error. Systematic error is due to uncertainty in sinker volume. This includes uncertainty in sinker volume determination at a reference temperature and pressure, as well as uncertainty in the functional dependence of sinker volume on temperature and pressure. Force transmission error also contributes to systematic error

The random error in density due to pressure, temperature and composition can be expressed as:

$$
\Delta\rho = \left\{
\begin{array}{l}
\left[\left(\dfrac{\partial\rho}{\partial P}\right)_{T,x}\Delta P\right]^2 + \left[\left(\dfrac{\partial\rho}{\partial T}\right)_{P,x}\Delta T\right]^2 + \\[2ex]
\displaystyle\sum_{i=1}^{C}\left[\left(\dfrac{\partial\rho}{\partial x_i}\right)_{P,T,x_{j\neq i}}\Delta x_i\right]^2
\end{array}
\right\}^{1/2}
\tag{B.1}
$$

Where C is the number of components.

The following procedure should be used for error analysis:

1. Convert experimental isotherms of density data to density at nearest round figures of pressure and temperature using any EOS; we can even use perfect gas law equation as temperature and pressure deviations are very small. These temperatures and pressures will serve as reference; i.e. densities at all near-by pressures and temperatures will be converted to densities at this pressure and temperature.

2. At each isotherm, get a functional relationship between ρ vs. P and calculate the derivative at each value of P. This will give us $\left(\dfrac{\partial \rho}{\partial P}\right)_{T,m_{\mathrm{v}},m_{\mathrm{a}},x}$ at each experimental point.

3. Similarly, at each isobaric point, get the functional relationship between ρ vs. T and calculate the derivative at each value of T. This will give us $\left(\dfrac{\partial \rho}{\partial T}\right)_{P,m_{\mathrm{v}},m_{\mathrm{a}},x}$ at each experimental point.

4. For original composition of gas, calculate the densities at all temperatures and pressures using any good EOS (GERG02 or AGA8-DC92 or Peng-Robinson). Then, very slightly change the composition of only one component and normalize so that $\Sigma x_i = 1$. Calculate the densities again using the EOS. Change the composition of the same component again and calculate densities. Repeat the steps, say six times. Now we have, for each set of pressure and temperature point, seven densities (including that of original composition). Similar to step 2 and 3, calculate $\left(\dfrac{\partial \rho}{\partial x_i}\right)_{P,T,m_{\mathrm{v}},m_{\mathrm{a}},x_{j\neq i}}$ for each set of temperature and pressure point.

5. Repeat steps 4 for all other components in the mixture, one at a time.

6. As supplied by the manufactures: $\Delta T = 10$ mk, $\Delta P = 0.02$ %* Full Scale = 1.2 psi for 6,000 psi transducer. Δx_i is found from calibration certificate supplied by DCG Partnership and Accurate Gas Products.

Table B.1 shows the percentage uncertainty due to temperature and pressure at 1σ while table B.2 and figure B.1 shows the uncertainty due to temperature, pressure and compositions at 2σ; it is observed that compositional uncertainty dominates the total uncertainty.

It is assumed that there is no systematic error in pressure, temperature and compositional measurements.

Table B.1. Percentage uncertainty due to temperature and pressure for gas samples

Temperature	Pressure					
K	**psia**					
	2000	2500	3000	3500	4000	5000
270	0.023	0.017	0.013	0.010	0.007	0.003
290	0.029	0.020	0.015	0.011	0.008	0.004
305	0.031	0.022	0.016	0.012	0.009	0.004
340	0.032	0.023	0.017	0.013	0.011	0.006

Table B.2. Percentage uncertainty due to temperature, pressure and compositions for gas samples

Temperature	Pressure					
K	**psia**					
	2000	2500	3000	3500	4000	5000
270	0.106	0.085	0.071	0.062	0.055	0.046
290	0.105	0.089	0.076	0.066	0.059	0.049
305	0.101	0.087	0.076	0.067	0.060	0.051
340	0.093	0.081	0.073	0.067	0.062	0.053

Random scatter in weighings is found from the measurement point position of the sinker under vacuum. Balance linearity has been obtained from the literature.

Drift in the sinker mass has been calculated by isolating the balance completely from the MSA and by putting weights (close to sinker weight) on the balance pan. The weights are kept on the pan continuously for 10 minutes (time for each experimental measurement point run) and the drift is taken as the difference between initial and final balance reading. During actual experiment, we take the most stable data. So, this time, the data with least amount of drift was considered. The average of two best run was 15 μg.
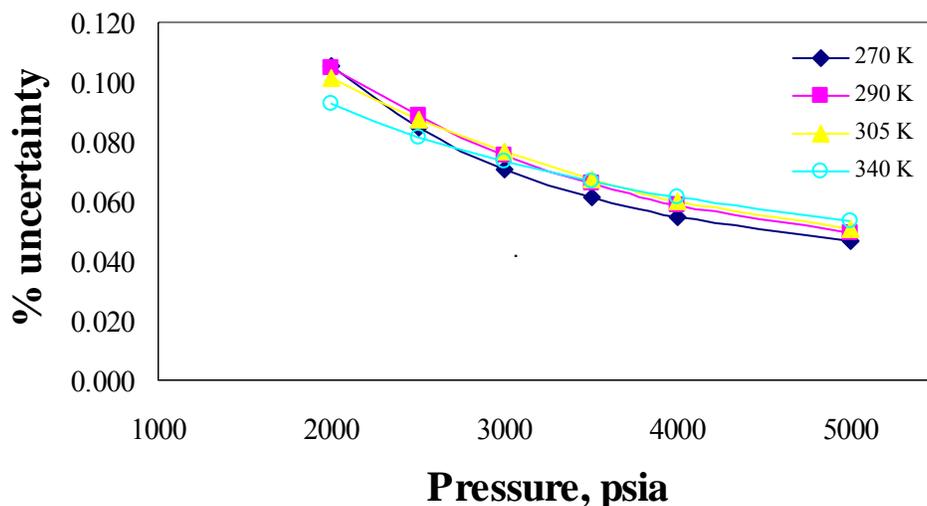
Figure B.1. Percentage uncertainty due to temperature, pressure and compositions

In case of the double sinker, the numbers for the sinkers are subtracted. This is why; the drift is usually very small, in the order of 5 μg.

Assuming 1 μg is equivalent to 0.0001 kg/m^3 in density (McLinden and Lösch-Will, 2006), the sum of absolute error (root sum of squares) could be written as $[\,0.0018 + 4.45*10^{-6}(T - 293.15)\,]$ when T ≥ 293.15 K.

The volume of the sinker is 6.74104 ± 0.00013 cm^3 (McLinden, 2005) measured at 293.15 MPa and almost at 0.1 MPa. Therefore, the relative error due to sinker volume at 293.15 K and 0.1 MPa is (0.00013*10^6)/6.74104 or 19 ppm.

The relative uncertainty due to sinker volume as $f\,(T)$ at 0.1 MPa has been determined using the concept of density-ratio gas thermometer (appendix D).The relative uncertainty in sinker volume at 350 K has been estimated to be 200 ppm and at 264.8 K; 300 ppm. Low measurement accuracy at low pressure has resulted in such large uncertainties. The sinker volume uncertainty should ideally be carried out using a two-sinker densimeter. Based on the two measurements, $f\,(T)$ has been determined to be $2*10^{-7}*T^2 - 0.0001*T + 0.0159$. The relative error due to sinker volume as $f\,(p)$ has been obtained from literature (McLinden and Lösch-Will, 2006; Smithells, 1997); it has

been assumed to be (1.25*p) ppm, where p is pressure in MPa. Force transmission error has been estimated to be 25 ppm.

The total uncertainty due to balance, force transmission error and sinker volume, as a function of temperature and pressure could be expressed

$$u(k=2) = \left\{ 25^2 + \left[2*10^{-7} * T^2 - 0.0001 * T + 0.0159 \right]^2 + \left[1.25 p \right]^2 \right\}^{0.5} (ppm)^{-1}$$
$$+ \left[0.0018 + 4.45 * 10^{-6} (T - 293.15) \right] (kg.m^{-3})^{-1}$$

The uncertainty due to MSA and balance such as sinker volume, balance weighings, force transmission error, etc are shown in table B.3.

Table B.3. Uncertainty due to MSA and balance

	Temperature		
	264.8 K	**293.15 K**	**350 K**
randon scatter in weighings	10 µg	10 µg	20 µg
balance linearity	3 µg	3 µg	3 µg
drift in mass of sinker	15 µg	15 µg	15 µg
Sum ("root sum of squares)	0.0018 kg/m3	0.0018 kg/m3	0.0025 kg/m3
Relative Errors			
sinker volume at reference temperature of 293.15 K	19 ppm	19 ppm	19 ppm
sinker volume as $f(T)$, p = 0.1 MPa	300	0	200
sinker volume as $f(T)$, p = 35 MPa	44 ppm	44 ppm	44 ppm
force Transmission Error	25 ppm	25 ppm	25 ppm
balance calibration and non linearity minimisation			
uncertainty in sinker mass	1 ppm	1 ppm	1 ppm
mass of Ta and Ti weights	5 ppm	5 ppm	5 ppm
Sum at p = 0.1 Mpa	302 ppm	32 ppm	203 ppm
Sum at p = 35 Mpa	305 ppm	54 ppm	207 ppm

Absolute Errors (1 µg equivalent to 0.0001 kg/m^3)

APPENDIX C

DENSITY RATIO GAS THERMOMETER

Uncertainty in sinker volume can be estimated by using the concept of density-ratio gas thermometer (McLinden, 2006). It involves the density measurement of a working gas at two temperatures and at multiple pressures. The ratios of the densities at each pressure (for two temperatures) are computed and the ratios are extrapolated to zero pressure or zero density.

The pressure of a low-density gas is given by a simple virial expansion:

$$p = \frac{RT\rho(1 + B\rho + C\rho^2 + D\rho^3)}{M} \tag{C.1}$$

Where T is the temperature, R is the molar gas constant, ρ is the mass density, M is the molar mass, and $B,\ C$ and D are the second, third and fourth virial coefficient on a mass basis.

In a constant-volume thermometer mass of gas is kept constant. However, in the density ratio gas thermometer, the pressure is held constant for measurements at the two temperatures. The density ratio is extrapolated to zero pressure (or density) to yield

$$\frac{T_x}{T_{ref}} = \frac{\rho(T_{ref})}{\rho(T_x)} \quad \text{as } p \longrightarrow 0 \tag{C.2}$$

Where T_{ref} is the reference temperature of 293.15 K where the sinker volume was determined hydrostatically.

Any real gas approaches the ideal–gas behavior in the limit of zero pressure, but measurements are carried out at finite pressures. This indicates that a very simple fluid like helium with a low critical temperature should be used for this purpose, as nearly ideal behavior is desirable at high pressure. On the other hand, mass density determination with a light gas would lead to large relative uncertainties in the densities. Thus one should use heavier gases with simple, symmetrical structure.

In our case, we are doing low-pressure measurements with nitrogen in the range of 0.5 MPa to 10 MPa at different isotherms, namely 260, 293.25, and 350 K with

293.25 K as the reference temperature. Then we plotted ρ_x/ρ_{ref} (measured at same pressure but at two different temperatures) against pressure in the low-pressure region and extrapolated to zero density using polynomial such as:

$$\frac{\rho_x}{\rho_{ref}} = a_0 + a_1 p + a_2 p^2 \qquad\qquad (C.3)$$

The difference between the value of the density ratio at zero pressure and temperature ratio should ideally be zero, as evident from (C.2). However, the actual difference could be interpreted as either the error in the measured temperature relative to the thermodynamic temperature (which is comparatively small) or the error in the sinker volume.

In future, we should investigate the matter further by testing with more gases such as helium, neon, argon etc at many temperature points. The uncertainty in sinker volume could be expressed as a cubic polynomial function of temperature. For helium, the density ratio should be almost flat.

Because of extrapolation to zero density, virials are not needed and this density method is not sensitive to gas purity. The working gas need not have to have high purity, it should be same for all the tests.

By repeating the process at different temperatures, density ratios at these temperatures to that at reference temperature should be calculated at different pressures. Then extrapolate to zero pressure. So, we will have uncertainty in sinker volume as a function of temperature.

APPENDIX D

SINKER VOLUME DEPENDANCE ON PRESSURE AND TEMPERATURE

Consider a rectangular solid of volume V (L, W, H), even though the following derivation is true for any geometry. The independent dimensions L, W and H change by infinitesimal amounts dL, dW and dH, respectively because of pressure and temperature effect (Dowling, 2007). Therefore, the normal strains along x, y and z-axis are:

$$\varepsilon_x = \frac{dL}{L}, \quad \varepsilon_y = \frac{dW}{W}, \quad \varepsilon_z = \frac{dH}{H} \tag{D.1}$$

$$V = L * W * H$$

$$dV = \left(\frac{\delta V}{\delta L}\right)_{W,H} dL + \left(\frac{\delta V}{\delta W}\right)_{L,H} dW + \left(\frac{\delta V}{\delta H}\right)_{W,L} dH$$

$$\frac{dV}{V} = \frac{1}{V}\left[W * H * \left(\left(\frac{\delta L}{\delta L}\right)_{W,H} dL\right) + L * H * \left(\frac{\delta W}{\delta W}\right)_{L,H} dW + L * W * \left(\frac{\delta H}{\delta H}\right)_{W,L} dH \right]$$

$$= \frac{dL}{L} + \frac{dW}{W} + \frac{dH}{H} = \varepsilon_x + \varepsilon_y + \varepsilon_z \tag{D.2}$$

Where ε stands for normal strain and suffix x, y and z stand for three axis.

Hook's law for any material, assuming that strains caused by each component of stress can be added together, can be written as:

$$\varepsilon_x = \frac{1}{E}\left[\sigma_x - v(\sigma_y + \sigma_z)\right]$$

$$\varepsilon_y = \frac{1}{E}\left[\sigma_y - v(\sigma_x + \sigma_z)\right] \qquad \text{D.3 (a, b, c)}$$

$$\varepsilon_z = \frac{1}{E}\left[\sigma_z - v(\sigma_x + \sigma_y)\right]$$

Where σ stands for normal stress, v for poison's ratio and E for Young's modulus (modulus of elasticity).

The previous equations do not take into consideration the affect of temperature. Taking temperature in to consideration for an isotropic material, where uniform thermal strain happens in all directions:

$$\varepsilon_x = \frac{1}{E}\left[\sigma_x - v\left(\sigma_y + \sigma_z\right)\right] + \alpha\Delta T$$

$$\varepsilon_y = \frac{1}{E}\left[\sigma_y - v\left(\sigma_x + \sigma_z\right)\right] + \alpha\Delta T \qquad \text{D.4 (a, b, c)}$$

$$\varepsilon_z = \frac{1}{E}\left[\sigma_z - v\left(\sigma_x + \sigma_y\right)\right] + \alpha\Delta T$$

Where, α is the linear expansion of thermal coefficient and $\Delta T = \text{T} - \text{T}_{\text{Reference}}$. At reference temperature, strains are taken to be zero.

$$\alpha = \frac{1}{L}\frac{dL}{dT} \qquad (D.5)$$

Plugging in D.4 (a, b, c) in to (D.2), we get:

$$\frac{dV}{V} = \frac{(1-2v)}{E}\left(\sigma_x + \sigma_y + \sigma_z\right) + 3\alpha\Delta T \qquad (D.6)$$

The first term on right accounts for pressure change and the second term accounts for temperature change.

The body is surrounded by gas on all sides, so pressure is same everywhere.

$$\sigma_x = \sigma_y = \sigma_z = \sigma = -\left(P - P_0\right) \qquad (D.7)$$

The last equality indicates that stress is working outward and pressure P is working inward. P_0 is the reference pressure where strains are taken to be zero.

Plugging in (D.5) and (D.7) into (D.6), we get:

$$\frac{dV}{V} = 3\frac{\Delta L}{L_0} - \frac{3(1-2v)}{E}\left(P - P_0\right) \qquad (D.8)$$

The factor 3 in the first term in the right hand side arises because the linear thermal expansion coefficient is very closely approximated as one-third the volumetric coefficient β in an isotropic material.

$$\beta = \frac{1}{V}\frac{\delta V}{\delta T} = \frac{1}{L^3}\frac{\delta L^3}{\delta T} = \frac{1}{L^3}\left(\frac{\delta L^3}{\delta L}\frac{\delta L}{\delta T}\right) \cong \frac{1}{L^3}\left(3L^2\frac{\delta L}{\delta T}\right) = \frac{3}{L}\frac{\delta L}{\delta T} = 3\alpha \qquad (D.9)$$

This is however true only when the change in volume is small. As the change in temperature increases, and as the value for the linear coefficient of thermal expansion increases, the error due to this assumption also increases. For non-negligible changes in volume, the total volume is:

$$(L + \Delta L)^3 = L^3 + 3L^2\Delta L + 3L\Delta L^2 + \Delta L^3 \tag{D.10}$$

The last three terms indicate the change in volume. This equation contains the main term $3L^2$ (as in equation (D.9)), but also has the term $3L\Delta L^2 = 3L^3\alpha^2\Delta T^2$, which shows that a large change in temperature can overshadow a small value for the linear coefficient for thermal expansion.

$$\frac{\Delta V}{\Delta L} = \frac{1}{\Delta L}\left(3L^2\Delta L + 3L\Delta L^2 + \Delta L^3\right) = 3L^2 + 3L\Delta L + \Delta L^2 \tag{D.11}$$

$$\beta = \frac{1}{L^3}\left(\frac{\Delta V}{\Delta L}\frac{\delta L}{\delta T}\right) = \frac{1}{L^3}\left(3L^2 + 3L\Delta L + \Delta L^2\right)\frac{\delta L}{\delta T}$$

$$\cong 3\alpha + 3\alpha\frac{\Delta L}{L}, \text{ ignoring the last term} \tag{D.12}$$

So, for large change in temperature, equation (D.8) should be re-written as:

$$\frac{dV}{V} = \left(3 + 3\frac{\Delta L}{L_0}\right)\frac{\Delta L}{L_0} - \frac{3(1 - 2\nu)}{E}(P - P_0) \tag{D.13}$$

$\frac{\Delta L}{L_0}$, ν and E can be calculated from curves supplied by Rubotherm.

APPENDIX E

PRT CALIBRATION COEFFICIENTS

International Temperature Scale of 1990 (ITS-90) is designed to represent the absolute thermodynamic scale as closely as possible throughout its range of 0.65 K to 1358 K. ITS-90 uses various defined points, to which temperature values have been assigned, that are based on various thermodynamic equilibrium states of fourteen pure chemical elements and water. Thermometers calibrated according to ITS-90 use formulas to interpolate between the defined points. ITS-90 uses rigorous control over variables to insure reproducibility from lab to lab. Therefore, ITS-90 is not a scale, rather an equipment calibration standard that facilitates the comparability and compatibility of temperature measurements internationally. It's subdivided into multiple temperature ranges which can overlap in some cases (Preston-Thomas, 1990).

Between 13.8033 K (the triple point of equilibrium hydrogen) and 1234.93 K, the ITS-90 has been defined by resistance ratios of standard platinum resistance thermometers (PRT). The ratios have been obtained by calibration at specified sets of the fixed points, by reference functions and deviations functions of resistance ratios which relate to ITS-90 temperatures (T_{90}) between the fixed points (NIST, 1990).

ITS-90 expresses the temperature in Kelvin in terms of the ratio of the measured resistance of the PRT at the temperature and its resistance at triple point of water; 273.16 K:

$$W(T_{90}) = \frac{R(T_{90})}{R(273.16\text{K})}$$ (E.1)

The deviation function is given by:

$$\Delta W (T_{90}) = W (T_{90}) - W_{ref} (T_{90})$$ (E.2)

Using a polynomial expression for the deviation function for calibration in the sub-range 83.8058 K to 273.16 K and plugging it in E.2, we get equation E.3 for

reference function. Finally equation E.4 is used to calculate the temperature below 273.16 K.

$$W_{\text{ref}}(T_{90}) = W(T_{90}) - a_4[W(T_{90}) - 1] - b_4[W(T_{90}) - 1]\ln W(T_{90}) \tag{E.3}$$

$$\frac{T_{90}}{273.16K} = B_0 + \sum_{1}^{15} B_i \left[\frac{W_{\text{ref}}(T_{90})^{1/6} - 0.65}{0.35} \right]^i \tag{E.4}$$

The coefficients a_4 and b_4 were obtained by MINCO by calibrating the PRT at triple points of argon (83.8058 K), mercury (234.3156 K) and water (273.16 K).

To be used throughout the sub-range 273.15 K to 692.677 K, the same PRT is calibrated at the triple of water, and at the freezing points of tin (505.078 K) and zinc (692.677 K). Using a different expression for deviation function, we calculate the temperature at and above 273.16 K.

$$W_{\text{ref}}(T_{90}) = W(T_{90}) - a_8[W(T_{90}) - 1] - b_8[W(T_{90}) - 1]^2 \tag{E.5}$$

$$T_{90} - 273.15K = D_0 + \sum_{1}^{9} D_i \left[\frac{W_{\text{ref}}(T_{90}) - 2.64}{1.64} \right]^i \tag{E.6}$$

The coefficients a_8 and b_8 were determined by Minco during the calibration. These coefficients and values of the coefficients B_0, B_i and D_0, D_i are given in Table E.1. The resistance of the PRT at the triple point of water measured during the original calibration done by Minco on November 16, 2000 was R (273.16K) = 100.4244 ohm. PRT resistance at triple point of water was again checked by Dr. McLinden of NIST in July 2005 and he found it to be 100.4293 ohm (McLinden, 2005).

Table E.1. Constants in deviation equations and reference functions of ITS-90

a_4	-0.000418264140	B_0	0.183324722
b_4	0.000080228227	B_1	0.240975303
a_8	-0.000568113400	B_2	0.209108771
b_8	0.000260761350	B_3	0.190439972
		B_4	0.142648498
		B_5	0.077993465
D_0	439.932854	B_6	0.012475611
D_1	472.418020	B_7	-0.032267127
D_2	37.6844940	B_8	-0.075291522
D_3	7.472018	B_9	-0.056470670
D_4	2.920828	B_{10}	0.076201285
D_5	0.005184	B_{11}	0.123893204
D_6	-0.963864	B_{12}	-0.029201193
D_7	-0.188732	B_{13}	-0.091173542
D_8	0.191203	B_{14}	0.001317696
D_9	0.049025	B_{15}	0.026025526

APPENDIX F

DEADWEIGHT GAUGE PISTON CALCULATIONS

There are various factors that affect the performance the performance of the piston gage in the dead weight gage or DWG (as discussed in section 5) and the following correctional procedures should be used:

Elastic distortion of the cylinder: The net change in the area of the piston/cylinder assembly at a constant temperature of 23 deg C could be expressed as a polynomial function of the applied pressure:

$$A_e = A_{0(t=23))} \left(1 + b_1 p + b_2 p^2 \right) \tag{F.1}$$

Where, A_e is the effective area at a pressure p and $A_{0(t=23))}$ is the area of the piston at a reference pressure of zero psig and at a reference temperature of 23 deg C. b_1 and b_2 are elastic distortion coefficients that are determined experimentally.

Effect of temperature: Dead-weight gages are temperature sensitive and should be corrected to a common temperature datum.

$$A_{0(t+\Delta t)} = A_{0(t=23)} \left(1 + C\Delta t \right) \tag{F.2}$$

Where, $A_{0(t+\Delta t)}$ is the area corrected to the working temperature and C is the coefficient of superficial expansion

Buoyant effect of the air: If X is the calibrated mass, M_X is the true mass in vacuum and $(M_A)_X$ is the apparent mass in air due to buoyancy, then:

$$
\begin{aligned}
\left(M_A \right)_X &= M_X - V_X \rho_{air} \\
&= M_X \left(1 - \rho_{air} / \rho_X \right)
\end{aligned} \tag{F.3}
$$

Where, V_X is the volume of the calibrated mass. If ρ_{air} and ρ_x are the densities of air and calibrated mass, respectively, g_c is a conversion constant and F is the force due to apparent mass, then:

$$F = \left(M_A\right)_X \frac{g}{g_c}$$

$$= M_X \left(1 - \rho_{air} / \rho_X\right)\frac{g}{g_c} \tag{F.4}$$

$(M_A)_{\text{X wrt brass}}$, apparent mass of X with respect to brass standards has been

defined such that $F = \left(M_A\right)_{X \text{ wrt brass}} \left(1 - \rho_{air} / \rho_{brass}\right)\frac{g}{g_c}$ (F.5)

Where, ρ_{brass} is density of the brass standards and taken as either 8.4 or 8.0 g/cm^3.

The calibration certificates report apparent mass rather than true mass. Therefore, we can do force calculation by using equation (F.5) rather than equation (F.4). Equation (F.4) requires the knowledge of density of calibrated weights; because of their irregular shapes, it's difficult to determine their volumes and densities.

Corrections should be made for the pressure head of the DWG fluid (Spinnestic 22 oil) between reference plane of measurement and DPI (differential pressure indicator) diaphragm; presently this distance is about 8.5 inches. The specific gravity of the Spinnestic 22 is 0.86 (15.6 deg C / 15.6 deg C).

Finally, corrections should also be made for surface tension of the fluid in terms of apparent mass, as provided in calibration certificates.

Table F.1. Parameter values from the calibration report of DWG

Parameter	Value
A0 at 23 deg C	1.301632E-02 in^2
b1	-1.54E-08 / psi
b2	-1.35E-13 / psi^2
C	9.10E-06 / deg C
L1	6.141E+00 in

Table F.2. Component weights from the calibration report of DWG

Component	Apparent Mass (8.4) Pound
Piston	0.0191751
Surface tension	1.20E-04
Weight Table	0.761864
Total Tare	0.781159

L1 in table F.1 is the distance between the top loading edge of the weight table and the reference plane. The calibration was done by Ruska Instrument Corp. (Now GE Sensing) on June 11, 2003. Table F.2 shows the component weights from calibration.

APPENDIX G

NI DAQ CARD PIN DESIGNATION

Table G.1. Designation of pins in NI DAQ-6527 card

Pin	Channel in DAQ	Line
67	4	7
69	4	6
71	4	5
73	4	4
75	4	3
77	4	2
79	4	1
81	4	0

Table G.1 shows the pin designation of NI DAQ-6527 card.

Comments: A logic low (FALSE, 0 V) closes the relay.

The designations are used in the LabView Program for temperature control and data acquisition.

Source: NI DAQ-6527 manual (www.ni.com, 2006)

VITA

Saquib Ejaz received his Bachelor of Science degree in chemical engineering from Bangladesh University of Engineering and Technology in 1995. He worked for two years as a process engineer in British Oxygen Company and two more as a lecturer in Bangladesh University of Engineering and Technology. He received a Master of Science degree in chemical engineering from the same school in 1999 and a Master of Engineering degree in chemical engineering from Texas A&M University, College Station in 2001. He enrolled in the PhD program in the Department of Chemical Engineering at Texas A&M University, College Station in 2002. His research area includes measurement of thermophysical properties.

Saquib is the father of two beautiful and precious daughters, Lamiya Zahin and Nashita Zahin. His wife Lufthansa R. Kanta is also pursuing a PhD degree in the Department of civil engineering at Texas A&M University.

His permanent address in Bangladesh is:

House: 49, Road: 14, Sector: 3

Uttara Model Town

Dhaka-1230, Bangladesh

Phone: (8802) 8912615

In the USA, he can be reached through Dr. Ken Hall, Department of Chemical Engineering, Texas A&M University, College Station, TX 77843